

A Dissertation

entitled

Eco-design of Emerging Photovoltaic (PV) Cells

by

Ilke Celik

Submitted to the Graduate Faculty as partial fulfillment of the requirements for the

Doctor of Philosophy Degree in

Engineering

Dr. Defne Apul, Committee Chair

Dr. Michael Heben, Committee Member

Dr. Randall Ellingson, Committee Member

Dr. Constance Schall, Committee Member

Dr. Cyndee Gruden, Committee Member

Dr. Kumar Ashok, Committee Member

Dr. Amanda Bryant-Friedrich, Dean

College of Graduate Studies

The University of Toledo

August, 2018

Copyright 2018, Ilke Celik

This document is copyrighted material. Under copyright law, no parts of this document may be reproduced without the expressed permission of the author.

An Abstract of
Eco-design of Emerging Photovoltaic (PV) Cells

by

Ilke Celik

Submitted to the Graduate Faculty as partial fulfillment of the requirements for the
Doctor of Philosophy Degree in
Civil Engineering

The University of Toledo
August, 2018

This dissertation explores the eco-design concepts for emerging PV cells. By conducting life cycle assessment (LCA) method, I addressed the following questions: (1) What is the environmental impact of a scalable perovskite PV cell? (2) How important are the metal emissions from the emerging thin film devices during the use phase? (3) What are the environmental impacts and costs of the materials used in emerging PVs? These questions are addressed in the analyses presented in the Chapters two, three and four, respectively.

Chapter two assesses the environmental impacts of perovskites PVs that have device structures suitable for low cost manufacturing. A structure with an inorganic hole transport layer (HTL) was developed for both solution and vacuum based processes, and an HTL-free structure with printed back contact was modeled for solution-based deposition. The environmental impact of conventional Si PV technology was used as a reference point. The environmental impacts from manufacturing of perovskite solar cells were lower than that of mono-Si. However, environmental impacts from unit electricity generated were higher than all commercial PV technology mainly because of the shorter lifetime of perovskite

solar cell. The HTL-free perovskite generally had the lowest environmental impacts among the three structures studied. Solution based methods used in perovskite deposition were observed to decrease the overall electricity consumption. Organic materials used for preparing the precursors for perovskite deposition were found to cause a high marine eutrophication impact. Surprisingly, the toxicity impacts of the lead used in the formation of the absorber layer were found to be negligible.

Chapter three addresses the life cycle toxicity of metals (cadmium, copper, lead, nickel, tin and zinc) that are commonly used in emerging PVs. In estimating the potential metal release, a new model that incorporates field conditions (crack size, time, glass thickness) and physiochemical properties (diffusion coefficient and solubility product) was introduced. The results showed that the use phase toxicity of copper and lead can be more toxic than that of the extraction phase. Thus, precautionary loss limits to manage toxic impacts from the use phase was proposed. Also, the toxicity from different layers of perovskite, copper zinc tin sulphide (CZTS), and quantum dot (QD) type of solar cells was compared. It was found that cadmium sulphide (compared to zinc oxide and tin oxide) and lead (II) sulphide (compared to lead (II) iodine and CZTS) were less toxic alternatives for electron selective layer and light absorber, respectively. Finally, in comparing the toxic metal releases of the PVs to today's coal power plants, it was seen that the metal emissions from PVs are expected to be several times less than the emissions from coal.

Chapter four aims to create inventories that offer insight into the environmental impacts, and cost of all the materials used in emerging PV technologies. The results show that CO₂ emissions associated with the absorber layers, are much less than the CO₂ emissions associated with contact and charge selective layers. CdS (charge selective layer) and ITO (contact layer) have the highest environmental impacts compared to Al₂O₃, CuI, CuSCN, MoO₃, NiO, P3HT, PCBM, PEDOT:PSS, SnO₂, Spiro-OMeTAD, and TiO₂ (charge selective layers) and Al, Ag, FTO, Mo, ZnO:In, and ZnO/ZnO:Al (contact layers). The cost assessments show that the organic materials such as polymer absorber, CNT, P3HT and Spiro-OMeTAD are the most expensive materials. Inorganic materials would be more preferable to lower the cost in solar cells. All the remaining materials have a potential to be used in commercial PV market. Finally, the eco-efficiency analysis showed that absorbers made from polymer, and CNT, charge selective layers made from Spiro-OMeTAD, PCBM and CdS and contact layers made from ITO, ZnO:In, and ZnO:ZnO:Al materials should be excluded from emerging PV market to lower the cost and environmental impacts from solar cells.

With hopes of a sustainable future...

Acknowledgements

I would like to express my deepest gratitude to my advisor Dr. Defne Apul for her guidance, encouragement and constructive feedbacks through my Ph.D. studies. I was lucky to have an advisor who truly wants her students to be successful and helps them every step of the way! I am also thankful to my dissertation committee members, Dr. Heben, Dr. Ellingson, Dr. Gruden, Dr. Schall and Dr. Kumar not only for enriching scientific discussion and efforts in evaluating my dissertation but also their supports and advices to me in my academic job applications.

I am greatly indebted to Dr. Yan, Dr. Song, Dr. Cimaroli and Dr. Phillips from Ohio's Wright Center for Photovoltaic Innovation and Commercialization. Without their technical support and guidance, I would never be able to realize this work. Special thanks to Miss. Ann Dougherty and Mr. Thierry Fabozzi, who are my supervisors at Roppe Holding Company and Plastic Technologies Inc, respectively. I would like to thank my friends from Anthony Wayne Toastmaster Club Heather, Ping, Brandon, Mary and Nancy, my dear neighbours Roy, Joyce and Kathrine and my parents Saime and Metin, and brother Avsar Celik. Their generous support was so valuable. Finally, my dear husband Ramez, without your unconditional love, I would never finalize my graduate education.

This study was supported by the National Science Foundation's Sustainable Energy Pathway (SEP) Program (grant # 1230246).

Table of Contents

| | |
|--|------|
| Abstract..... | iii |
| Acknowledgements | vi |
| Table of Contents | vii |
| List of Tables | viii |
| List of Figures..... | ix |
| List of Abbreviations..... | x |
| 1 Background... .. | 1 |
| 1.1 Solar Photovoltaic..... | 1 |
| 1.2 Problem Statement..... | 3 |
| 1.3 Theory of LCA..... | 5 |
| 1.3.1 History of LCA..... | 5 |
| 1.3.2 LCA Framework..... | 8 |
| 1.3.3 LCA Software..... | 9 |
| 1.4 Strategy | 10 |
| 1.4.1 Overview of the dissertation | 10 |
| 2 Life Cycle Assessment (LCA) of perovskite PV cells projected from lab to fab . | 12 |
| 2.1 Introduction | 12 |

| | | |
|-------|---|----|
| 2.2 | Methodology..... | 15 |
| 2.2.1 | Goal and scope | 15 |
| 2.2.2 | Selection of the Perovskite PV Cell Device Architecture | 16 |
| 2.2.3 | Selection of the Manufacturing Processes | 20 |
| 2.2.4 | Life Cycle Inventory..... | 24 |
| 2.2.5 | Life cycle impact assessment | 27 |
| 2.3 | Results and Discussion..... | 28 |
| 2.3.1 | Impacts from Manufacturing of the Cells..... | 28 |
| 2.3.2 | Impacts from Generating 1 kWh of Electricity..... | 29 |
| 2.3.3 | Uncertainty and Sensitivity Analysis..... | 32 |
| 2.3.4 | Energy Requirements of Perovskite Cells | 36 |
| 2.3.5 | EPBT and GWP impacts..... | 37 |
| 2.3.6 | Hot spot analysis of Perovskite Solar Cells | 42 |
| 2.3.7 | Which steps in cell preparation use the most electricity? | 45 |
| 2.3.8 | Which materials in cell preparation contribute more to the impacts..... | 47 |
| 2.4 | Conclusions | 50 |
| 3 | Life cycle analysis of metals in emerging photovoltaic (PV) technologies..... | 52 |
| 3.1 | Introduction | 52 |
| 3.2 | Methodology..... | 56 |
| 3.2.1 | Life Cycle Based Modeling Approach | 56 |

| | | |
|-----|--|----|
| | 3.2.2 Estimation of metal leachate from PV..... | 59 |
| 3.3 | Results | 61 |
| | 3.3.1 Metal Loss Factor | 61 |
| | 3.3.2 Comparing Upstream and Downstream Toxicities | 64 |
| | 3.3.3 Application of metal toxicity results to emerging PV structures | 68 |
| | 3.3.4 Comparing the metal emissions from emerging solar PV to those from coal power plants | 72 |
| 3.4 | Conclusions | 74 |
| 4 | Eco-design of Emerging PV Materials | 75 |
| | 4.1 Introduction | 75 |
| | 4.2 Methodology..... | 78 |
| | 4.2.1 Life Cycle Inventories | 78 |
| | 4.2.2 Cost Assessment..... | 80 |
| | 4.3 Results | 81 |
| | 4.3.1 Life Cycle Carbon Emissions..... | 81 |
| | 4.3.2 Life Cycle Costing..... | 84 |
| | 4.3.3 Eco-Efficiency of the Material Selection..... | 86 |
| | 4.4 Conclusions | 87 |
| 5 | Conclusions..... | 88 |

| | | |
|-----|---|-----|
| 6 | Limitations and Recommendations to Future Works | 91 |
| | References..... | 93 |
| A.1 | Stoichiometric Reactions Assumed for Synthesis of Compounds | 107 |
| A.2 | Life Cycle Inventory of the Solution and Vacuum Based and HTL Free Models.. | 108 |
| A.3 | Comparison of Primary Energy Demand (PED) of Selected Metals | 114 |
| A.4 | Comparison of Electricity Consumption Mix of Different Regions and Countries | 118 |
| A.5 | EPBT Calculation | 120 |
| A.6 | Environmental Impacts of Materials Use..... | 120 |
| B.1 | Typical PV Structure..... | 122 |
| B.2 | Derivation of LF | 122 |
| B.3 | Estimation of LF | 124 |
| B.4 | Do results change in Usetox was used instead of ReCiPe | 126 |
| B.5 | Metal Releases from Coal-fired Power Plants..... | 129 |
| B.6 | Metal Releases from Mining the Metals Used in Emerging PV Technologies | 129 |
| C.1 | How to start using GaBi? | 132 |
| C.2 | How to data can extract from GaBi?..... | 132 |
| C.3 | How do I create PV LCA models? | 132 |
| C.4 | How do I create PV LCA models? | 133 |

List of Tables

| | | |
|-----|---|-----|
| 2-1 | Alternatives for device layers..... | 17 |
| 2-2 | Environmental impacts from generation of 1kWh of electricity..... | 31 |
| 2-3 | Comparison of the modeling assumptions in published studies..... | 40 |
| 3-1 | The estimated metal lost factor (LF) values..... | 57 |
| 3-2 | Precautionary metal lost limit (LL). | 62 |
| 3-3 | The comparison of metal emission rates between coal-fired power generations and emerging PV cells | 68 |
| 4-1 | Deposition methods used in layer processing. | 76 |
| 4-2 | The GWP of commercial PVs | 79 |
| A-1 | Synthesis of the compounds..... | 95 |
| A-2 | Routes for solution and vacuum based methods and HTL free structure models. | 96 |
| A-3 | Inventory for solution, vacuum based and HTL free Perovskite PV cell devices. | 96 |
| A-4 | Material comparison with a literature study..... | 103 |
| A-5 | Impacts of solution-based perovskite PV production (per m ²) | 104 |
| A-6 | Impacts of vacuum based perovskite PV production (per m ²). | 104 |
| A-7 | Impacts of HTL free perovskite PV production (per m ²). | 105 |

| | | |
|-----|---|-----|
| A-8 | Toxicity of materials used in Modeled PV Technologies..... | 108 |
| B-1 | Synth Physical parameters of metal compounds and the estimated metal LFs... | 112 |
| B-2 | R The variation of LF among the different scenarios. | 113 |
| B-3 | Physical parameters of metal compounds and the estimated metal LFs..... | 113 |
| B-4 | Downstream and upstream metal emissions of coal-fired power plants..... | 117 |
| B-5 | Grams of metals emitted per gram of metal mined. | 118 |
| B-6 | Upstream metal emissions from emerging PVs | 119 |

List of Figures

| | | |
|-----|---|----|
| 1-1 | Types of main solar PV technologies. | 4 |
| 1-2 | Contribution of LCA method to Eco-design | 5 |
| 1-3 | A representation of the generic life cycle of a product..... | 7 |
| 1-4 | The LCA Framework..... | 9 |
| 1-5 | The classification of the studies performed in this dissertation | 12 |
| 2-1 | Device architecture (a) and deposition techniques (b) of Perovskite devices..... | 21 |
| 2-2 | Possible routes for deposition of perovskites. | 24 |
| 2-3 | Comparison of perovskite devices with commercial PV technologies..... | 28 |
| 2-4 | Sensitivity of total environmental impacts to lifetime..... | 32 |
| 2-5 | Probability of perovskite cells having lower total impacts | 35 |
| 2-6 | Comparison of GWP and EPBT data from this study with prior studies | 40 |
| 2-7 | Comparison of environmental impacts among the alternatives | 44 |
| 2-8 | Breakdown of direct process energy requirements in each layer | 46 |
| 2-9 | Comparison of material impacts..... | 47 |
| 3-1 | The modelling framework for the three analyses | 53 |
| 3-2 | Downstream/Upstream toxicities (D/U) of the metals..... | 61 |
| 3-3 | The structures of selected emerging PV technologies | 64 |
| 3-4 | Normalized metal toxicity scores from different layers in emerging PV cells | 66 |
| 4-1 | Emerging PV types (a) and the cell structure of PV cells (b). | 72 |

| | | |
|-----|---|-----|
| 4-2 | The GWP breakdown of emerging materials..... | 78 |
| 4-3 | Material cost of the different layers used..... | 81 |
| 4-4 | The cost of CO ₂ emissions from different PV layers..... | 83 |
| A-1 | Comparison of primary energy consumption of selected metals | 103 |
| A-2 | Normalized impact comparison of unit production-mixture..... | 106 |
| A-3 | Comparison of Perovskite devices with commercial PV technologies | 107 |
| B-1 | Typical PV structure and possible representations of a damage on glass layer .. | 110 |
| B-2 | Downstream (D) and upstream (U) toxicity from metals | 115 |
| B-3 | Toxicity impacts of the metals used in different studies | 116 |

List of Abbreviations

| | |
|--------------------------------------|--|
| Al ₂ O ₃ | Aluminum (III) Oxide |
| CdS..... | Cadmium Sulfide |
| CdTe..... | Cadmium Telluride |
| CIGS..... | Copper indium gallium selenide |
| CZTS..... | Copper zinc tin sulfide |
| CNT..... | Carbon nanotube |
| CTU..... | Comparative toxicity unit |
| CZTS..... | Copper zinc tin sulfide |
| FTO..... | Fluorine doped tin oxide |
| ITO..... | Indium doped tin oxide |
| MoO ₃ | Molybdenum trioxide |
| P3HT..... | Poly(3-hexylthiophene) |
| PbI ₂ | Lead(II) Iodine |
| PbS QD..... | Lead sulfide quantum dot |
| PEDOT:PSS..... | Poly(3,4-ethylenedioxythiophene) polystyrene sulfonate |
| PCBM..... | [6,6]-phenyl C61 butyric acid methyl ester |
| PSC..... | Perovskite Solar Cell |
| Spiro-OMeTAD.. | 2,2',7,7'-Tetrakis[N,N-di(4-methoxyphenyl)amino]-9,9'spirobifluorene |
| ZnO:In..... | Indium doped zinc oxide |
| ZnO/ZnO:Al..... | Aluminum doped zinc oxide |

Chapter 1

Background

1.1. Solar Photovoltaic

Increasing interest in atmospheric carbon reduction and a fast-growing demand for renewable energy promise a great future for large-scale use of solar cells. While photovoltaics (PV) currently contribute to less than 1 % of the global electricity generation, this small contribution is expected to grow remarkably reaching 18 % in the US and 16 % globally by 2050 (IEA, 2013; IEA, 2014).

Solar PV technologies are typically named per the primary light-absorbing material of PV cells. As shown in Figure 1-1, PV technologies can be classified using two categories: wafer-based and thin-film cells. Wafer-based cells are fabricated on semiconducting wafers and can be made without an additional substrate, although modules are typically covered with glass for mechanical stability and protection. Thin-film cells consist of semiconducting films deposited onto a glass, plastic, or metal substrate. Compared to wafer based (crystalline mono and poly Si) solar cells, commercial thin films (e.g. a-Si, CdTe and Cu(In,Ga)(Se,S)_2) have lower conversion efficiency but their lower manufacturing and material costs have made them quite competitive in recent years.

The past decade has already witnessed the rapid growth of the global PV market, and total global capacity was close to 250 gigawatts (GW) in 2016 mainly due to the substantial reduction in the manufacturing costs of market-dominant crystalline Si solar cells. Between 2010 and 2016 the total installed cost of utility-scale PV systems fell by 29 - 65%. Although the current cost of PV electricity continues to decline based on technological advances in conventional crystalline silicon and thin film modules, it is still higher compared to other sources (fossil fuel, nuclear, coal etc). The manufacturing cost of solar PV energy will be further reduced if emerging PV technologies being developed in laboratories can be commercialized.

Perovskite solar cells (PSC), carbon nanotube solar cells (CNTs), quantum dots solar cells (QDSC), $\text{Cu}_2\text{ZnSnS}_4$ (CZTS) and polymer PVs are key alternative technologies that emerged because of intense R&D efforts in materials discovery and device engineering to achieve low cost manufacturing. These emerging thin-film technologies employ nano-structured materials that can be engineered to attain desired optical and electronic properties. Although these technologies are early in R&D stage, reliance on earth-abundant materials and relatively simple processing methods compared to established PV technologies offer potentially large-scale manufacturing and deployment. In the long term, emerging thin-film technologies may overcome many of the limitations of today's deployed technologies at low cost, assuming improvements in efficiency and stability are realized. Yet, if these cells were to enter the commercial market and ultimately play an important role in supplying electricity globally, it will be important to understand their environmental impacts.

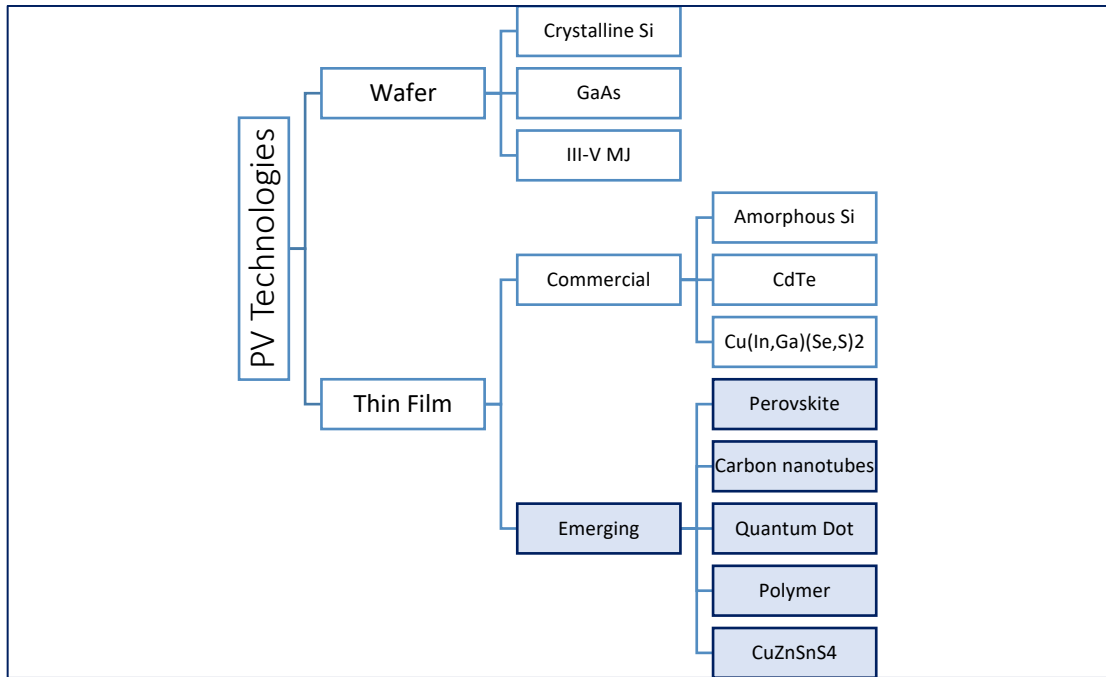


Figure 1-1 Types of main solar PV technologies. In contrast to wafer and commercial thin films, emerging PV cells (boxes shaded with blue) have not been used in any industrial applications to date. These cells were investigated in this dissertation.

1.2. Problem Statement

Life cycle assessment (LCA) has been widely used in understanding the environmental impact of emerging PV technologies in case these PVs scale-up from lab to industrial fabrication (fab). However, most of the prior LCA studies on these solar cells have been modeled to reflect the environmental performance of the lab scale devices. Lab scale devices are often made with expensive materials (e.g. gold, silver, Spiro-MeOTAD, PCBM, PEDOT:PSS) and are manufactured via methods that could be applied only in

laboratories (e.g., spin coating, dip coating). These lab-based devices hardly match the expected large-scale manufacturing conditions that will be based on low-cost production and scalability parameters. Therefore, the results from these LCA models have limited use in understanding the environmental performance of ultimate PV cells that may enter the commercial market in the future.

Also, most of the PV LCA studies neglect the impact from the use phase of the devices when calculating the life cycle environmental footprint. Use phase has typically not been considered due to the expectation that PV materials are water-insoluble inorganic compounds and that modules are deployed in robust, hermetically sealed packaging that would preclude emissions during the use phase (Fthenakis, 2009; Raugei and Fthenakis, 2010). However, recent studies experimentally demonstrated that the environmental performance of several emerging PV technologies based on perovskite or polymer materials could be affected by serious toxic emissions due to physical damage of modules during the use phase (Espinosa et al., 2016; Hailegnaw et al., 2015; Zimmermann et al., 2012a).

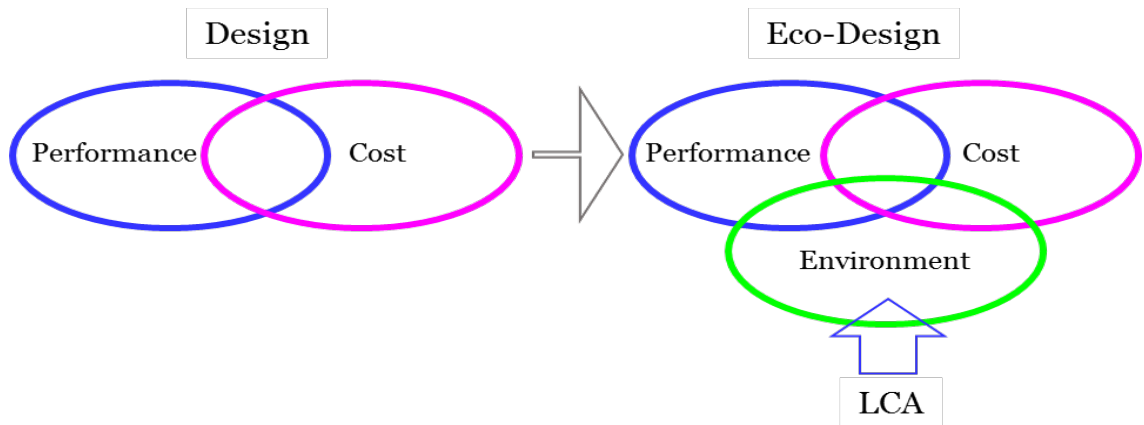


Figure 1-2 Contribution of LCA method to Eco-design

The scope of my dissertation is to increase the resolution of the environmental footprint of the emerging PV's by conducting LCA studies that have three perspectives namely cost, scalability and end-use toxicity. Consequently, this research may affect the emerging PV design transformation into eco-design which is supported by life cycle assessment methodology (Figure 1-2). This research assesses various possible designs of emerging PVs and identifies those life cycle phases, materials and manufacturing techniques that can be improved or replaced to increase environmental performance of the devices. Finally, it offers an eco-design tool for the future emerging PV cells that can reduce the environmental impacts of today's PVs.

1.3. Theory of LCA

1.3.1. History of LCA

Studying of environmental impacts of products and processes have a history that dates back to 1960s. Manufacturing facilities and their emissions raised environmental concerns and

start to take public interest. In the beginning, all the efforts were put in controlling the facilities and their emission when they operate. In 1990s, the scope of the interest was enlarged to consider the entire life cycle of products and the product life cycle scheme was developed (Figure 1-3).

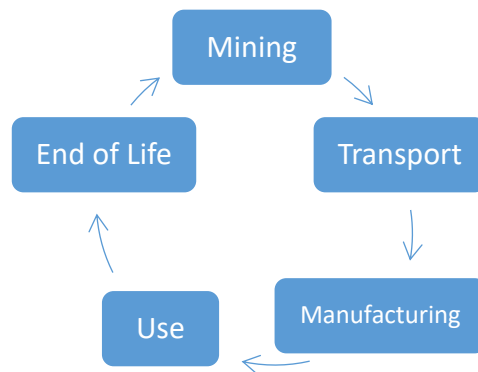


Figure 1-3 A representation of the generic life cycle of a product

There are five components of a product life cycle: (1) material mining/extraction, (2) transportation, (3) Manufacturing (4) use and (5) end of life. In the end of life of a product, materials can be either recycled or sent to landfills. The environmental impact of materials, and electricity consumed, and wastes generated are evaluated for each stage of the entire life cycle. The LCA method was first used by Coca Cola in 1969 to compare the environmental impacts of alternative materials used in beverage containers (Journey Staff, 2012).

In 1990s, a remarkable growth of scientific activities took place. Society of Environmental Toxicology and Chemistry (SETAC) organized number of workshops, forums and engaged scientist to publish on LCA guidelines and handbooks. In 1994, the International Organization for Standardization (ISO) prepared the first guideline regarding the methods and procedure of LCA. Also, the first scientific manuscripts started to publish in the journals of Journal of Cleaner Production, Resources, Conservation and Recycling, International Journal of LCA.

LCA was first applied to the PV technologies to perform the health, safety (Owens et al., 1980), and energy flow assessments of silicon PV cells manufacturing (Hagedorn, G., and Hellriegel, 1992; Hagedorn, G., S. Lichtenberg and H. Kuhn, 1989). Over the intervening 25 years, numerous LCA studies have been performed on relatively mature PV technologies such as Si (Bailie et al., 2014; Hong et al., 2016; Phylipsen and Alsema, 1995; Wong et al., 2016), CdTe (Fthenakis, 2004; Fthenakis et al., 2005; Raugei et al., 2007; Sinha, 2013), amorphous-Si (Engelenburg and Alsema, 1993), and $\text{CuGa}_{1-x}\text{In}_x\text{Se}_2$ (Collier et al., 2014; Raugei et al., 2007; Zimmermann et al., 2014). These LCA studies have quantified the energy flows, material flows, and emissions from manufacturing, and raw material purification (Fthenakis et al., 2011, 2008; V. M. Fthenakis and Kim, 2011). Recycling of PV cells and the impacts of manufacturing waste have also been assessed (Fthenakis, 2000; Goe and Gaustad, 2014; Latunussa et al., 2016; Zimmermann et al., 2014). Energy related metrics such as energy payback time, energy return on investment, and CO_2 equivalent avoidance has been discussed as well (Alsema, 2006; Bhandari et al., 2015; Raugei et al., 2007).

1.3.2. LCA Framework

ISO delineated the framework of LCA (Figure 1-4) which contains four steps: Goal and scope, inventory analysis, impact assessment and interpretation. In the first step, the possible questions to be answered (goals) and the encompassed product life cycle (scope) are defined. In this step, the impact assessment tool, the impact categories to be considered, the functional unit of the study, system boundaries, and the life time of the product are

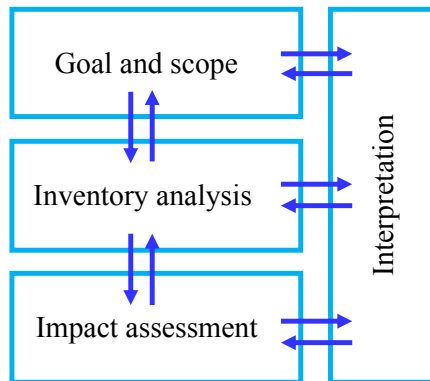


Figure 1-4 The LCA framework

also determined. In the second step, the quantitative data such as the energy and material inventories used throughout the scope of the work are prepared. The third step is the impact assessment and involves relating extraction and emissions of the system to environmental impact. In this step, environmental influences of the inventories are characterized. Usually, a software is used in this step. In the background of the software, the following formula is used:

$$S_j = CF_{i,j} \times E_i$$

where E_i is the mass flow identified for species i in the inventory assessment, $CF_{i,j}$ is the characterization factor for species i and category j , and S_j is the category impact indicator for category j .

The interpretation of results is where the findings from one or more of the three steps are analyzed to reach the conclusions and making recommendations.

1.3.3. LCA software

There are number of research organization as and private companies that have developed software to facilitate life cycle assessment. Among many of LCA software packages, there are two alternatives that are used by the scientific community: GaBi and SimaPro. These software packages allow users select the inventories used in the product under study and enter their quantities into an available database available. The software, taking the advantage of internal databases relates materials to impacts of various types of categories. The software packages also have normalization and weighting parameters to convert different impact categories into a single score. In this dissertation, GaBi 8.0 software package and EcoInvent 3.2 database are used.

1.4. Strategy

1.4.1. Overview of the dissertation

Figure 1-3 shows the central aspects of the five emerging PVs that were analyzed. The solid lines depict the studies published in peer-reviewed journals. The first study covered PSC and the aspects including life cycle assessment, scalable manufacturing and market criteria. The first published study attained the goals shown in the green box (Celik et al., 2016a). The second study focuses on the end use toxicity of metals used in PSC, QDSC, Polymer and CZTS. This study has two significant goals including, comparing the metal related toxicities from upstream and downstream processes and showing the relative importance of PV deployment locations on the toxicological profile of PVs. The third study covers all the cost and LCA approaches and aims to assess all the emerging PVs in-depth. The yellow dashed lines in the figure indicates that the manuscript regarding this study has not published yet.

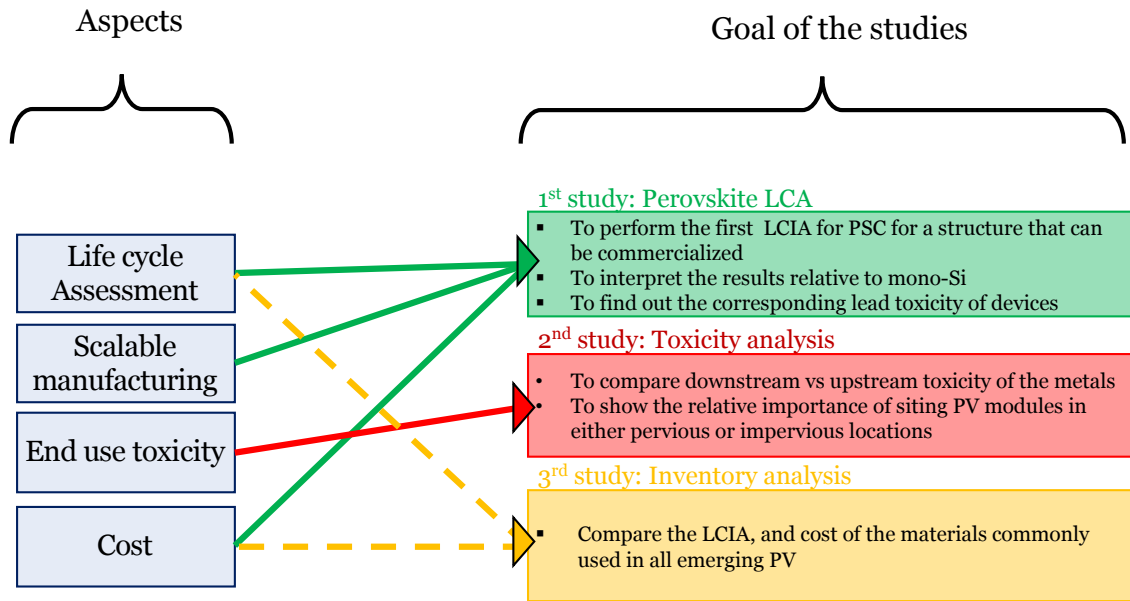


Figure 1-5 The classification of the studies performed in this dissertation. The goals given in green, red, and yellow boxes correspond to each research question 1, 2 and 3 given in Section 4, respectively.

Chapter 2

Life Cycle Assessment (LCA) of perovskite PV cells projected from lab to fab

2.1. Introduction

Increasing interest in atmospheric carbon reduction and a fast-growing demand for renewable energy promise a great future for large-scale use of solar cells. While photovoltaics (PV) currently contribute ~1 % of the global electricity generation, this percentage is expected to grow remarkably reaching 18 % in the US and 16 % globally by 2050 (IEA, 2013; IRENA, 2016). The past decade has already witnessed the rapid growth of the global PV market, and total global capacity was close to 180 gigawatts (GW) in 2014 mainly due to the substantial reduction in the manufacturing costs of market-dominant crystalline Si solar cells. Between 2010 and 2014 the total installed cost of utility-scale PV systems fell by 29 - 65% (Taylor et al., 2015a). While the levelized cost of electricity (LCOE) can vary greatly as a function of discount rate, conversion efficiency, system degradation, solar insolation, and operation and maintenance conditions (Darling et al., 2011), most of the utility scale projects in 2014 delivered electricity at a reasonable LCOE of \$ 8 ¢/kWh in 2014 (Taylor et al., 2015a). Compared to first generation wafer based

(crystalline mono and poly Si) solar cells, second generation thin-film solar cells (e.g. CdTe and Cu(In,Ga)(Se,S)₂) have lower conversion efficiency but their lower manufacturing and material costs have made them quite competitive in recent years, reaching a current global market share of ~10% in 2015, which was double their share in 2007 (Taylor et al., 2015). The manufacturing cost of solar PV energy will be further reduced if promising alternatives being developed in laboratories can be commercialized.

One emerging promising PV technology is based on methylammonium lead halide perovskites. These organic-inorganic hybrid materials have progressed rapidly over the past few years and become one of the most attractive areas for PV research (Song et al., 2016). A large number of studies emerged with a variety of different material preparation methods and diverse device architectures. To date, the best performing perovskite device has achieved 21% efficiency (NREL, 2017), which is competitive with the established PV technologies. This fast learning curve for perovskites is extraordinary considering more than three decades were required to achieve similar efficiency advances with either Si, CdTe, or Cu(In,Ga)(Se,S)₂.

Perovskites, named after the Russian mineralogist Lev Perovski, are materials that have the same crystal structure as calcium titanium oxide (CaTiO₃). In the field of PV research, the term perovskites mainly refer to a class of organic-inorganic hybrid methylammonium lead halide (CH₃NH₃PbX₃, where X= I, Br, or Cl). These perovskites have a tunable direct bandgap ranging from 1.5 to 2.2 eV (Noh et al., 2013) that covers the whole visible solar spectrum and high optical absorption.

High-efficiency devices can be fabricated with very thin layers, which promises reduced materials costs. For example, ~300 nm is needed to form a high efficiency perovskite cell, while Si and thin film (e.g. CdTe or Cu(In,Ga)(Se,S)₂) absorber layers are typically ~300 μm and ~2 μm thick, respectively (Yin et al., 2015). These characteristics along with other important properties such as ultrafast charge generation (Jr et al., 2014), high carrier mobilities for both electrons and holes (Stoumpos et al., 2013), and relatively long carrier lifetimes (Stranks et al., 2013) lead to excellent performance in PV devices. Furthermore, perovskites exhibit a large degree of tolerance in synthesis (Song et al., 2015) and may be easier to manufacture into high-efficiency devices than current silicon and thin film cells. Despite this promise, there remain significant technical challenges that must be overcome before perovskites can be fabricated in modules at a large scale. For example, perovskite solar cells display hysteresis in their current-voltage characteristics (Snaith et al., 2015), and more importantly their stability issues have not been resolved. Perovskite solar cells degrade due to oxygen, light, moisture, and high temperatures (Snaith et al., 2015).

Most of the prior work on perovskite solar cells have focused on their technical properties and performance. Yet, if perovskite cells were to enter the commercial market and ultimately play an important role in supplying electricity globally, it will be important to understand their environmental impacts as well. To date, four *ex-ante* life cycle assessment (LCA) studies have been conducted on perovskite PV cells to shed light on their potential environmental impacts (Espinosa et al., 2015; Gong et al., 2015a; Serrano-Lujan et al., 2015; Zhang et al., 2015). One of these studies focused on liquid perovskite solar cells. The other three focused on solid perovskite solar cells but modeled materials (e.g. gold, silver, Spiro-MeOTAD) and methods (e.g. spin coating) (Espinosa et al., 2015; Gong et

al., 2015; Serrano-Lujan et al., 2015; Zhang et al., 2015) that may be difficult to scale up from lab to commercial fabrication. In this paper, we evaluate the environmental impacts of perovskite PV technology at scale by modeling device architectures that we believe represent the expected low-cost production conditions. As described in the methods section, we went through a rigorous elimination process and determined and modeled the materials (FTO-coated glass, SnO₂, perovskite, CuSCN, and MoO_x/Al) and manufacturing methods (spray deposition and co-evaporation under vacuum) that we believe are more likely to be used during commercialization. In addition, seeing as the hole transport layer (HTL) was found to have significant environmental impacts (*vide infra*), a new promising HTL-free device was modeled. The global PV market share is currently dominated by mono-Si (36 %) and poly-Si (56 %) (ISE, 2016) . Mono-Si has higher environmental impact than other commercial PVs (poly-Si, a-Si, CdTe and CIGS) (Gong et al., 2015). To more clearly interpret the results, we present the results after normalizing the impacts to mono-Si. We discuss the relative importance of different PV components and electricity use in manufacturing the cells. A sensitivity and uncertainty analysis was also conducted.

2.2. Methodology

2.2.1. Goal and scope

The goal of this study was to evaluate the life cycle environmental impacts from perovskite solar cell designs that may be commercially fabricated. Life cycle assessment is a technique for assessing the environmental impacts of a product or service throughout its life cycle from raw material acquisition, to production, through use and disposal/recycling phases (ISO, 2006). Since perovskite cells are not currently commercially fabricated, we conducted an ‘ex-ante’ LCA study. We anticipated and modeled the most scalable methods

and materials for a commercial PV market. Evaluation of ex-ante LCA results can identify potential opportunities for improvement, inform research directions and guide the sustainable design of perovskite solar cells.

The system boundary of the study was cradle to gate. Since the perovskite technology is still far from scalable manufacturing, the operation and end of life phases include much greater uncertainty than the production phase and were not included in the LCA model for this reason.

LCA guidelines suggest that the environmental profiles be interpreted based on the function of the product (ISO, 2006). The function of PV modules is to generate electricity and our selected functional unit was 1 kWh of electricity generated for the entire life time of the PV. All results were presented for this functional unit. In addition, following the approach of recent PV LCA studies we present the impacts from manufacturing 1m² of module (Darling and You, 2013; Gong et al., 2015; Zhang et al., 2015).

2.2.2. Selection of the Perovskite PV Cell Device Architecture

The conventional structure of perovskite PV cells typically consists of a fluorine-doped tin oxide (FTO) coated glass substrate, a TiO₂ electron transport layer (ETL), a perovskite absorber, a Spiro-MeOTAD hole transport layer (HTL), and a gold back contact. Each layer of the device can be made from these or other alternative materials (Table 1). The performance of perovskite solar cells is mainly determined by the quality of the perovskite

absorber. Changing other layers in the perovskite solar cell into alternative materials with similar functionality does not significantly affect the physics of the device, and consequently, results in similar device performance (Song et al., 2016). In this study, we selected the materials that are most likely to be used in low-cost commercial scale fabrication.

The first layer, also known as the top contact layer, is commercially available TCO coated glass; coated either with fluorine doped tin oxide (FTO) or indium tin oxide (ITO). We modeled FTO because it is lower in cost and is already used more frequently in the solar industry for this reason (Michael, 2012). Moreover, realizing the challenges with the global availability of indium, U.S. Department of Energy's Solar Energy Technologies Program aims to reduce the amount of indium used in thin film technology; indium has been designated a 'critical metal' with high supply risk and high importance for the clean energy industry (Bauer et al., 2011).

For the electron transport layer, of the four available materials, SnO₂ was selected as offering the most promise for commercial production due to the low-temperature process used for deposition and energy band match with the perovskite. TiO₂ has been commonly used in perovskite solar cells, however, it typically requires temperatures as high as 450 °C to 500 °C which may be incompatible with low-cost solar technology (Sum and Mathews, 2014). Similarly, Al₂O₃ and ZnO were found to be not suitable for low cost production due to the highly energy intensive methods that are used for their manufacturing (Chen et al.,

2014). Among all the alternative materials, SnO₂ provides a low-temperature and solution-processable approach for high efficiency (>18%) perovskite device, which is compatible with roll-to-roll manufacturing of low-cost perovskite solar cells (Ke et al., 2015).

Table 2-1 Alternatives for device layers. The materials selected and modeled in this study are in bold. In the structure without the HTL, CuSCN was not used and MoO_x/Al was replaced with C-Paste.

| Layer | Function | Alternative Chemicals |
|--------------------------|--------------------|--|
| Top Contact Layer | Collects electrons | FTO ITO |
| Electron Transport Layer | Conducts electrons | TiO ₂ ZnO Al ₂ O ₃ SnO₂ |
| Absorber Layer | Harvests light | CH ₃ NH ₃ PbI _x Br _{3-x} CH ₃ NH ₃ PbI _x Cl _{3-x} CH₃NH₃PbI₃ |
| Hole Transfer Layer | Conducts holes | Spiro-MeOTAD P3HT PTAA CuSCN CuI NiO |
| Back Contact Layer | Collects holes | Au MoO_x/Al Ag C-Paste |

For the absorber layer, we considered that compositional engineering of CH₃NH₃PbI₃ is made possible by incorporating/substituting other species such as chlorine, bromine, and formamidinium (FA) to achieve improved device performance and stability (Jeon et al.,

2015; Lee et al., 2012; Noh et al., 2013). However, since the amounts of additive chemicals can vary from lab to lab and the necessity of such compositional modification is yet to be proven, we chose pure $\text{CH}_3\text{NH}_3\text{PbI}_3$ for our study. Note that devices based on pure $\text{CH}_3\text{NH}_3\text{PbI}_3$ alone have shown efficiencies of 19.7%, which is very close to the current record value. To provide scalable manufacturing by an easy processing method, pure $\text{CH}_3\text{NH}_3\text{PbI}_3$ was selected in our study.

In the HTL, dozens of organic small molecules, conducting polymers, organometallics, and inorganic compounds have been used in perovskite solar cells. Among them, the most commonly used organic HTL materials include 2,2',7,7'-tetrakis (*N,N*-di-*p*-methoxyphenylamine) 9,9'-spirobifluorene (Spiro-MeOTAD) (Burschka et al., 2015; Zhou et al., 2014), poly(3-hexylthiophene-2,5-diyl) (P3HT), (Conings et al., 2014; Guo et al., 2015) and poly(bis(4-phenyl) (2,4,6-trimethylphenyl)amine) (PTAA), (Heo et al., 2013; Jeon et al., 2015). However, these materials are very expensive (Lizin et al., 2013) and their instability may represent a potential hurdle to the commercialization of this type of solar cell (Christians et al., 2013). To solve this problem, alternative inorganic HTLs, including CuI, CuSCN (Qin et al., 2014; Ye et al., 2015), and NiO (Park, 2015; Xu et al., 2015) have been developed. Use of inorganic HTL material can lead to high performance perovskite devices with high hole mobility, better stability, ease of synthesis, and thus low production cost (Docampo et al., 2013; Jung and Park, 2015). For our study, we selected CuSCN, a copper-based semiconductor, which shows the highest energy conversion efficiency (15.6%) so far for an inorganic HTL (Ye et al., 2015).

To complete the PV device, a patterned metal contact is deposited. Gold, silver, and aluminium are among the common materials reported in the literature (Collier et al., 2014; Green et al., 2014). Among them, gold and silver anode contacts provide better device performance due to the higher work function and better energy band alignment. However, both of these metals are relatively expensive and are not suitable for mass production. Aluminium is commonly used as a cathode electrode due to a low work function, but it can be used as an anode electrode with a MoO_x interface layer to achieve a 11.4% efficiency (Zhao et al., 2014). Thus, we propose to use less expensive MoO_x/Al as the back contact for the solution- and vacuum-based perovskite cells in this study.

Besides the standard device architecture, an HTL-free structure that was developed in a recent study has also attracted much attention. The device without a HTL shows a potential to reduce material costs and process complexity by using low-cost solution-processed carbon-paste back contact. The HTL-free perovskite cells have recently demonstrated a reliable stability during a 3-month outdoor test in Saudi Arabia, showing a potential to realize perovskite PV cells (Li et al., 2015). To compare it with standard devices, we also modeled the environmental impacts for the HTL-free device with the carbon electrode.

2.2.3. Selection of the Manufacturing Processes for the Perovskite Cell

We sought to optimize not only the materials but also the manufacturing processes. The ultimate device architecture and deposition methods that we expect to see in industrial scale production are shown in Figure 2-1. For the solution-based method we followed steps 1, 2,

3a, 4 and 5b shown in Figure 2-1. For the vacuum-based method we followed steps 1, 2, 3b, 4, 5b (for the device with HTL) and steps 1, 2, 3a, 5a (for the HTL-free structure).

Steps 1 and 2 are common for all three of the devices we modeled. In step 1, the FTO coated glass substrates (Pilkington, TEC 8 or TEC 15) are sequentially cleaned with acetone and isopropanol in an ultrasonic bath for 10 min each (García-Valverde et al., 2010). Then, in step 2, a 60 nm compact layer of tin dioxide (SnO_2) is deposited on FTO by spraying a 0.1 M $\text{SnCl}_2 \cdot \text{H}_2\text{O}$ in ethanol and annealing it at 180 °C for 1 h. In Step 3, the $\text{CH}_3\text{NH}_3\text{PbI}_3$ perovskite can be deposited as the absorber layer using several possible methods that can be classified as either solution or vapor based (Figure 2-2) (Jung and Park, 2015). Solution-based processes for depositing $\text{CH}_3\text{NH}_3\text{PbI}_3$ include spin-coating, spraying, dip coating, and printing (Hwang et al., 2015). Among these deposition techniques, spin coating is the most widely used for fabricating uniform thin films with nanoscale thickness for small-sized PV devices. However, most of the solution is spun off the substrate during the processing, leading to a material loss around 90 % (Espinosa et al., 2015). Thus, spin coating may not be a feasible option for large-scale commercial fabrication of thin film PV devices. Sequential deposition method consisting of a PbI_2 thin film deposition followed by dipping the film into a $\text{CH}_3\text{NH}_3\text{I}$ solution can be used to achieve high-performance perovskite devices in the laboratory. Although this dipping technique is partially employed in the fabrication of other thin film solar modules (Romeo et al., 2004), the extra step to deposit PbI_2 thin films would add complexity and lower fabrication efficiency. Thus, the dip coating technique is not considered optimal for commercialization. Consequently, we concluded that spray and inkjet coating would be the

most feasible deposition methods for the commercialization of perovskite solar cells. These two techniques are known to promise low-cost production of solar PV by reducing material usage and energy input in the thin film deposition process, and are similar in that, both employ piezoelectric nozzles to generate micron-sized liquid droplets to deposit precursor solutions. Here, spray deposition was chosen to represent the solution-based deposition approach because it is used for device fabrication in University of Toledo's PV labs.

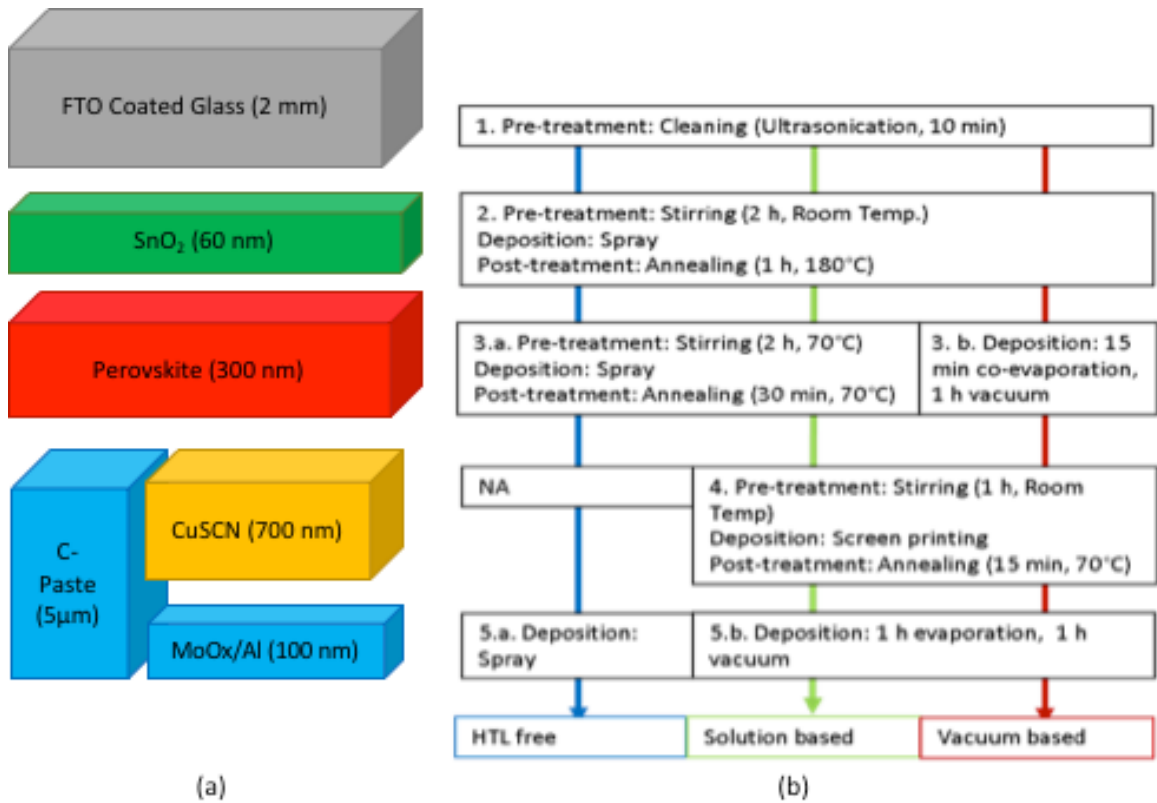


Figure 2-1 Device architecture (a) and deposition techniques (b) of Perovskite devices expected to be commercialized.

Vapor based deposition can be achieved by vacuum (Liu et al., 2013) and non-vacuum (Chen et al., 2014) methods. As for the perovskite deposition, co-evaporation of $\text{CH}_3\text{NH}_3\text{PbI}_3$ and PbI_2 offers better control of the thickness, uniformity, and the grain structure of the perovskite layer (Jung and Park, 2015) than non-vacuum, and therefore, has potential to be commercialized in the future (Bishop, 2011). Also, in contrast to non-vacuum methods that combines vacuum and solution-based methods, it can be applied one step. Therefore, for practical consideration for mass production, one step vacuum method was chosen.

We assumed that the commercial scale perovskite cell fabrication would include a 300 nm perovskite absorber prepared by either the solution-based spray deposition or the vapor based vacuum deposition method. In the solution-based deposition shown as Step 3a in Figure 2-1, the precursor solution consisting of 0.1 M PbI_2 (Sigma-Aldrich, 99 %) and 0.3 M $\text{CH}_3\text{NH}_3\text{I}$ (synthesized in house) are dissolved in N, N dimethylformamide (Sigma-Aldrich, 99.8 %) (DMF) and spray-deposited at 70 °C for 30 min followed by drying at 100 °C for 1h. In the vacuum-based deposition shown as Step 3b in Figure 2-1, PbI_2 and $\text{CH}_3\text{NH}_3\text{I}$ are co-evaporated in a vacuum chamber ($< 10^{-6}$ Torr base pressure, $< 10^{-4}$ Torr deposition pressure) for around 30 min. During the deposition, the source temperatures for PbI_2 and $\text{CH}_3\text{NH}_3\text{I}$ are fixed at 270 and 100 °C, respectively.

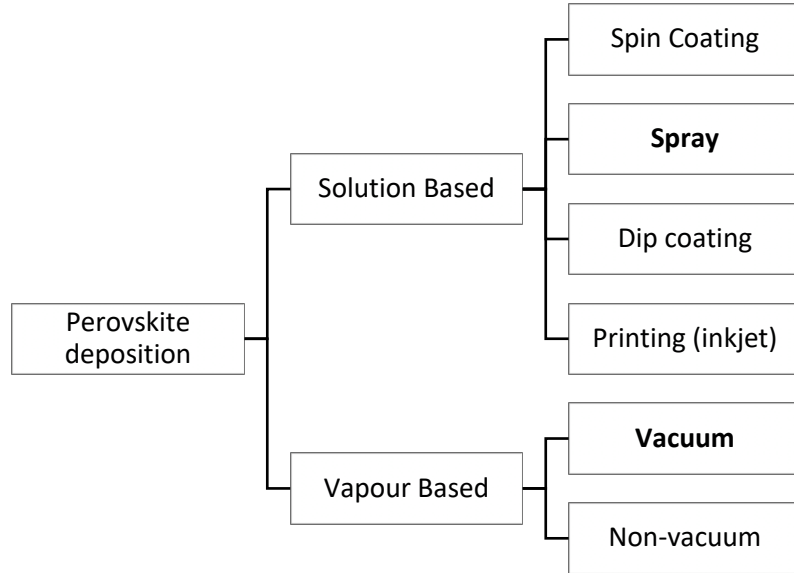


Figure 2-2 Possible routes for deposition of perovskites. The techniques used in this study are shown in bold.

In step 4, a 700 nm HTL is deposited by printing the precursor solution of 0.1 M CuSCN (Sigma-Aldrich, 99.5%) in chlorobenzene (Sigma-Aldrich, 99.8%)(Qin et al., 2014). For the HTL-free device, no process is needed for this step. Finally, in step 5a, a 100 nm metal back contact (MoO_x/Al) is deposited by evaporating at around 700 °C. The back contact for the HTL-free structure was deposited from a solution of commercial graphite paste in isopropanol by spray or printing (step 5b in Figure 2-1).

2.2.4. Life Cycle Inventory

At the University of Toledo, the Photovoltaic Innovation and Commercialization (PVIC) center produces perovskite and other thin film cells in research labs. Life cycle inventory data were collected from the PVIC lab for manufacturing of 2 inch X 2 inch lab scale cells.

We assumed 65 % of the area to be active, which is the average of previously reported values (Gong et al. used 70 % and Zhang et al used 60 %). We also collected inventory data from the literature and from the Ecoinvent database. All modeling was done using GaBi 6.0 software.

Electricity consumption values were taken from the literature, and necessary assumptions were made in order to scale-up lab data to an industrial fabrication (García-Valverde et al., 2010) (García-Valverde et al., 2010; Kushnir and Sandén, 2008). Intermediate products that are not included in the EcoInvent database were synthesized within the model assuming 100 % reaction efficiency (i.e. all inputs would react completely to form the desired product) (Table A.3). Electricity consumption for these chemical syntheses were not done on a reaction specific basis; average values were taken from the study of García et al. which incorporates a methodology from Geisler (García-Valverde et al., 2010; Geisler et al., 2004). We note that the eventual contribution of electricity consumption during chemical syntheses was less than 0.1% to the total electricity consumption in this study.

Vacuum apparatus (e.g. control systems and vacuum pumps) used for the perovskite absorber and the metal back contact would likely run nonstop in a manufacturing facility. In absence of other data, we assumed these apparatuses to run only during the deposition. While some of the material is wasted during deposition, deposition efficiencies are not well documented in the literature. For vacuum efficiencies a range of 30 to 50 % have been recommended (Bishop, 2011; Espinosa et al., 2015). We used the upper value (50 %) of

this range in our analysis assuming the manufacturers will prefer more efficient processes that reduce total waste and cost. For solution deposition a higher efficiency of 80 % (Liu et al., 2013) was used.

Emissions and waste streams associated with deposition were modeled as being released to different mediums during the production stage. Volatile organic compounds and waste from thermal annealing and vacuum deposition were assumed to be emitted to air. Lead emissions used for the perovskite layer were assumed to be emitted to fresh water. Other solid wastes in the solution-based methods were assumed to be released to industrial soil. All the energy input was modeled by waste heat output.

To compare the environmental impacts from perovskite cells to those of commercial technologies, we also modeled the first (mono-Si, Poly-Si) and second (amorphous-Si(a-Si), CdTe and CIS) generation solar cells. There is some variation in published energy and greenhouse gas emission metrics for these commercially fabricated solar cells (Yue et al., 2014) (Bishop, 2011) and part of this variation stems from the variability in the location the solar cells are manufactured (Yue et al., 2014) . To be consistent, we extracted all data for the commercial technologies from the Ecoinvent database. To further help with interpretation, we show the effect of the electricity mix in the appendix (See Appendix, Figures A2 and A3).

2.2.5. Life cycle impact assessment

Nine midpoint environmental impact categories were modeled using TRACI impact assessment model: acidification (kg SO₂ equiv.), ecotoxicity (CTU,e), eutrophication (kg N equiv.), global warming potential (GWP) (kg CO₂ equiv.), human toxicity (CTU,h), cancer and non-cancer, and primary energy demand (PED) (MJ). TRACI is the most commonly used impact assessment method in the U.S. while some other impact assessment methods like ReCiPe, EcoIndicator and ILCD are more commonly used in Europe. Our preliminary analysis using different impact assessment methods suggested some interesting findings with the marine eutrophication impact. Therefore, we also include results for this impact category, modeled using the ReCiPe method. Finally, using the approach in Bhandari et al. we also present the energy payback time (EPBT).

One important goal of perovskite deployment should be to reduce the total environmental impact from electricity generation. Yet, the meaning of the ‘total’ impact has been interpreted in different ways in PV LCA studies. Since the different types of environmental impacts are all calculated in different units, they are not directly additive or comparable to each other. Often, researchers use normalization methods embedded in existing life cycle impact assessment methods such as Ecoindicator 99, CML, and ReCiPe to compare across different impact categories or to add the different impact categories towards estimating a single ‘total’ impact score. In the U.S. the normalization is done using the US emissions and population data presented by Ryberg (Ryberg et al., 2014). The fundamental concept in all of these normalization approaches is to divide the impact from PV LCA (for each impact category) with the total impact for a region and with the population in that region

(e.g. for Europe, U.S. or global). The challenge with this approach is that the normalization factors are dependent on the region and different results and interpretations can be obtained depending on the normalization method. In addition, the absolute values resulting from normalization are not easy to interpret in this way. To overcome these challenges, in this paper, we use crystalline mono-Si as the reference point (Roes et al., 2009). Since crystalline mono-Si is the second most dominant PV technology in the market and has the largest environmental impacts compared to commercial PVs, it is important to understand the impacts of new technologies in reference to the technology it may displace. To facilitate this interpretation, we normalized each impact from the different technologies to the corresponding impact from mono-Si.

2.3. Results and Discussion

2.3.1. Impacts from Manufacturing of the Cells

The impacts from manufacturing of the cells are shown in Figure 2-3. Based on the Ecoinvent database, and as was also reported by Gong et al., mono-Si has the highest and a-Si has the lowest total manufacturing environmental impact among commercial technologies (Figure 2-3). For each environmental impact category, the impacts from manufacturing mono-Si are higher than those of other commercial technologies. Total impacts from the three perovskite solar devices were about 10 to 30 % lower than that of mono-Si but still higher than those of second generation technologies. The acidification impacts from perovskite cells were considerably higher than in mono-Si. Checking our life cycle inventory, we note that the reason for high acidification in our model is due to the

upstream emissions of sulfur compounds (sulphate, sulfur and sulphide) to freshwater during electricity production and tin extraction.

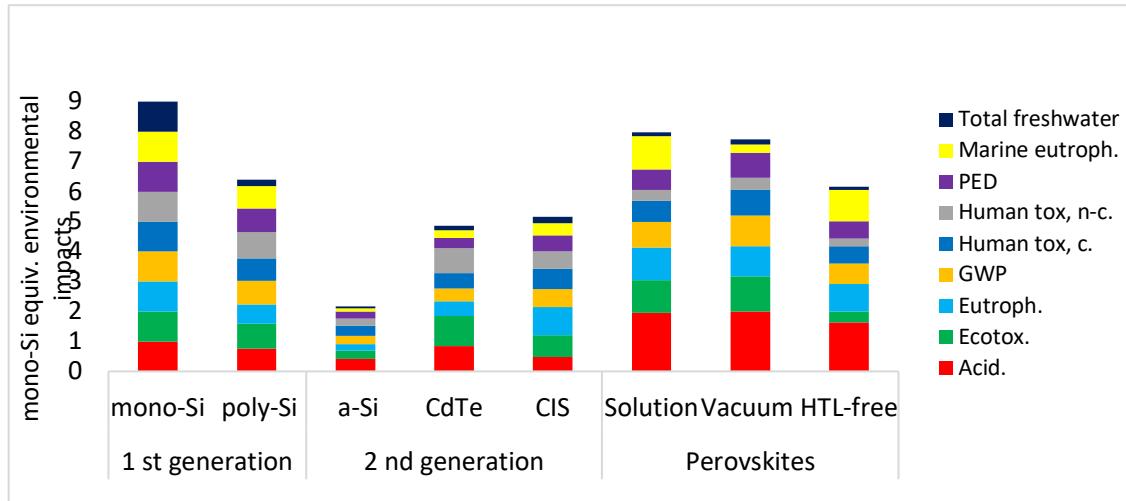


Figure 2-3 Comparison of perovskite devices with commercial PV technologies when normalized to mono-Si for selected impact categories. Note that GWP and PED stand for global warming potential and primary energy demand. Within each impact category, the impact (per m² of module manufactured) from each technology was divided by the impact from mono-Si. For mono-Si the bar height is unity for each impact category. For nine impact categories, the total impact for mono-Si is given as nine units. The data for mono-Si, poly-Si, a-Si, CdTe and CIS are directly extracted from EcoInvent database.

2.3.2. Impacts from Generating 1 kWh of Electricity

While the impacts per unit area given in Section 2.1 are helpful for direct comparison of manufacturing of the cells, the ultimate goal for solar PV sustainability is the reduction of

the total impact per unit electricity generated. To convert the impact results from manufacturing of the cells to impact results from unit electricity generated (i.e. the functional unit of the study), several other parameters are needed as shown in Equation 1;

$$Impact_{kWh} = \frac{Impact_{m^2}}{I \times \eta \times PR \times LT} \quad \text{Equation 1}$$

where,

I = insolation constant (kWh/m²-yr);

η = module efficiency (%);

PR = performance ratio of the module (%);

LT =lifetime of the PV technology (yr).

Impact_{m²}=Impact per 1m² module area

Impact_{kwh}=Impact per 1 kWh of electricity generated

Some of these parameters can be kept constant when comparing different technologies. For example, performance ratio and insolation are often kept constant at 75 % and 1700 kw/m²-yr, respectively; and module lifetime is often estimated as 30 years (Bhandari et al., 2015). For perovskite solar cells, module lifetime does not currently exist but values of 1, 2, 5, 15 and 30 years have been used in the literature (Espinosa et al., 2015; Gong et al., 2015; Zhang et al., 2015). For efficiencies, once again, there is some ambiguity and different perspectives in what value should be used. In evaluating perovskite LCA results, Gong et

al. made the comparison with Laleman's inventory, which was based on 2011 efficiency data. However, since 2011 the module efficiencies have increased from 14.0 to 22.9 % for mono-Si, 13.2 to 18.5 % for poly-Si, 6.5 to 10.9 % for a-Si, and 7.1 to 17.5 for CdTe and 10.7 % to 17.5% for CIGS (ISE, 2016). The latest best cell efficiencies reported by NREL are 25.0 % for mono-Si, 20.8 % for poly-Si, 13.6 % for a-Si, 21.5 % for CdTe and 21.7 % for CIGS (NREL, 2017). Darling and You reported that efficiencies may decrease 19.6 % to 49.6 % from cell to module (Darling and You, 2013). With the intent of comparing perovskite cells to other technologies in a future scenario, we used 15 % efficiency for our modeled perovskite cells which is 25 % lower than the champion perovskite cell efficiency (20.1%) (Noh et al., 2013). This efficiency value is in the higher part of the efficiencies (6.4 %, 6.5 %, 9.1 %, 11 %, 11.5 %, 15.4 %) used in prior perovskite PV LCA studies(Espinosa et al., 2015; Gong et al., 2015; Serrano-Lujan et al., 2015a; Zhang et al., 2015). We assumed a 30 year lifetime for all technologies except perovskite solar cells where an average value of 5 years was assumed. When perovskite lifetime is assumed to be much shorter than others, this has a large effect causing perovskite PV devices to have 5-8 times higher impacts than mono-Si (Table 2). The difference between perovskite and commercial technologies other than mono-Si is even more drastic suggesting perovskite is not environmentally competitive with a 5 year lifetime. While both the efficiency and lifetime affect the impacts per kWh, the short lifetime assumption is the primary reason for the very high environmental impacts from perovskite cells.

Table 2-2 Environmental impacts from generation of 1kWh of electricity.

| | mono-Si | poly-Si | a-Si | CdTe | CIS | Solution | Vacuum | HTL-free |
|---|---------|---------|---------|---------|---------|----------|---------|----------|
| Acidification [kg SO ₂ -equiv.] | 9.3E-05 | 8.0E-05 | 7.6E-05 | 9.5E-05 | 5.3E-05 | 1.4E-03 | 1.5E-03 | 1.2E-03 |
| Ecotoxicity [CTUe] | 1.8E-01 | 1.6E-01 | 9.3E-02 | 2.1E-01 | 1.6E-01 | 1.5E+00 | 1.6E+00 | 5.0E-01 |
| Eutrophication [kg N-equiv.] | 1.2E-04 | 8.7E-05 | 4.8E-05 | 6.7E-05 | 1.3E-04 | 1.0E-03 | 9.2E-04 | 8.4E-04 |
| GWP [kg CO ₂ -equiv.] | 2.3E-02 | 2.0E-02 | 1.2E-02 | 1.2E-02 | 1.7E-02 | 1.5E-01 | 1.8E-01 | 1.2E-01 |
| Human toxicity, [CTUh] | 1.7E-09 | 1.4E-09 | 1.1E-09 | 1.0E-09 | 1.3E-09 | 9.4E-09 | 1.1E-08 | 7.5E-09 |
| PED [MJ] | 1.1E-08 | 1.1E-08 | 4.9E-09 | 1.1E-08 | 8.0E-09 | 3.1E-08 | 3.7E-08 | 2.4E-08 |
| Marine Eutrop. [kg N-equiv.] | 4.6E-01 | 4.1E-01 | 2.1E-01 | 1.9E-01 | 2.9E-01 | 2.5E+00 | 3.0E+00 | 2.0E+00 |
| Total fresh- water use [kg] | 1.1E-05 | 8.1E-06 | 1.2E-06 | 2.8E-06 | 4.4E-06 | 9.3E-05 | 2.4E-05 | 8.9E-05 |

2.3.3. Uncertainty and Sensitivity Analysis

As shown in Section 3.2, deploying perovskite cells in the market at expected efficiency and relatively short lifetime would not reduce the environmental impacts of PV technologies. Therefore, we asked a relevant question for these two parameters. Figure 4a shows how the improvement in lifetime of perovskite PV cells can bring a fast reduction in their total environmental impacts. The environmental performance of HTL-free perovskite cells may supersede that of mono-Si cells within 26 years lifetime. For HTL-free perovskite device to supersede many of other commercial technologies, its lifetime has to be 40 years. Solution and vacuum based cells need even longer lifetimes for them to perform better than commercial technologies. With 15 % efficiency, solution and vacuum based perovskite cells need 33-34 year lifetimes to perform better than mono-Si. In contrast, if the lifetimes of perovskite cells are fixed to five years, perovskite solar cells would not have lower environmental impacts than commercial technologies even if their

efficiency could increase up to 30 % (Figure 4b). Therefore, a longer lifetime should be targeted for further improvement of perovskite technology.

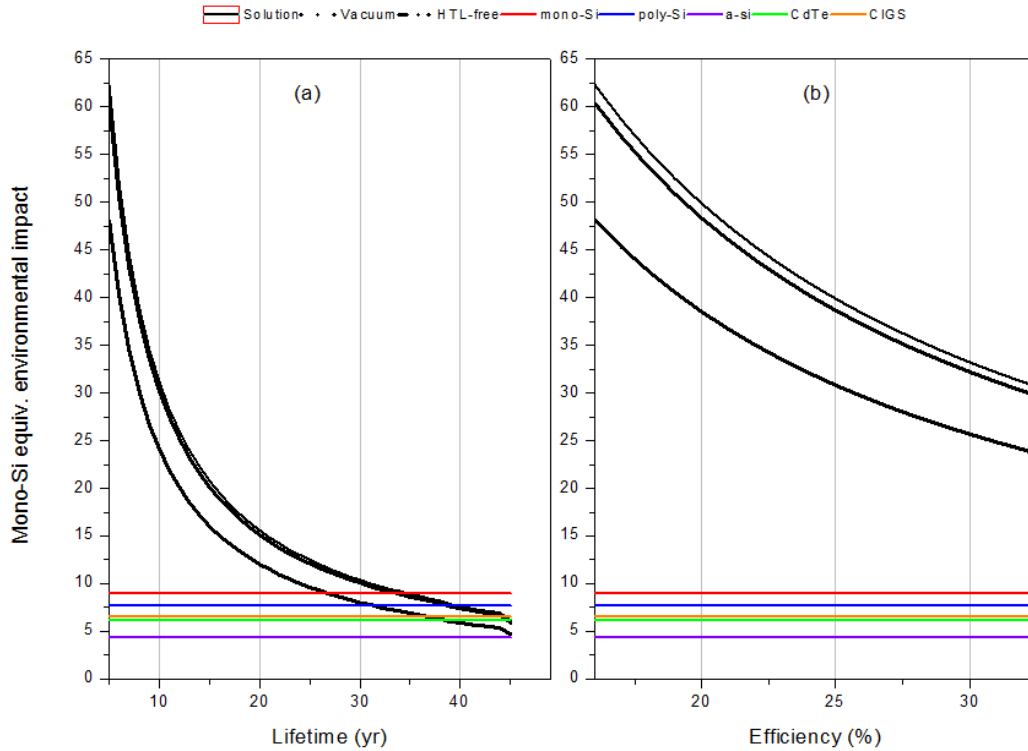


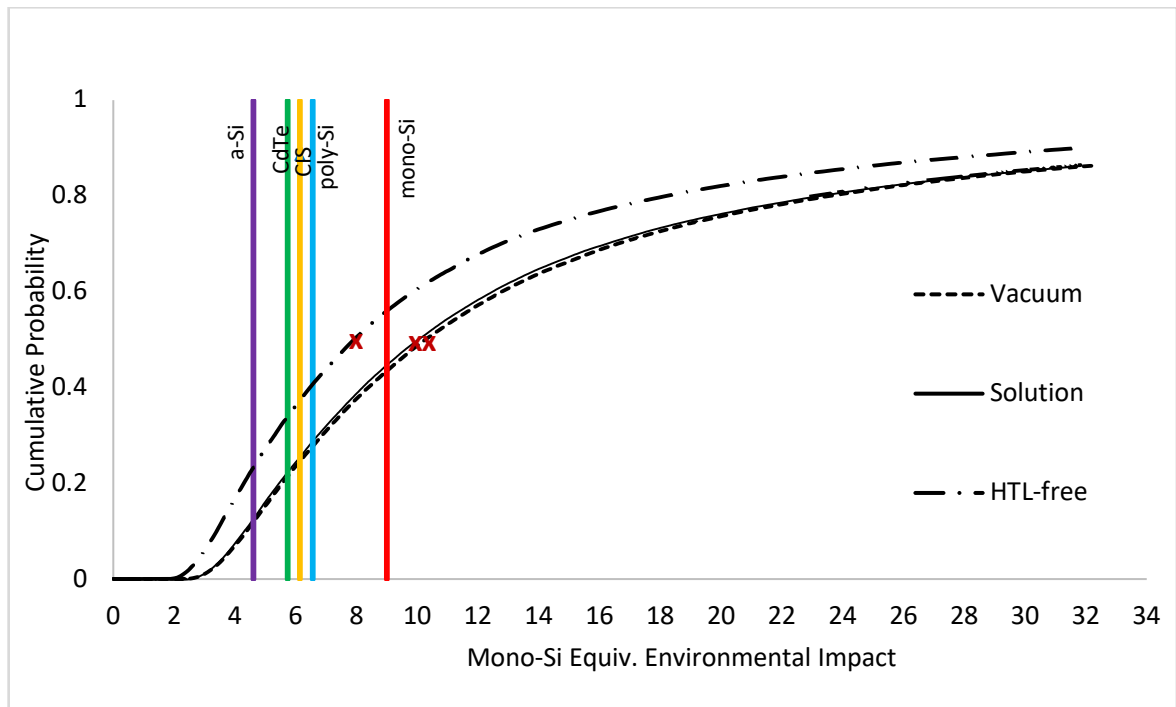
Figure 2-4 Sensitivity of total environmental impacts to lifetime (Figure 4a) and efficiency (Figure 4b) assumptions. Baseline perovskite cells efficiencies and lifetime assumed were 15 % and 5 years. This graphs test whether it is possible for perovskite cells to reduce overall impacts with efficiency or lifetime. Figure 4a shows the variation of perovskite impacts when perovskite cell lifetime is varied. Figure 4b shows the variation of perovskite impacts when its efficiency is varied. The parameters for commercial technologies were kept constant as in Section 3.2. All results are presented as total impacts normalized to mono-Si impacts as in Figure 2-3. Unlike Figure 1-3, the mono-Si equivalent impact is

calculated for 1kWh electricity generated not for manufacturing of 1m² of module.

From Figure 2-4, we can conclude that improvements in both the efficiency and the lifetime of perovskite solar cells are needed for perovskite cells to have lower environmental impacts than commercial technologies. Given the challenges with prediction to a future date, the relevant question to ask is about the probability of perovskite solar cells having impacts less than commercial technologies. We analyze this question in Figure 2-5. Based on the resulting cumulative density functions, we would expect the total environmental impact of HTL-free structure to be lower than that of mono-Si 55 % of the time. The HTL-free structure intersects with the other technologies at cumulative probabilities ranging from about 25 to 40 %. For solution and vacuum based perovskite cells, the chances of them having lower impacts are even lower.

The uncertainty analysis clearly depends on the input distribution (uniform assumed) used in Monte Carlo analysis which results in a cumulative probability distribution that is steep at first but then levels off very slowly suggesting that the total impacts from perovskite solar cells could be many times higher than those of mono-Si. (The x-axis scale was cut off at 35 but extends 266.) On the other hand, there is also a probability of all three perovskite cells having lower environmental impacts from all commercial technologies but this chance is only 10 %. In this analysis we did not incorporate the uncertainty resulting from the LCA model itself which is difficult to characterize but we estimate that the current

modeling of perovskite cells reveal higher energy requirements (and corresponding higher impacts) than commercial technologies due to lack of commercial scale data for their production (see section 3.4). Once perovskite solar cells are being manufactured commercially, it is quite possible that their environmental impact data obtained not from lab estimation but from actual facilities will be lower. As we obtain facility level data for perovskite manufacturing and as we gain more confidence in perovskite cells having higher lifetimes and efficiencies, the shape of the cumulative density function will shift towards being steeper early on suggesting that the chances of perovskite cells having lower total environmental impacts than existing technologies will be higher than what we currently estimate in Figure 2-5.



**x shows median of total mono-Si equiv. of the perovskite cells*

Figure 2-5 Probability of perovskite cells having total impact less than that of commercial technologies. Monte Carlo simulations were run using @Risk software to create

the data in Figure 2-5. Uncertainties in three parameters were propagated using uniform distributions. Insolation constant was varied from 1266 to 2187 kWh/m²/yr to represent the variation across the USA. Efficiency was varied from 10 to 30 % with the higher value representing the thermodynamic limit for photovoltaic conversion, known as the Shockley-Queisser limit (Darling and You, 2013; Shockley and Queisser, 1961). Lifetime was varied from 1 to 30 years following Zhang et al.'s approach. Median values are indicated with a red x. Median/mean values were 7.90/14.3, 9.97/18.18 and 10.25/18.56 for HTL-free, solution based and vacuum based cells, respectively.

2.3.4. Energy Requirements of Perovskite Cells

We had anticipated the perovskite PV cell energy requirements to be lower than those of the thin film PV cells due to their simpler manufacturing methods and simpler structures. Contrary to our expectations, the PED of perovskite solar cells were lower than that of mono-Si but higher than the thin film cells (see the heights of the purple bars in Figure 2-3). PED incorporates the direct energy requirements of processing the materials and the manufacturing of the cells. If we leave out the energy requirements of the materials and analyze only the electricity demand of the perovskite solar cell manufacturing facility, the electricity requirement for vacuum, solution, and HTL-free devices are 821, 665, and 504 MJ/m², respectively. These values are among other perovskite studies (Espinosa et al., 2015; Serrano-Lujan et al., 2015a; Zhang et al., 2015) (See Section 2.3.5 for the comparisons). In the EcoInvent database the electricity requirements for first and second-

generation solar cells range from (59 to 484 MJ/m²). Contrary to our expectations, the manufacturing electricity requirements of perovskite solar cells are higher than those of all current commercial technologies. We believe the reason for this is the incomplete specification of an industrial scale perovskite manufacturing process and the modeling assumptions that reflected this situation.

2.3.5. EPBT and GWP impacts: Comparison to Prior Perovskite LCA studies

Recent LCA studies on perovskite PV cells have shown large variation in results. Here we compare only the EPBT and GWP metrics since they were the only ones we could directly extract and compare from prior studies (Figure 2-6). In GWP impacts, the reported values vary by almost 50-fold among the three published cradle to gate studies. For solution and vapor-based deposition methods, Espinoza et al. found GWP emissions to be around 1100 g CO₂ eq. per kWh. However, Gong et al. found 24 and 32 g CO₂ eq. per kWh for the perovskite cells with ZnO and TiO₂ ETL, respectively. Zhang reported GWP as 414 g CO₂ eq per kWh for liquid titania perovskite cells and Serrano-Lujan calculated this value as 1880 g CO₂ eq. per kWh. The GWP in our study was in the lower end of the reported values (99 to 147 g CO₂ equiv. per kWh).

There is a large variation in the literature in perovskite solar cells' estimated EPBTs as well. Our estimates of the EPBT of the three perovskite structures varied between 1.05-1.54 years whereas values reported by both Gong et al. (0.19-0.27 years) and Espinoza et al. (1.1 years) were lower. (Espinoza et al. also reported EPBT of around 17 and 1 years

when they assumed the lifetime of the perovskite to be 1 and 15 years, respectively, but we assume this was an error. We omitted these values from the comparison since EPBT should not depend on system lifetime.) In contrast, estimates from Zhang et al are much greater (5.3-55.4 years).

Ultimately, it is helpful to compare the EPBTs not only among perovskite solar cells but also with existing commercial technologies. Bhandari et al recently compiled and harmonized the EPBTs for Si and thin film based solar cells. These data also display a wide variation in EPBT for a given technology even when the data are harmonized to the same insolation and performance ratios. Yet, if we consider the mean of the harmonized EPBTs given in Bhandari et al (4.1 yr for mono-Si, 3.1 yr for poly-Si, 2.3 yr for a-Si, 1.0 yr for CdTe and 1.7 yr for CIGS (Khagendra et al., 2015)) the perovskite solar cells that we modeled appear quite competitive with all of the commercial technologies.

Another way to interpret the perovskite EPBTs is to compare them to standard organic PV which has shown great advances in the last decade (Anctil and Fthenakis, 2006) and seem to promise much lower environmental impacts than commercial technology due to the use of inexpensive materials and solution processing methods. For example, Espinosa et al. (Espinosa et al., 2011) report that polymer PVs with 3 % efficiency can have lower environmental impacts than crystalline silicon technology and deliver EPBT as low as 1.35 yr. In another study with a 10 % efficiency assumption, an EPBT of as short as 12 days was estimated for organic PV (Darling and You, 2013). Roes estimates that a polymer

module on a flexible substrate can have lower CO₂ equiv. than poly-Si even at a 2.6 yr lifetime (Roes et al., 2009). More LCA studies directly comparing organic PV to perovskite PV would be helpful in the future to improve our understanding of the environmental impacts of perovskites in relation to organic PV.

The variations in results among the published perovskite LCA studies stem from the different materials, deposition methods, electricity inventories, and assumptions used in the models (See Table 2.3). For example, performance ratios, power conversion efficiencies, and active area assumptions are slightly different among the published data. If we analyse the choice of electricity mix in the models, we note that in our study, we extracted the data from Ecoinvent database and used the average US electricity mix in the models. Yet, Espinoza et al. and Serrano et al. used Denmark's low-voltage electricity. Similar to our study, Gong et al. and Zhang et al. used the average U.S. electricity mix, which is higher GWP emissions per unit of MJ electricity produced (Figure A2).

While there could be many reasons for variations, we estimate that the large CO₂ equiv. difference between Espinosa and Gong can be contributed to the direct process energy to deposit the layers. Gong estimated the direct process energy needed to fabricate 1 m² module as 7.78 kWh (TiO₂) and 4.56 kWh (ZnO) while Espinosa found the same value as 1080 kWh (Solution) and 1460 kWh (Vacuum). We can see this difference more clearly in the deposition of Spiro-MeOTAD (HTL). For the deposition of that layer Gong only considered the spin coating process which consumes 0.244 kWh (per m²) while Espinosa

modeled annealing and nitrogen glovebox energy requirement in addition to spin coating and reported 276 kWh (per m²). In contrast, a much higher direct process energy value is reported by Serrano-Lujan et al.; this study is based on the model given in Espinoza et al. 2015 and reports a value of 31,700 kWh (per m²) for direct process energy. Since Zhang modeled dye synthesized solar cell, the materials (layers) and processes are quite different in that study and cannot be directly compared.

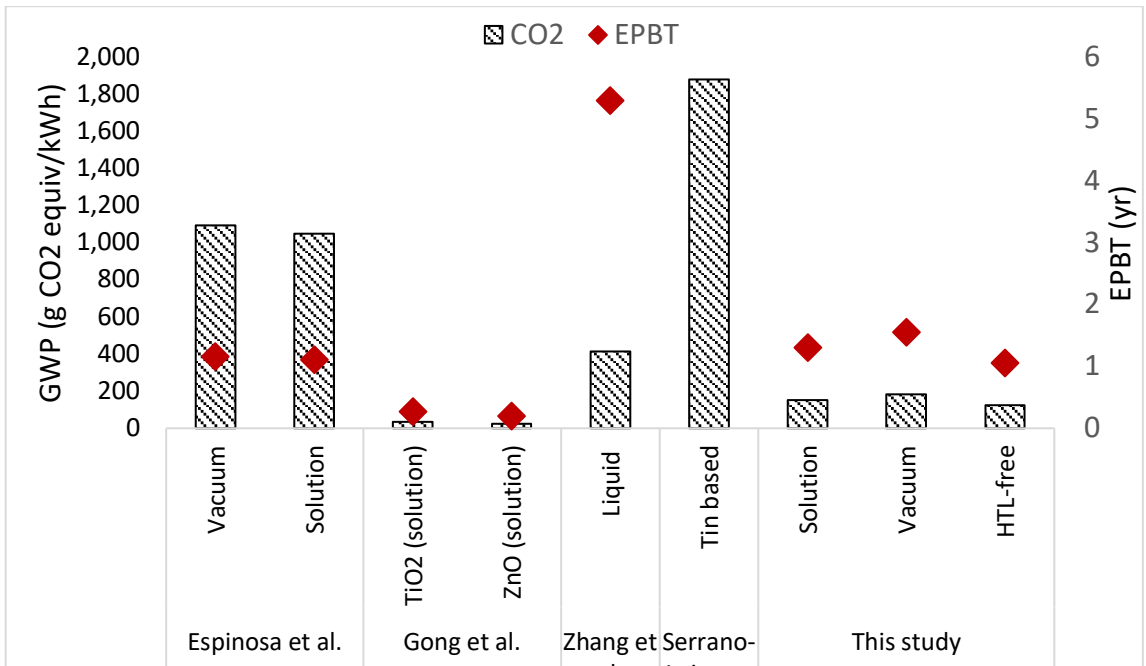


Figure 2-6 Comparison of GWP and EPBT data from this study with prior studies. Data shown are for cradle to gate and 5 year lifetime assumption for all studies. Since Zhang et al did not provide an average EPBT value, we plotted the lowest point of the uncertainty range they reported. Also, EPBT value of tin based perovskite cell was not available provided.

Table 2-3 Comparison of the modeling assumptions in published Perovskite PV LCA models

| | Espinosa et al. 2015 | Gong et al. 2015 | Zhang et al. 2015 | Serrano-Lujan et al. 2015 | This study |
|-----------------------------|---|---|--|---|---|
| System boundary | Cradle-to-gate | Cradle-to-grave | Cradle-to-gate | Cradle-to-gate | Cradle-to-gate |
| Lifetime | 1 - 15 yr | 2 yr | 1 to 30 yr | 1 yr | 5 yr |
| Performance Ratio | 80 % | 80 % | 75 % | 80 % | 75 % |
| Active Area | Not provided | 70 % | 60 % | Not provided | 65 % |
| Power conversion efficiency | 11.5 % (solution) 15.4 % (vacuum) | 9.1 % (TiO ₂) 11.0 % (ZnO) | 6.5 % | 6.4 % | 15 % |
| Material Structure | FTO/TiO ₂ /Lead-P/S-MeOTAD/Ag (for solution) ITO/REDOT:PSS/Lead-p/PCBM/Al (for Vacuum) | FTO/TiO ₂ /Lead-p/S-OMeTAD/Au ITO/ZnO/Lead-p /S-OMeTAD/Ag | FTO/TiO ₂ /Lead-p /electrolyte/ Pt. | FTO/TiO ₂ /Tin-P+TiO ₂ /S-MeOTAD/Au | FTO/SnO ₂ /Lead-P/CuSCN/MoO _x - Al (for solution and vacuum) FTO/SnO ₂ /Lead-P/C-paste (for HTL-free) |
| Fabrication methods | SD: Oxygen plasma treatment, Spin coating, Drying, Sintering, evaporation, annealing VD: Evaporation, Spin coating, Vacuum | TiO ₂ : Screen printing, Sintering, Spray pyrolysis, spin coating ZnO: Ultrasonic cleaning, spin coating, | Spin coating, dipping, annealing | Spin coating/annealing/evaporation | Ultrasonic cleaning, spray pyrolysis, Screen printing, co-evaporation vacuum, annealing, |
| Electricity inventory | Denmark Electricity, low voltage | US Electricity mix | US Electricity mix | Denmark Electricity, low voltage | US Electricity mix |

As another example of the effect of the materials and modeling assumptions, we note that both our study and Gong et al. used FTO as the top contact layer but the percentage

contribution of the PED of this layer is much lower in this study (15 %) than in Gong's study (27 %). The PV companies have been using commercially available TCO glasses for this layer (e.g., Pilkington, TEC 15). In our study, we selected the low-iron solar glass available in the EcoInvent database to model this glass. However, Gong separately modeled the glass and the FTO deposition. Similarly, in contrast to our study where we modeled aluminum as the metal electrode, Gong et al. modeled gold, silver paste, and found the embedded energy to be primarily dominated (70 to 85 % of total) by the energy demand for these materials. This is an expected result since gold and silver are considered precious materials and embedded energy of gold and silver are much higher than aluminum (see Figure A.2).

2.3.6. Hot spot analysis of Perovskite Solar Cells: Comparison of Electricity versus Material Impacts

In sections 3.6-3.8 we present hot spot results that can help guide researchers and manufacturers on how to reduce the impacts from perovskite cells. A possible question to ask is whether the impacts come mainly from electricity use versus materials (section 3.6). If the impacts are from electricity, then this means the focus should be in reducing electricity use during manufacturing. In that case, the relevant question is which layer one should focus on to reduce the impact (section 2.3.7). Finally, the hot spot analysis can also be done for the specific materials to evaluate if some materials should be substituted with others to decrease impact (section 2.3.8).

For all of the impact categories studied, except ecotoxicity and marine eutrophication, the major impacts were from electricity consumption during manufacturing, which contributed from 50 to 90 % of the different impacts (Figure 2-7). In particular, impacts from electricity are around 80 % for GWP, human toxicity (cancer and non-cancer), PED and freshwater use. These results emphasize the importance of using electricity efficient manufacturing methods and clean electricity sources to reduce environmental impacts.

From our data, it is possible to roughly estimate how the impacts may change if more energy efficient processes are used by a manufacturer. For instance, in scaling up the vacuum-based model to commercial production, if we consider that our approximation using lab data were low and that the industry may reduce the processing energy by 20 % (in comparison to our current model), we can say that the electricity dominates 40 to 90 % of the impacts (see Figure 2-7). A 20 % reduction in processing energy would therefore results in 8 to 18 % reduction in final impacts. Corresponding LCIA can be calculated by using values given in Table 2.

Interestingly, prior perovskite LCA studies reported contradictory results for electricity versus materials impacts. In Espinoza's study, electricity contributed to more than 90 % of the impacts likely due to energy intensive deposition choices used in that study. Yet, in Gong's study the material choices such as gold or silver, resulted in a dominant contribution of materials to the impacts categories. Our study lies somewhere in between Espinoza's and Gong's results. These differences are a good example of how sensitive PV

LCA results are to the specific device architecture and deposition methods modeled. More research in comparing specific materials and deposition methods would be helpful in guiding future research and better interpreting the variation of results in the literature.

Figure 2-7 is also helpful in comparing the three devices with respect to the individual impact categories. From this comparison, we see that for all except the marine eutrophication impact, the highest, medium, and lowest impacts are observed for vacuum, solution, and HTL-free devices, respectively. The differences are fairly small with solution and HTL-free devices being about 10 to 20 % lower than the vacuum-based device. The primary reason for the lower impacts in these two devices is that the solution-based deposition of the perovskite layer in solution and HTL-free devices result in the lower energy consumption which then reduces the environmental impacts for these devices compared to the vacuum deposition. (In Figure 2-2, the solution-based device had higher impact than the vacuum-based device primarily due to the marine eutrophication impact.)

Marine eutrophication shows an exception to the general order of impacts with vacuum having the highest and HTL-free having the lowest impacts. Marine eutrophication is also the primary reason the solution-based device had higher impact than the vacuum-based device in Figure 2-7. Marine eutrophication impact is largely affected by the use of DMF in solution-based deposition of perovskite which caused a much greater marine eutrophication impact in solution and HTL-free devices compared to the vacuum-based device.

Another interesting observation is with the use of copper thiocyanate. HTL free device does not use this compound and results in about a 60 % lower ecotoxicity and 30 % human toxicity compared to vacuum and solution-based devices.

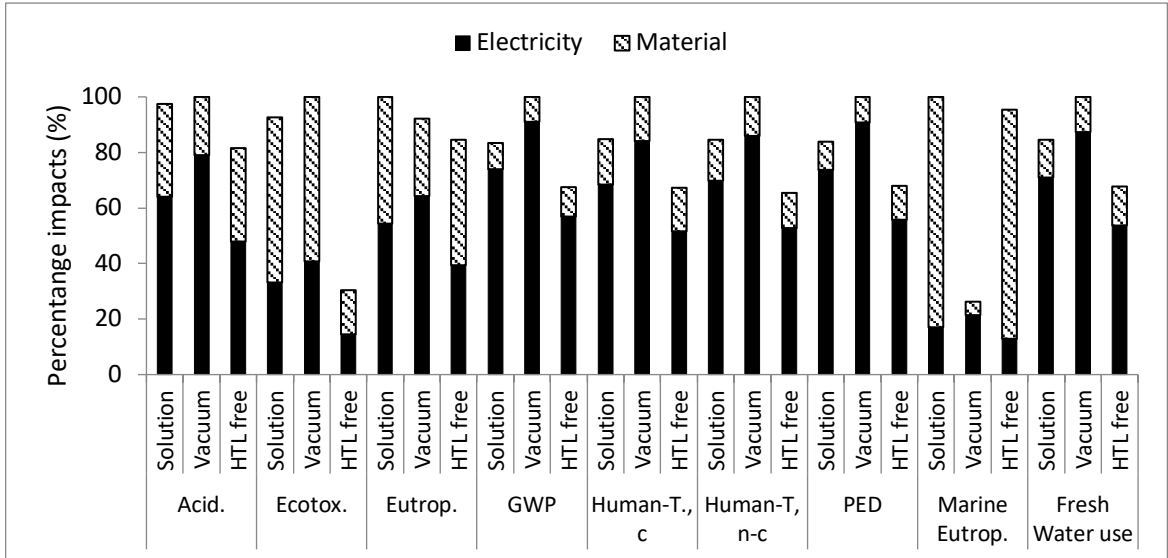


Figure 2-7 Comparison of environmental impacts among solution, vacuum and HTL-free devices. The results are plotted as normalized to the highest value within each impact category.

2.3.7. Hot Spot analysis of Perovskite Cells. Which steps in cell preparation use the most electricity?

Process breakdown of the electricity consumption during manufacturing of perovskite solar cells is shown in Figure 2-8. Pre-treatment consists of the processes that have to be done before depositions, including cleaning of solar glass or stirring and heating the chemicals necessary for solution-based depositions (steps 1, 2, 3a and 4). Depositions include the processes such as screen-printing, spray, or vacuum (steps 2, 3a, 3b, 4 and 5). This analysis shows that the highest electricity requirement for processing the cells come from the

absorber layer (perovskite deposition) for all three devices. In the case of solution-based deposition of perovskites, pretreatment process also has high electricity requirements, larger than the deposition process itself. As was expected, vacuum-based deposition of perovskites was found to be much more energy intensive (about twice as much) than solution-based perovskites. This caused the perovskite deposition in the vacuum-based device to require about three quarters of the total energy consumption during cell manufacturing.

From Figure 2-8 we also see that post processing contributes to about less than seven percent in all three devices suggesting that the focus in reducing electricity consumption should be in pre-processing and deposition steps. With respect to deposition the preference should be in solution-based deposition. In the back contact layer, the HTL free device was deposited using vacuum whereas the other two devices were deposited using solution processing. As was in the perovskite deposition, the high energy requirements of vacuum processing are also evident in this layer. These results show that to reduce electricity usage in thin film manufacturing, vacuum deposition should be avoided and instead solution deposition should be used.

Among the three modeled device architectures, the substrate and ETL were the same and therefore contributed equal amounts of electricity to cell production. Cleaning of the solar glass using sonication was responsible for 9 to 14 % of the electricity consumption. Using

detergent based chemicals instead of sonication may be a way to reduce energy consumption for the substrate layer.

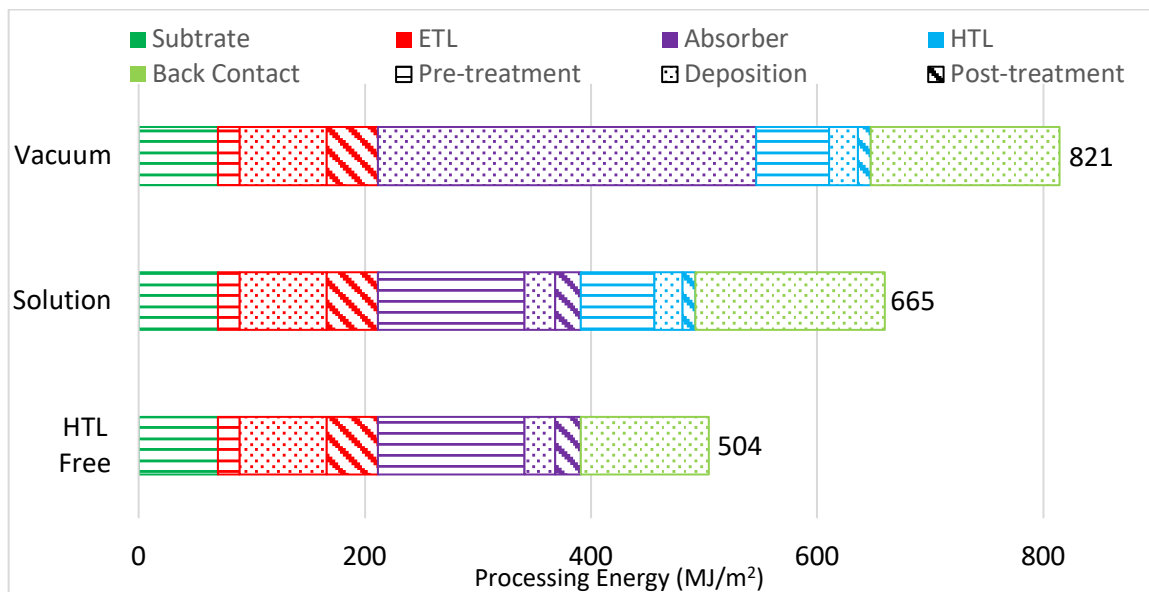


Figure 2-8 Breakdown of direct process energy requirements in each layer

2.3.8. Hot spot analysis of perovskite cells: Which materials in cell preparation contribute more to the impacts?

Material impacts from the vacuum-based method were lowest for most of the impact categories (Figure 2-7). Part of the reason for this is that vacuum based method uses less organic compounds (e.g. DMF and chlorobenzene) that contribute a lot to the impacts from materials (Figure 2-9). Marine eutrophication impact of the solution and the HTL-free structures were especially dominated by organics (around 95 %) and were 16 to 20 times higher than that of the vacuum-based method. The primary reason for this was the use of DMF in the solution-based deposition of the perovskites.

Other than the organic compounds, tin and the waste stream contributed considerably to the impacts from materials in all three perovskite cell devices. Raw tin usage dominated acidification, GWP, human-toxicity, cancer and non-cancer, PED and fresh water use categories. High toxicity findings of this study is consistent with Serrano-Lujan. Waste streams (that were dominated by copper and tin including waste to industrial soil) dominated the ecotoxicity and eutrophication impacts. This result is quite higher than what we expected; however similar to ours, Ryberg et al. also found questionably high impacts from waste released to industrial soils (Ryberg et al., 2014).

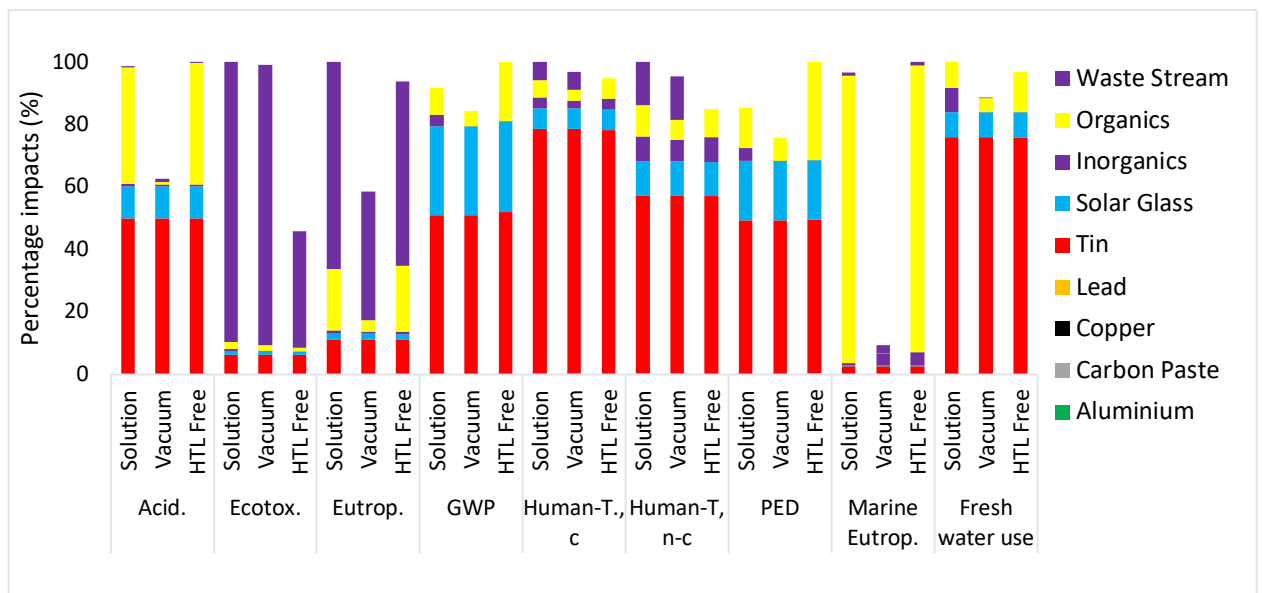


Figure 2-9 Comparison of material impacts among solution, vacuum and HTL-free devices.

The results are plotted as normalized to the highest material impact value within each impact category (For raw data see Table A. 8).

We note that the contribution from lead is insignificant in all impact categories in all three perovskite devices (Figure 2-9). Cradle-to-gate environmental impacts of lead used in the

PV solar cell come from mining of lead and the release of lead back into the environment when some lead waste is created during deposition of the absorber. These impacts contributed less than 0.2% of total impacts in all of the impact categories. Thus, our results confirm the conclusions from previous studies (Espinosa et al., 2015; Gong et al., 2015; Serrano-Lujan et al., 2015; Zhang et al., 2015). However, to our knowledge, Espinosa and Gong did not include any lead emissions during manufacturing. Although Zhang et al. discussed the release of metals to the environment (iron, magnesium, and aluminum), lead emissions may not have been considered in that study either. Unlike prior studies, we modeled a direct freshwater release of the lead which was assumed as a material loss during perovskite layer deposition. The negligible impact from lead may be due to the limited mass of lead used in the cell. Another likely reason is the limited accuracy in modeling the toxicity of metals in LCA studies. For example, the TRACI model used in this study is based on the Usetox model which has 'interim' characterization factors for metals (Henderson et al., 2011). Also, ecotoxicity characterization in Usetox is only valid for fresh water. Usetox model is embedded in the other LCA studies as well. For example, Espinosa et al., Serrano-Lujan et al., and Zhang et al. used the International Reference Life Cycle Data System (ILCD) in their models which is also based on the Usetox model. In contrast, Gong et al. used Ecoindicator and CML, both of which are based on USES-LCA. USES-LCA has differentiated characterization factors for lead related to aquatic, sediment and terrestrial ecotoxicity potentials (Huijbregts et al., 2000). Based on this different toxicity model, Gong et al. did not find lead to pose a major concern either. The only study that showed significant toxicity from lead is Serrano-Lujan's cradle-to-grave lead perovskite model. In this study, lead emissions at the end of life were modeled in a landfill scenario

which included leaching of 70% of total lead content of the module into soil (Serrano-Lujan et al., 2015a). This model resulted in >10 times higher fresh water toxicity compared to the cradle-to-gate system boundary. Much uncertainty still remains at the end-of-life phase of perovskite cells. More work in this area is needed to better understand the environmental impact of lead in perovskite cells.

2.4. Conclusions

The goal of this study was to evaluate the environmental impacts of vacuum, solution, and HTL-free perovskite solar cell devices using fabrication approaches that are amenable to large scale manufacturing. A comparison of environmental impacts was made with mono-Si as a reference point. We found that manufacturing of perovskite solar modules causes 10 to 30 % lower impacts than manufacturing mono-Si PV. However, if perovskite cells were to enter the market, their environmental impacts would be higher than those of all commercial PV technologies mainly because of their shorter lifetimes. Monte Carlo analysis varying lifetime and efficiencies of perovskite cells showed that HTL-free structure could perform equal or better than mono-Si cells with about 55 % cumulative probability.

To our surprise, the energy requirements of perovskite solar cells were not lower than those of commercial technologies. This result is likely due to incomplete specification of the commercial scale fabrication of perovskite solar cells. The EPBT and GWP varied from 1.0 to 1.5 years and 100-150 g CO₂ equivalence (per kWh). These values are within previously reported data for other perovskite solar cells. Solution-based methods with

spray used in perovskite deposition were observed to decrease the overall electricity consumption.

Among the three structures modeled, the HTL-free structure had the lowest environmental impacts in all impact categories, except marine eutrophication. Marine eutrophication impact of the solution and HTL-free structure were dominated by organics (around 95 %). Material impacts attributed to the vacuum-based method were lower than other two methods, except for ecotoxicity. The ecotoxicity value of HTL free structure was around 30 % of the vacuum and solution-based methods because it is missing the HTL made from copper thiocyanate. The impact of lead used in the absorber layer was negligible, which is consistent with the literature.

Chapter 3

Life cycle analysis of metals in emerging photovoltaic (PV) technologies: A modeling approach to estimate use phase leaching

3.1. Introduction

Driven by the increasing demand for green energy, solar photovoltaics (PV) have rapidly developed in the past decade. The global installed PV capacity increased from 5 GW (Fthenakis et al., 2011) in 2005 to approximately 250 GW (Shahan, 2015) in 2015, advancing the progress towards the goal of electricity generation at the multi-terawatt (TW) scale (Zweibel, 2005). This fast-growing implementation of PV is due to a rapid **reduction** (up to 65%) of solar module cost over the past six years (Taylor et al., 2015b), a reduction in the balance of system cost due to improved installation methods (Dhere, 2005), longer inverter lifetimes, and innovative financing methods. Conventionally, solar energy development efforts have focused on commercial crystalline Si, and thin film (e.g., CdTe, and $\text{CuIn}_{1-x}\text{Ga}_x\text{Se}_2$) technologies. Yet, more recently, a host of emerging PV technologies, such as those based on dye-sensitizers, organic polymers, earth-abundant

inorganic materials (e.g., $\text{Cu}_2\text{ZnSnS}_4$ or CZTS), and inorganic-organic hybrid perovskites are being pursued to develop new options that can be scaled-up at an even greater rate than the conventional technologies. These emerging PV cells are expected to provide several advantages including high device efficiencies, low materials costs, and easy manufacturing, due in part to the possibility of using ultra-thin substrates (Michael Graetzel et al., 2012; Z. Song et al., 2017) In addition, they can reduce both the energy and mass requirements of manufacturing and potentially lower the environmental footprint of solar PV by combining lightweight and flexible substrates with scalable high-rate processes that do not require high temperatures (Ilke Celik et al., 2017b; Gong et al., 2015)

The potential environmental impacts of solar PV technologies can be determined using life cycle assessment (LCA) (Celik et al., 2016a; Collier et al., 2016). The LCA framework divides the analysis into separate life cycle stages such as (1) extraction/mining, (2) manufacturing, (3) transportation, (4) use, and (5) end-of-life. The environmental impact of materials, and electricity consumed, and wastes generated are evaluated for each stage of the entire life cycle. The LCA method was first used by Coca Cola in 1969 to compare the environmental impacts of alternative materials used in beverage containers (Journey Staff, 2012). LCA was first applied to the PV technologies to perform the health, safety (Owens et al., 1980), and energy flow assessments of silicon PV cells manufacturing (Hagedorn, G., and Hellriegel, 1992; Hagedorn, G., S. Lichtenberg and H. Kuhn, 1989). Over the intervening 25 years, numerous LCA studies have been performed on relatively mature PV technologies such as Si (Bailie et al., 2014; Hong et al., 2016; Phylipsen and

Alsema, 1995; Wong et al., 2016), CdTe (Fthenakis, 2004; Fthenakis et al., 2005; Raugei et al., 2007; Sinha, 2013), amorphous-Si (Engelenburg and Alsema, 1993), and $\text{CuGa}_{1-x}\text{In}_x\text{Se}_2$ (Collier et al., 2014; Raugei et al., 2007; Zimmermann et al., 2014). These LCA studies have quantified the energy flows, material flows, and emissions from manufacturing, and raw material purification (Fthenakis et al., 2011, 2008; V. M. Fthenakis and Kim, 2011). Recycling of PV cells and the impacts of manufacturing waste have also been assessed (Fthenakis, 2000; Goe and Gaustad, 2014; Latunussa et al., 2016; Zimmermann et al., 2014). Energy related metrics such as energy payback time, energy return on investment, and CO_2 equivalent avoidance has been discussed as well (Alsema, 2006; Bhandari et al., 2015; Raugei et al., 2007).

In general, LCA studies concluded that the environmental impacts of solar PV electricity are dominated by the upstream emissions associated with (1) mining and purification of raw materials and (2) the emissions associated with the electricity needed for manufacturing the modules (Chatzisideris et al., 2016; V. Fthenakis and Kim, 2011; Meijer et al., 2003; Rand et al., 2007). However, these conclusions were reached by neglecting the impacts from non-routine breakage events during the use, and emissions to landfills at the end of life of solar cells. These phases were typically not considered due to the expectation that PV materials are typically water-insoluble inorganic compounds, and that modules are deployed in robust, hermetically sealed packaging which would preclude emissions during the use phase (Fthenakis, 2009; Raugei and Fthenakis, 2010).

Recently, it has been experimentally demonstrated that the environmental impacts from several emerging PV technologies made from perovskite or polymer materials can significantly increase due to metal emissions resulting from exposure to moisture during the use phase (Berhe et al., 2016; Espinosa et al., 2016; Hailegnaw et al., 2015; Serrano-Lujan et al., 2015a; Zimmermann et al., 2012a). These effects have not been considered as being a problem for the more established solar modules, even if the module packaging is mechanically damaged or otherwise compromised because the components are not emitted to the environment during interactions with moisture (rain) or air (oxygen) even under extreme heat (Espinosa et al., 2016; Hailegnaw et al., 2015; Jørgensen et al., 2008a). However, in the effort to reduce materials and manufacturing costs and eventually the cost from solar (Graetzel et al., 2012), emerging solar cells often contain water-soluble metal compounds, and these are often packaged in polymeric materials that allow ingress and egress of species even without damage (Wang et al., 2016). Consequently, the assumption that the use phase emissions can be neglected has been reanalysed in several recent studies (Brun et al., 2016; Celik et al., 2016b; Celik et al., 2017a; Espinosa et al., 2016; Hailegnaw et al., 2015; Zimmermann et al., 2013, 2012b). This recent work raises the question of whether and under what condition the downstream emissions may still be neglected in comparison to upstream emissions from mining and materials processing. This question coupled with the toxicity concerns of using heavy metals (Benmessaoud et al., 2016) often found in emerging PV is important to consider as society scales PV use to address the Terawatt challenge (Zweibel, 2005).

In this contribution, we compare the relative importance of the upstream and downstream emissions of the several important metals that are components in emerging PV technologies such as methylammonium lead iodide perovskite solar cells (PSCs), copper zinc tin sulphide (CZTS), and lead sulphide quantum dot solar cells (QDSCs). In order to estimate the downstream (use phase) emissions we developed a new theoretical model that incorporates field conditions (e.g. leaching time, crack area, initial mass of metal in the PV module, and thickness of the module) and thermodynamic concepts (e.g. solubility product of metal ions, diffusion coefficient) into the calculation. This is the first approach that estimates the metal release from PV cells from a theoretical basis as opposed to field experiments. In addition, since materials with similar functionalities may be interchangeable within an emerging PV technology, we determined which materials should be avoided in scenarios when use phase emissions are expected to be significant. Lastly, we put our results in the context of coal-based electricity by comparing possible emissions from emerging PV to those from coal fired power plants.

3.2. Methodology

3.2.1. Life Cycle Based Modeling Approach

Life cycle of metals used in a PV module is shown in Figure 3-1. Extraction, manufacturing, transportation, use and end of life are typical life cycle phases of any product. In this study, we focus on upstream toxicity resulting from metal extraction (and purification), and downstream toxicity resulting from potential leaching of metals during the use of the cells when the cells are damaged due to physical impact, rain, heat and wind.

In LCA, toxicity impact (Eq. 1) is calculated by multiplying the mass (M , in kg) of compound emitted per functional unit with the corresponding characterization factor (CF , in $1,4\text{ DCB}$) (Graedel and Allenby, 2010):

$$\text{Toxicity} = M \times CF \quad (1)$$

Metals, organic, and inorganic compounds are emitted to water, soil, and during the extraction and purification of any given metal that is included within the structure of a PV device. The mass of these upstream emissions (M) were obtained for each metal from EcoInvent v.3.0 (Wernet et al., 2016). For downstream toxicity, we estimated the mass of metal that may leach out from solar PV during use due to physical damage, rain, acidity, heat, and wind. The approach for this estimation is explained in Section 2.2.

In Equation (1), the CF converts the emissions of different compounds to a common toxicity unit so the toxic effects of the different compounds can be summed. CF can be extracted from several toxicity assessment models, including CalTOX (Maddalena et al., 1995), IMPACT 2002 (Jolliet et al., 2003), BETR (MacLeod et al., 2001), USES-LCA (Van Zelm et al., 2009), and Usetox (Hauschild et al., 2008). In this study CF s were extracted from USES-LCA which is embedded in the ReCiPe life cycle impact assessment model. Once the toxicities to marine, freshwater, terrestrial, and humans were calculated, these toxicities were normalized into a single toxicity score using hierarchist normalization factors (Goedkoop et al., 2008).

Three quantitative analyses were performed. The first analysis (A1) compared the toxicity resulting from downstream mining of the metals to the toxicity resulting from upstream emission of the metals. This analysis was performed for a unit mass (e.g. 1kg) of metal that might be used in any PV device. The second analysis (A2) considered the actual mass used within the different PV device architectures. With this analysis, we were able to compare the toxicities from different layers within a device and among different devices. In both A1 and A2 we considered a realistic scenario that corresponds to a damage on hermetically sealed packaging of the cell under investigation, coupled with the exposure of precipitation in outdoor conditions. For the final analysis (A3), we compared the emissions from electricity generated from emerging PV technologies to those from conventional coal plants.

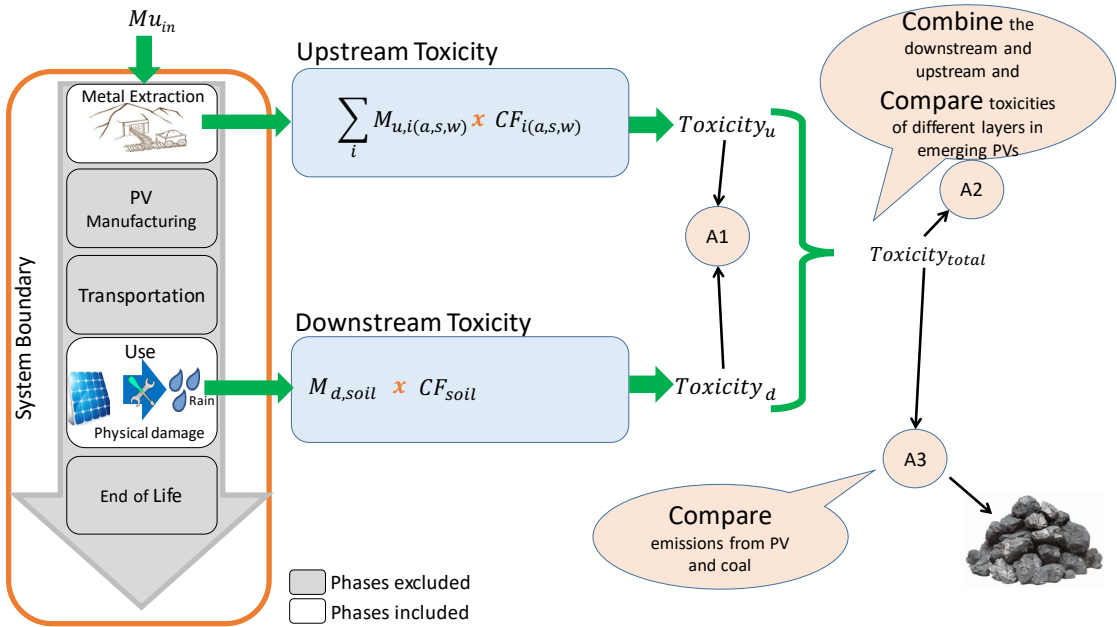


Figure 3-1 The modelling framework for the three analyses in which we compare (u) upstream and (d) downstream toxicities (A1); sum the upstream (to air (a), soil (s) and water (w) compartments) and downstream toxicities to evaluate

the total toxicity resulting from different PV layers used in emerging solar cells (A2); and compare the downstream metal emissions from emerging PV to emissions from coal electricity (A3).

3.2.2. Estimation of metal leachate from PV

As seen in *Equation(1)* the toxicity is directly proportional to the mass of the materials used in the device. Here, we distinguish between the metal mass related to downstream (M_d) and upstream emissions (M_u). M_u is the mass of each metal used for fabricating solar cells. This mass determines the upstream emissions associated with obtaining and producing the needed materials. M_d , on the other hand, is the mass of this metal that is released into the environment from a damaged module. We linearly relate M_d to M_u using loss factor (LF) which represents the percentage of initial mass released to the environment:

$$M_d = LF \times M_u \quad (2)$$

LF depends on the crack size, encapsulation method, substrate thickness, ambient temperature and humidity, and exposure time (Jørgensen et al., 2013, 2008b). A few pioneering studies measured LF from lab and field experiments but did not suggest any mechanistic models for its estimation (Espinosa et al., 2016; Hailegnaw et al., 2015; Sinha and Wade, 2015). Our proposed model estimates LF values -based on field conditions and thermodynamic properties of the metals. We use a semi-empirical approximation based on the Noyes-Whitney equation (Noyes and Whitney, 1897). We assume that after exposure to moisture (rain), the metals in the different layers dissolve and diffuse due to

a crack in the encapsulation. The dissolution rate of a substance (dm/dt) in an open environment can be expressed as:

$$\frac{dm}{dt} = A \left(\frac{D}{d} \right) (C_s - C_b) \quad (3)$$

where m (kg) is the mass of the dissolved material; t is time (in seconds, s); A is the surface area exposed to the solvent (m^2); D (cm/s) is the diffusion coefficient of the metal ion; d is thickness of the boundary layer (encapsulation glass); C_s is the saturated mass concentration at the surface (kg/m^2), and C_b is mass concentration in the bulk solvent. We assume that the concentration of metals in rainwater as it lands on the PV module is negligible ($C_b = 0$). C_s can be written in terms of the solubility of the metal (K_{sp}) in compound (A_xB_y) (See details in the *Appendix – Equation(A.1) to (A.3)*):

$$K_{sp(A_xB_y)} = (y/x)^y (C_s)^{x+y} \quad (4)$$

Integrating Equation (3) and merging with Equation (4), an expression is obtained for the ratio of dissolved mass to initial mass ($m_{(time@t)}/m_{(time@0)}$). Dissolved mass and initial mass represent the downstream (M_d) and upstream (M_u) metal emissions given in Equation 2. Their ratio provides LF, Equation (5):

$$LF = \frac{M_d}{M_u} = \frac{A * D * t * MW}{d * M_u} \left(\frac{x}{y} \right)^{\frac{y}{x+y}} K_{sp}^{1/(x+y)} \quad (5)$$

where MW is the molecular weight (kg/mol) of metal compounds used in PVs.

We analysed eight different metal compounds: CdS, CuSCN, PbI₂ and PbS, NiO, SnO₂, SnS, and ZnO. These compounds are commonly used as hole selective, electron selective or absorber layers of emerging PVs. The assumptions used to estimate LFs for sections A1 (in Figure A-1) are as follows: 1) The crack size (Area=A) is 3 cm², (on the surface of module) equivalent to 0.03 % of the unit module area; 2) The diffusion time (t) that allows the diffusion of metal ions is 6.48 x 10⁶ s, assuming 1-year lifetime of PV panels and ~80 days of rain; 3) boundary layer thickness (d) is 1 mm; 4) The initial mass of metal in a 1 m² of PV panel is 0.5 g ($M_u = 0.5$ g). This initial mass is representative for a variety of current PV modules with 100 nm to 1000 nm thickness (Ilke Celik et al., 2017c). The crack size is representative of 1 mm X 30 cm sized macro crack that may be caused by a hit from a ball to the top glass layer, can be representative for this assumption (See Figure (A.1) for a typical PV structure). The wet period of 80 days is representative for Toledo, OH and assumes the module remains wet for about a day when it rains. In the paper, we present the results for these assumptions as a realistic scenario (See Table A. 1 for all the parameters used in this study). We also varied these parameters for a best and worst-case scenario and presented the effects of these on LF in the Appendix (See Table A.2).

3.3 Results

3.3.1 Metal Loss Factor

Table 1 shows the LF calculated from the proposed leachate model. The effects of the different parameters on LF (Table A.2) show that given the same external physical conditions, the material loss is mainly determined by K_{sp} . This is because solubility (K_{sp})

of the materials vary by many orders of magnitude (Table 1). The LFs were found to be negligible for CdS, PbS, and SnO₂, somewhat noticeable for NiO and ZnO, and high for CuSCN, and PbI₂.

Table 3-1 The estimated metal lost factor (LF) values. The K_{sp} value for quantum dot PbS is assumed to be the same as the K_{sp} of bulk PbS material. The corresponding LF for quantum dot is expected to be even lower due to the existence of non-water soluble ligands (*Kim et al., 2015*)

| | K _{sp} (Gustafsson, 2006) | LF |
|------------------|---------------------------------------|-----------|
| CdS | 1.00E-27 | << 0.01 % |
| CuSCN | 1.77E-13 | 11.1% |
| PbI ₂ | 9.80E-09 | 100% |
| PbS | 3.00E-28* | << 0.01 % |
| NiO | 5.48E-16 | 0.4% |
| SnO ₂ | 1.09E-38 | <<0.01 % |
| SnS | 1.00E-26 | <<0.01 % |
| ZnO | 2.19E-17 | 0.09% |

Two research groups conducted field experiments to measure leaching of ZnO and PbI₂ from PV devices. These studies did not provide detailed kinetic leaching data and were not done in any standardized conditions but they provide the only point of reference against which the LF results from our proposed model can be compared. Espinosa *et al.* (2016) investigated the amount of ZnO leaching from polymer solar cells in varying states of damage. They found that for modules cut with scissors, nearly all of the ZnO was removed with rainwater. The amount of ZnO in the rainwater decreased with decreasing damage, with a well sealed device retaining all of the ZnO. These data were used to

complete an LCA for the end-of-life stage which suggested that to reduce environmental impacts, modules should be recycled and not landfilled (Espinosa et al., 2016). Hailegnaw et al (2015) measured the LF of an unsealed PbI_2 -based device. They showed rapid loss of PbI_2 with water and concluded that with catastrophic encapsulation failure, a large fraction of the material (~70 % of PbI_2) would leach into the environment. These results were also used to determine the environmental impacts for the end-of-life of perovskite solar cells (Serrano-Lujan et al., 2015b) which showed that landfilling is less favorable than incineration. While the conditions of the reported LF values are different from the proposed damage here, the trends are consistent. For minimally damaged cells, little ZnO leached in to the water, and unsealed PbI_2 was shown to quickly leach when exposed to water. For comparison, Table 1 shows that 0.09% ZnO and 100% of the PbI_2 are lost over the one year lifetime. Unlike the other LCAs that use these reported values to determine the impacts of the end-of-life phase, the LCA reported here focuses on the use-phase of a damaged device.

The assumptions stated in Section 2.2, leads to significant loss of PbI_2 and CuSCN . Losses of this magnitude would result in a non-functioning device. It is likely that the damaged module would be replaced well before the one-year time scale used in these assumptions. In order to provide a more realistic estimate for material lost before replacement, we also modeled a monolithically integrated panel. A thin film PV module is constructed by monolithically depositing each layer over the entire area. The module is then scribed to form individual cells connected in series with each other. The performance of the entire module can be dominated by a single bad cell. Consequently, significant loss of material

from one cell would be enough to require panel replacement. Assuming each module has 100 cells with area of 100 cm² and that a maximum of 10% loss of material/performance is tolerable, the lifetime of a perovskite module would be ~ 2 hr. Note that adjusting the area of the fracture or the percentage of time with rain will have a similar effect. Equation (5), thus, can provide valuable risk assessment to PV companies and policy makers when considering PV deployment location.

3.3.2 Comparing Upstream and Downstream Toxicities

The ratio of downstream to upstream toxicities (D/U) of the metals varied by several orders of magnitude (1.E-09 for SnS to 4.0E+01 for CuSCN) (Figure 3-2) (See FigureS. 2 for the raw data of toxicity scores). For the metals that have D/U less than one, the toxicity resulting from these metals in solar cells will mainly be experienced at the mining sites, not where PV is deployed. In order to reduce impacts for these metals, the policy regulations should focus on the mining and purification activities. Six of the eight metals analyzed in this study had D/U less than one. Each of these six metals have small LF values ($LF_{CdS, PbS, SnO_2} \ll 0.01\%$, $LF_{NiO}=0.4\%$ and $LF_{ZnO}=0.09\%$) suggesting that very little metal mass escapes the panel. For these compounds, D/U results also confirm the validity of the common PV LCA practice of omitting use phase emissions since this omission would have minor effects on total life cycle toxicity.

In contrast, if D/U is greater than one, the downstream toxicity of the metal is higher than the upstream toxicity, and policy measures within the life cycle framework should focus on reducing the emissions during deployment. Two metals have D/U values ~ 4 (Pb from

PbI₂ and CuSCN). The cause of these high D/U ratios for CuSCN and PbI₂ is the high solubility in water which results in LF values ranging from ~11% to 100% (See Table 1). With more aggressive deployment time, rainy days or breakage density on the PV surface, the downstream toxicity of CuSCN could potentially be ~8 times higher than the upstream toxicity (See Table A. 2). These results indicate that the downstream impacts from these metals should not be ignored in a life cycle assessment framework.

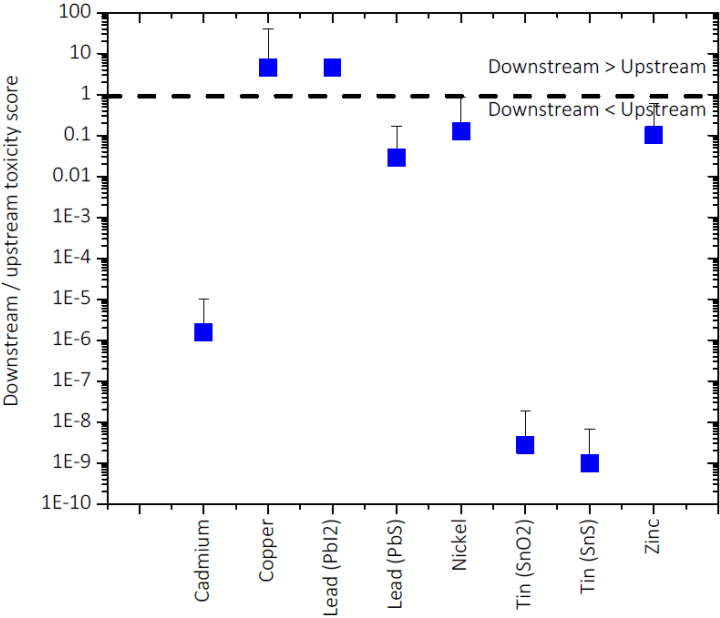


Figure 3-2 Downstream/Upstream toxicities (D/U) of the metals. See Table A. 2, the data points are created using the realistic assumptions and the error bars are added using the worst-case scenario as shown in Table A. 2). Omission of use phase toxicity may result in significant errors in the life cycle analysis of emerging PV for those metals shown above the dashed line. The error bar for PbI₂ is not included since the complete dissolution of the layer content occurs (20 hrs) within a shorter time

A clear example of the impact of LF on the D/U ratios can be seen by comparing PbI_2 ($\text{D/U}=4.6$) and PbS ($\text{D/U}=0.03$). For these two compounds, the upstream toxicity are the same but the downstream toxicities differ by two orders of magnitude due to the large difference in LF ($\text{LF}_{\text{PbS}} \ll 0.01\%$ vs $\text{LF}_{\text{PbI}_2} = 100\%$) due to the difference in K_{sp} of the compound(See Figure 3-2). The LF_{PbS} would be even lower due to the existence of non-water soluble ligands in the PV structure. Consequently, one way to reduce the downstream toxicity is to design solar cells such that metal LF is low during use phase.

We propose a precautionary metal ‘loss limit (LL)’ for each metal defined as the maximum percentage of metal loss that can occur before the toxicity from use phase exceeds the toxicity from mining the metal (i.e. to be below the dashed line in Figure 3-2). The results indicate that CuSCN and PbI_2 may exceed the suggested LL values, and thus, these metals should be deployed in PVs carefully. For example, the emerging solar cells can be encapsulated with thicker layers to withstand harsh weather conditions that would restrict leaching below the limits in Table 2 within the lifetime of the solar cells. Similarly, the LLs could be benchmarks for PV manufacturers in material selection process. Perhaps, the proposed LL limits can innovate R&D efforts to produce eco-friendly PV cells. A clear example for this can be observed in PbS . Contrary to PbI_2 , more stable compound PbS that would not exceed the LL criteria can be preferred for emerging PVs.

The precautionary LL can also be considered in the scope of regulatory directives that restrict the use of specific materials in electronic equipment. Currently, the European

Union uses the precautionary principle for Restriction of Hazardous (RoHS) to limit Cd (0.01 % weight) and Pb (0.1 % weight) in electronics. Photovoltaics are excluded from the scope of RoHS; however, this principle may eventually result in a complete ban of electronic products containing these metals to avoid environmental contamination (Sinha et al., 2008). If this were to occur, this principle may lead to increase in pollution of mining sites because some Cd and Pb is extracted as by-product of copper and zinc mining (Fthenakis et al., 2009). The ban on use of these metals in industry would cause the copper and zinc manufacturers to consider Cd and Pb as nuisance waste products. Instead, we propose to convert these toxic metals to valuable raw materials for PV industry and indirectly, enhance the pollution prevention activities in mining sites. The precautionary LL would allow regulation of these materials in the PV industry to limit the environmental impacts of these materials.

Table 3-2 Precautionary metal lost limit (LL). The LL is the maximum percentage of metal loss that can occur during PV use before the toxicity from use phase exceeds the toxicity from mining the metal. If the metal loss during use phase exceeds LL, then the solar cell causes more toxicity at the location it is used than at the location where it is mined.

| | LL | Comparison with estimated LF |
|----|--------|---|
| Cd | 0.2 % | Does not exceed |
| Cu | 1.2 % | Exceed (CuSCN) |
| Pb | 3.8 % | Exceed (PbI ₂) Does not exceed (PbS) |
| Ni | 3.32% | Does not exceed |
| Sn | 0.07 % | Does not exceed |
| Zn | 1.1 % | Does not exceed |

3.3.3 Application of metal toxicity results to emerging PV structures

This section calculates the total toxicity of downstream and upstream emissions of the metals used in selected emerging PV devices. In order to apply the toxicity results from previous sections to emerging PV structures, details on the PV layers are needed. For each layer in a solar cell, different metals can be used. Even if the same metal is used, the mass of the metal may still vary depending on the design of the cell. In order to evaluate the toxicity implications of this variability, we modeled four types of emerging PV cells previously reported elsewhere. These are PSC (Celik et al., 2016a; You et al., 2014), CZTS (Wang et al., 2014), and QDSC (Kim et al., 2015) (Figure 3-3). It is worth noting that there is a variability in the selection of materials and layer thicknesses for each type of solar cell, as in the given example of the two different PSC architecture. The estimation method used for analyzing the selected PV structures (Figure 3-3) is applicable to other devices once the materials, and metal masses are known. In order to determine the impacts for the representative devices, the analysis (*Equation (5)*) was repeated using the correct mass for each layer (m_o) (see Table A. 3). All other parameters remain the same as Section 3.2.

The metals analysed are shown in bold in the corresponding layer. Mass of metals are estimated based on layer thickness data provided in the papers. Several other metals (Al, In, Au, Ti, Pt, and Mg) have also been used in these structures but were not modelled in this study because the compartment-specific toxicity values do not exist for these metals in the ReCiPe model. Similarly, some layers have organic compounds that were not modelled in this study. The toxicity tools are capable of modelling organic materials' CFs

in very high accuracy. Therefore, organic vs. metal comparisons can be misleading due to the difference in accuracy of the CFs.

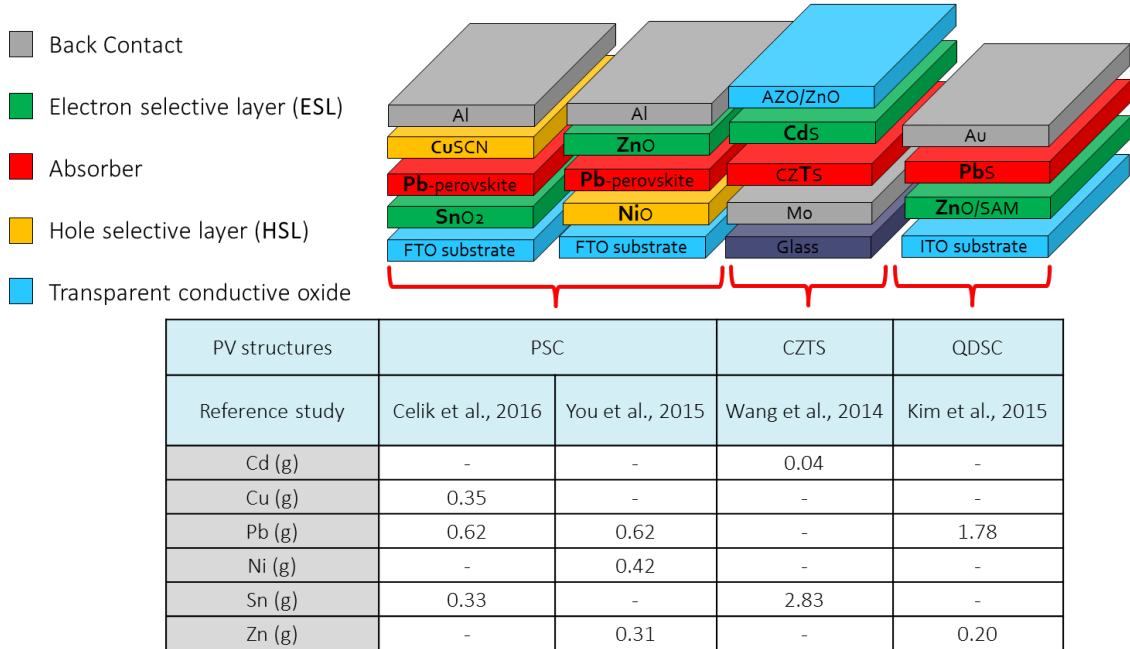


Figure 3-3 The structures of selected emerging PV technologies and the mass of each metal used within 1 m² of PV cell.

The toxicities resulting from the metals used in different functional layers are shown in Figure 3-4. SnO₂, ZnO, and CdS are the three commonly used materials in the electron selective layer (ESL) and their toxicity varied by a factor of 25 (from 0.03 to 0.80). These results are attributed to the upstream toxicity of the metals, and as such, would be similar if the use phase impacts were omitted. CdS used in QDSC had the lowest toxicity because the mass for a very thin layer (25 nm) of CdS layer is low (0.04 g) compared to the mass required for ZnO (0.74 g and 0.40 g) and SnO₂ (0.33 g) layers.

The toxicity of the absorber layers, $\text{CH}_3\text{NH}_3\text{PbI}_3$ (as PbI_2), CZTS, and PbS, vary by a factor of ~ 15 . While the toxicity of the Cu of CZTS and Pb of PbS are primarily due to upstream processing, the downstream toxicity of the Pb has an impact for the PSCs and dominates the total toxicity of these devices. This results in the PSC having the highest impact of the absorber materials. Interestingly, Pb used in the absorber layer of QDSC is ~ 3 times greater in mass than in PSC but its toxicity is much lower due to low solubility product of PbS. These results demonstrate the importance of the LF when determining total toxicity of the device.

Only the two PSC devices utilize a hole selective layer (HSL), and the toxicity of Cu is eight times larger than that of Ni. For Ni, upstream and downstream toxicities are comparable. For Cu, on the other hand, the downstream impacts dominate the total toxicity because the LF is high. As a result, NiO is clearly the low-toxic HSL.

These results show that from an LCA perspective Pb and Cd can be less toxic options than Cu, Zn and Ni. In order to determine if the low toxic impact of these metals is a tool-driven result, the analysis was also performed using Usetox (see Figure A.3). Usetox also confirms that the toxicity of metals from CdS and PbS are comparatively lower than other assessed ESLs and absorbers in this study, respectively. This low toxicity of heavy metals in stable compounds is consistent with the results obtained by others for Cd toxicity in CdTe solar cells (Fthenakis et al., 2005; Kim et al., 2014; Sinha, 2016, 2015; Sinha et al., 2012). These results should alleviate the toxicity concerns raised for metal use in PVs

(Benmessaoud et al., 2016), especially for Pb and Cd. In fact, they show that CdS is the preferred ESL over ZnO due to the lower environmental impacts, and PbS is the preferred absorber over Pb-based PSC and CZTS. This ion specific approach may be considered in the scope of regulatory directives rather than complete bans that restrict the use of specific metals in electronic equipments or PVs. Particularly, the large difference between the toxicities of PbI₂ and PbS, two alternative PV absorbers, support this conclusion.

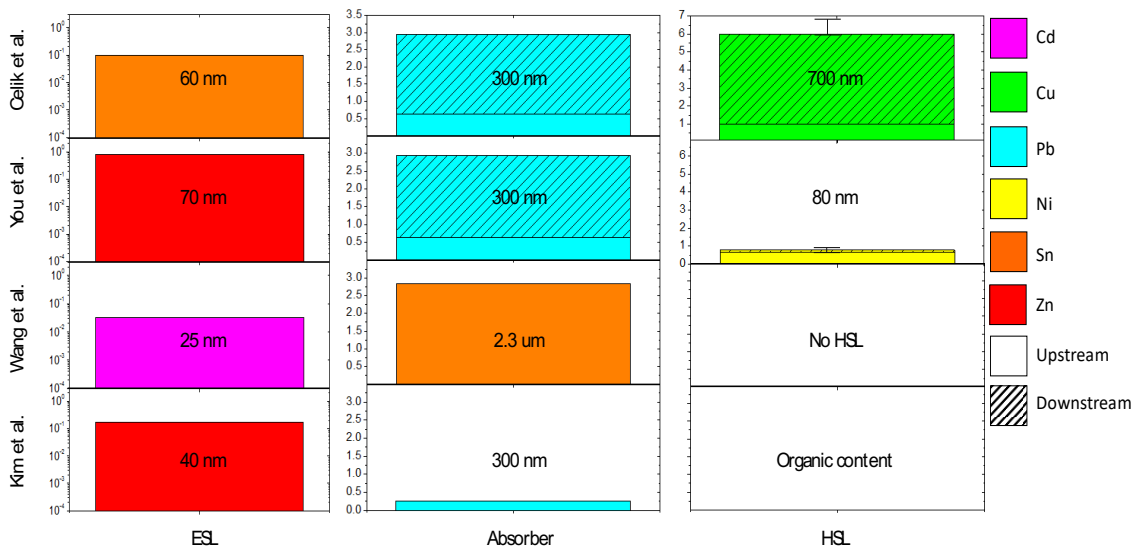


Figure 3-4 Normalised metal toxicity scores from different layers in emerging PV cells

(The raw data before normalisation is provided in Figure A.2 and see Appendix Section 3 for the error bars used in Cu and Ni.). Note that (a) and (c) graphs are in log scale while the other graphs are linear. Also, Sn modeled in CZTS is SnS. Downstream toxicities portion of Pb, Cu and Ni are patterned since only those of downstream have visible toxic impacts. The associated uncertainty of PbI₂ was not given since the complete leach out of Pb from PV module is expected to happen in ~1 day. Among the metal content of each layer, the most soluble compound was chosen for the toxicity comparison.

3.3.4 Comparing the metal emissions from emerging solar PV to those from coal power plants

If emerging PV cells were to be commercialized, an immediate comparison for emissions would be against those from coal-fired power plants (Celik, 2014) that PVs would replace. Table 3 shows a comparison between the mass of upstream and downstream metal emissions per MWh of energy produced from today's coal-fired power plants and emerging PVs. The upstream emissions from emerging PV are three to five orders of magnitude smaller than those of coal power plants.

Downstream emissions are also lower for PV about 25 to 10^5 times lower. Note that this analysis assumes that Pb emissions derive from PbI_2 which resulted in leaching out all the metal content. However, Pb emissions from emerging PV are still lower than those from coal. This conclusion is consistent with the literature (Hailegnaw et al., 2015; Hauck et al., 2017). Similar results can be observed in other emissions. These results point out that major criticisms on the toxicity of metals used in the thin film PVs are not valid since the possible impacts of the emissions would be limited due to the nature of emerging thin film PVs consisting low amounts of metals. Also, note that this analysis assumes a worst-case scenario for emerging PVs in which all the PV modules are damaged in the field conditions. However, in a realistic scenario, the actual breakage is expected to be 1 %, as reported by First Solar (Sinha and Wade, 2015). Inclusion of such a breakage rate would result in 100 times less metal emissions. Based on the realistic estimations, use phase metal emissions due to the emerging PVs are much lower than those from coal power plants.

Table 3-3 The comparison of metal emission rates between coal-fired power generations and emerging PV cells. Coal-fired power plant metal emissions were extracted from the literature (*Babbitt and Lindner, 2005; Rix et al., 2015*) (See details in Section 5 in Appendix B). The data for emerging PV cells were prepared considering the following points: A hypothetical cell was assumed. This cell includes six metals that are covered in this study. For the mass inventory of corresponding materials, the highest values are selected from Figure 3-3. Therefore, emissions due to mining and use phase reflects the highest amounts. For example, to estimate Zn release, 70 nm ZnO layer was used per You et al. (see Figure 2-3.) since it has the highest metal content in Figure 3-3. In order to convert emissions data from per m² to per kWh we assumed a power conversion efficiency of 20 %, Southern European insolation of 1700 kWh/m²/yr, 25 years life time and a performance ratio of 75 %. See the details of calculations in Section 6 in Appendix B.

| (g/MWh) | Emerging PVs | | Coal-fired power plant | |
|---------|---------------------------|---|---------------------------|--|
| | Downstream (Use phase) | Upstream (Metal- extraction phase) | Downstream (Use phase) | Upstream (Coal-extraction phase) |
| Cd | 1.89E-08 | 1.96E-06 | 2.00E-03 | - |
| Cu | 1.99E-01 | 4.39E-04 | 4.87E+00 | 3.94E+00 |
| Pb | 1.00E-01 | 1.26E-04 | 4.57E-01 | 3.67E-01 |
| Ni | 7.19E-03 | 6.54E-06 | 5.84E-01 | 4.69E-01 |
| Sn | 1.02E-07 | 2.82E-07 | - | - |
| Zn | 1.60E-03 | 1.33E-04 | 1.37E+00 | 1.10E+00 |

3.4 Conclusions

We conducted a life cycle toxicity analysis on the metals used in the emerging PV technologies. We developed a dissolution model to estimate LF of metals when PV devices are exposed to moisture. The model incorporates PV properties and outdoor conditions. Using the LF information, we compared the toxic impacts from downstream and upstream emissions of emerging PVs. Our results show that the use phase (downstream) emissions of Pb and Cu in perovskite PVs can be more toxic than those of extraction phase (upstream) and, as such, omitting the toxicity from use phase may result in significant errors in the life cycle analysis of emerging PV. The suggested precautionary limits for LL can be considered to keep the metal related downstream toxicity lower than upstream. From analysing four different PV structures, we found that CdS (compared to ZnO and SnO₂) and PbS (compared to MAPbI₂) are less toxic alternatives for ESL and light absorber, respectively. In addition, we showed that the metal emissions from PVs are expected to be several times less than the emissions from coal.

Chapter 4

Eco-design of Emerging PV Materials

4.1 Introduction

Today's global power consumption is ~6 TW, and this number is expected to increase up to 18 TW by 2050. The projected increase in global energy demand from 2020 and 2050, is approximately 1 GW a day. Addressing 1GW a day challenge, an average nuclear power plant should be built in each day in the next 30 years (globally) (Espinosa et al., 2012). This also means investing \$ 1.6 to \$ 2.7 billion on a daily basis (Wec, 2013). World Energy Council forecasts that the low-carbon energy sources tackling the mitigation of climate change, will play a central role in addressing this challenge and solar PV will be the major driver in the coming renewable energy market (Anctil, 2011; Wec, 2013).

Today, the global installed capacity of solar PV is 300 GWh. 88 % of this capacity are incorporated within wafer-based crystalline silicon (c-Si) technology. c-Si technology is fabricated on semiconducting wafers and can be built without an additional substrate, although modules are typically covered with glass for mechanical stability and protection. The remaining 12 % of the solar PV market relies on thin-film technology. Thin film cell

consist of semiconducting films deposited onto a glass, plastic, or metal substrate. There is a limitation of large scale global market penetration of these technologies due to production costs, material availability, and slow manufacturing (Collier et al., 2014 Espinosa et al., 2012). Emerging PV technologies were developed to overcome these limitations of PV technologies and potentially address the 1 GW-a day challenge.

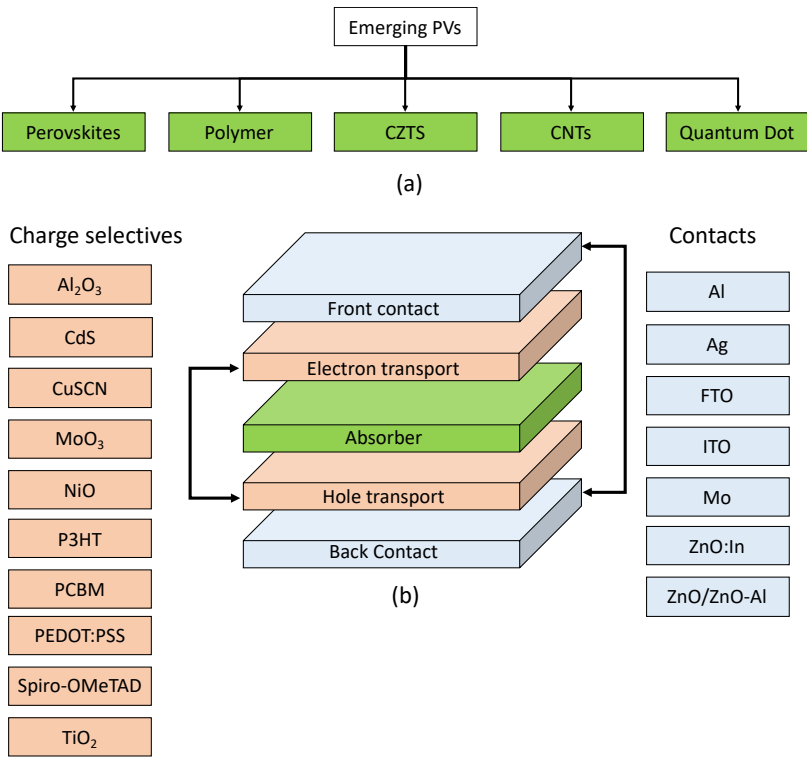


Figure 4-1 Emerging PV types (a) and the cell structure of PV cells (b). The color coding shows the alternative materials that can be used in emerging PV devices. P3HT stands for Poly(3-hexylthiophene-2,5-diyl), PCBM is for phenyl-C61-butyric acid methyl ester and PEDOT:PSS is for poly polystyrene sulfonate.

There are five different emerging PV technologies (Figure). The five technologies are: methylammonium lead halide perovskites ($\text{CH}_3\text{NH}_3\text{PbX}_3$, where $X=\text{I}$, Br , or Cl), polymer, $\text{Cu}_2\text{ZnSnS}_4$ (CZTS), carbon nanotubes (CNTs) and quantum dots (Figure 4-1 a). These PV cells have five thin layers (Figure 4-1 b). The cell mainly consists of an absorber in the middle, two charge selective layers (electron and hole transports) and contact (front and back) in the edges. Each layer has a distinctive purpose within the structure. The purpose of the overall device is to harness the sunlight and create a current by the flow of electrons flow between front and back contacts. The light is transmitted into the absorber layer and excites electron and holes. Electrons and holes flow in and out to the selective layers and moves to the contact, and the current occurs. There are a lot of alternative materials that can be used as charge selective and contacting layer (Figure 4-1 b). Most of these materials are relatively new and purposely optimized to be used in emerging PVs.

Despite the clear interest in analyzing the environmental and economic impacts of emerging materials used in these technologies (Albrecht and Rech, 2017; Ellingson et al., 2005; Jørgensen et al., 2013; Katagiri et al., 2009; Po et al., 2012), the detailed inventories used in the devices have largely been overlooked. The assumptions in modeling the emerging materials and the approaches in estimating manufacturing electricity result in different results from different studies which have not been comparable. For example, Gong et al found the total CO_2 emissions from perovskite device structure as ~ 22 g/kWh while Espinosa (2015) et al. reported the same value as 2,700 g/kWh. Similarly, the CO_2 emissions from fabricating only the perovskite component of the devices also varies ~ 28 times between these studies. Similar to environmental assessments, the economic analysis

on perovskite devices were found to vary 3-4 fold (\$ 30 to \$140) (Cai et al., 2017; Chang et al., 2017; Zhaoning Song et al., 2017). While the cost and environmental impacts of perovskite PVs have been analysed many times by various researcher in different device structure, other emerging PVs have not been explored in detail.

In this study, I aimed to create inventories that offer insight into the environmental impacts, and cost of all the materials used in emerging PV technologies. This study reveals which charge selective and contact materials should be more preferable compared to other alternatives. This question was addressed by assessing the CO₂ emissions and cost of the each alternative layer. The assessments reflect the effect of materials and their processing techniques on the device's economic and environmental performances. Similarly, the alternative absorber layers were investigated to inform the decisions-makers regarding which emerging technologies should enter the commercial market. Finally, an eco-efficiency concept that incorporates the environmental impacts and cost of materials were developed to promote eco-design perspective for emerging PV materials.

4.2 Methods

4.2.1 Life Cycle Inventories

The life cycle inventories for the alternative layers used PV cells, shown in Figure 4-1, were prepared. These materials are shown as promising for commercial production since either they offer low cost production or high efficient solar modules. For example, the use

of inorganic materials such as NiO, CuSCN, SnO₂, MoO₃ and ZnO have been proven in perovskite PV cells as low-cost materials that can also supply high efficiencies (> 20 %). Other inorganic materials such CdS and TiO₂ materials have been already used in commercial thin film technologies. Particularly, CdS could be a low-cost charge selective for CZTS PVs. Al₂O₃ has been assessed in quantum dot PVs that can reach 12 % power conversion efficiency. Organic materials such as P3HT, PEDOT:PSS, PCBM and Spiro-OMeTAD have been analysed in polymer and perovskite materials. Indeed, the flexible polymer solar modules used these organic materials was manufactured in mid-scale by the Technical University of Denmark. Al, Ag, FTO, and ITO layers have been studied in all emerging PV technologies while Al and FTO materials have been already used by PV industry.

The energy inventories for the depositions of the materials were modeled. Table 4.1 lists the methods used for deposition of each layer. These deposition techniques are the most commonly used methods in fabricating of emerging PVs, extracted from the literature. Note that among these methods doctor blading, printing, and spinning are solution-based methods and they can be used interchangeably between the layers. Sputtering and evaporation are thermal methods that are used in the PV market. The electricity consumptions of these methods were scaled up for large scale manufacturing. These efforts were built on the University of Toledo Photovoltaic Innovation Center(PVIC)'s experiences in manufacturing these cells in lab scale. All the deposition methods given in Table 4-1 are used at PVIC labs. The estimation incorporates the time and power required for depositions, pumping, and annealing of each material.

The life cycle inventories for each layer component was built using GaBi 8.0 software. The data for CdSe quantum dots, P3HT, CuI, and Al₂O₃ were created using literature data (Şengül and Theis, 2011; Tsang et al., 2016), while the remaining inventories were taken from our group’s previous studies (Celik et al., 2018, 2016a; I. Celik et al., 2017; Ilke Celik et al., 2017a).

Table 4-1 Deposition methods used in layer processing

| Deposition methods | Layers |
|--------------------------|--|
| Chemical bath deposition | CdS |
| Doctor blading | CNT |
| Printing | CuSCN, CdSe, CuI |
| Spinning | CZTS, Perovskite, NiO, PCBM, PEDOT:PSS, Spiro-OMeTAD, TiO ₂ |
| Sputtering | Mo, ZnO:In, ZnO:ZnO:Al |
| Thermal evaporation | Al, Ag, MoO ₃ , Al ₂ O ₃ |

4.2.2 Cost Assessment

The cost data for the assessment model includes the PV materials and their depositions on the device structure shown in Figure 4-2. The raw cost data for the inventories were taken from Song et al., 2017, Supporting Information Table S1-S3. For the materials, there is little publicly available information on the costs and prices from PV companies. The assumptions and cost data were created using the literature and online sources, including global trading websites, as well as from reports from governments and other

organizations. Some of the data were directly extracted from our group's previous publication (Zhaoning Song et al., 2017). For the manufacturing cost, the processing time, degree of automation for each step and the US electricity price were used.

4.3 Results

4.3.1 Life Cycle Carbon Emissions

The life cycle carbon emissions (global warming potential, GWP) of the absorber (a), charge selective (b) and contact (c) materials are shown in Figure 4-2. GWP results show that CO₂ emissions resulting from one of the back contact material (ITO) and three of the charge selective (CdS, ZnO:In, and ZnO:ZnO-Al) materials are several times higher than those of emissions from absorber materials.

GWP of the absorber materials varied ~2 – 52 g CO₂/ m². These values are three to four orders of magnitude smaller than the GWPs of c-Si, CdTe and CIGS absorber materials commonly used in today's commercial market. Among the absorber materials, CdSe quantum dot material has the highest GWP value (51.54 g CO₂/ m²). The reasons for this high GWP values are the electricity (~55 % of the total CO₂ emissions) and chemicals (butanol, ~24% and methanol, 20 % of the total CO₂ emissions) used in preparing (synthesising, isolation & purification steps) quantum dots. CZTS has the second highest GWP values. High GWP value of CZTS layer is due to electricity consumption for CZTS deposition. CZTS is the thickest absorber layer among the alternatives (2000 nm). Thus, despite the solution-based methods used in deposition (spinning, annealing), the CO₂

emissions due to electricity consumption (4.89 MJ/m²) contributes to the high GWP impact. CNT, perovskite and polymer (mixture of PCBM and P3HT) have low GWP values. For all of these absorber layers, chemicals used in material synthesis dominate the GWP values. The most impactful chemicals used in preparation of perovskite, polymer, and CNT absorber materials are dimethylformamide (84 % of the total impacts), ultrapure water (37 %) and carbon monoxide (90 %), respectively.

Table 4-2 The GWP of commercial PVs

| | c-Si | CdTe | CIGS |
|-------------------------------------|-------|------|-------|
| kg CO ₂ / m ² | 130.2 | 56.3 | 51. 2 |

GWP of the alternative charge selective layers varied by a factor of ~300. CdS has the largest CO₂ emissions among the all the alternatives. The reason for such a high impact is mainly the plasma-enhanced chemical vapor deposition (PECVD) method in preparing CdS. This deposition technique is currently used in manufacturing process of CdTe technology. Among inorganic charge selective materials such as NiO, SnO₂, CuSCN, MoO₃ and TiO₂, NiO has the highest GWP value while TiO₂ has the lowest. For both the layers, the electricity required for depositing the layers is the main contributor. However, the difference between electricity consumption is because of the time required NiO deposition is ~20 times longer than TiO₂. Similar to inorganic charge selective materials, the organic transport layers have low GWP values. All of these organic materials are deposited by solution-based methods. Among the four alternatives, Spiro-OMeTAD was found to be the lowest GWP (50 g CO₂ per m²) charge selective option.

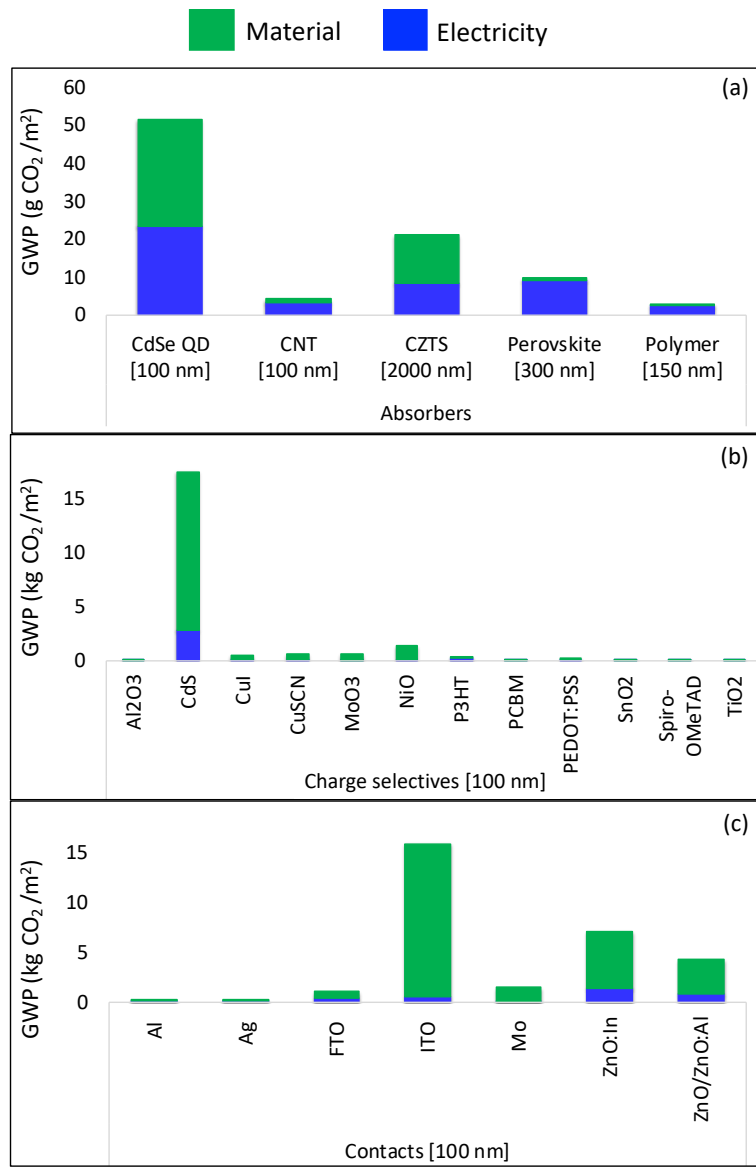


Figure 4-2 The GWP breakdown of emerging materials. Note that the y axis for the absorber materials is in g whereas it is in kg for contacts and charge selectives.

GWP of contact materials varied by several times (from ~100 g CO₂/m² for Al to ~15 kg CO₂/m² for ITO). High GWP of ITO was reported in the literature (Ilke Celik et al., 2017d;

Chatzisideris et al., 2016; García-Valverde et al., 2010). Many studies showed that ITO is the most impactful component of the device when it is used as a back contact of perovskite (Gong et al., 2015b), polymer (Espinosa et al., 2011) and CNT (Ilke Celik et al., 2017a) solar cells. ITO material is deposited by the sputtering method. Mo, ZnO:In and ZnO/ZnO:Al are also sputtered to deposit the materials onto the thin film surface. The main difference for lower GWP values compared to ITO is attributed to the differences in time required for pumping for the sputter and material deposition.

4.3.2 Life Cycle Costing

Figure 4-3 shows the cost of the materials used in emerging PV technologies. CNT and polymer absorbers were found to be the most expensive materials. Although CdSe QD are nanomaterials that requires a lot of step for synthesising process, their costs are much less expensive. CZTS and perovskite are the most promising materials due to their lowest cost.

Similar to absorber materials, the material cost of charge selective materials varies in a large range. Organic materials such as Spiro-OMeTAD and PCBM are the most expensive charge selective alternatives. The cost of P3HT and PEDOT:PSS are relatively lower than other organics since they have been used in the solar industry for a longer time, and as such, their costs have reduced. As it is seen, all the other inorganic materials are much cheaper, as such, are estimated to be more favourable alternatives than organic materials for commercial production.

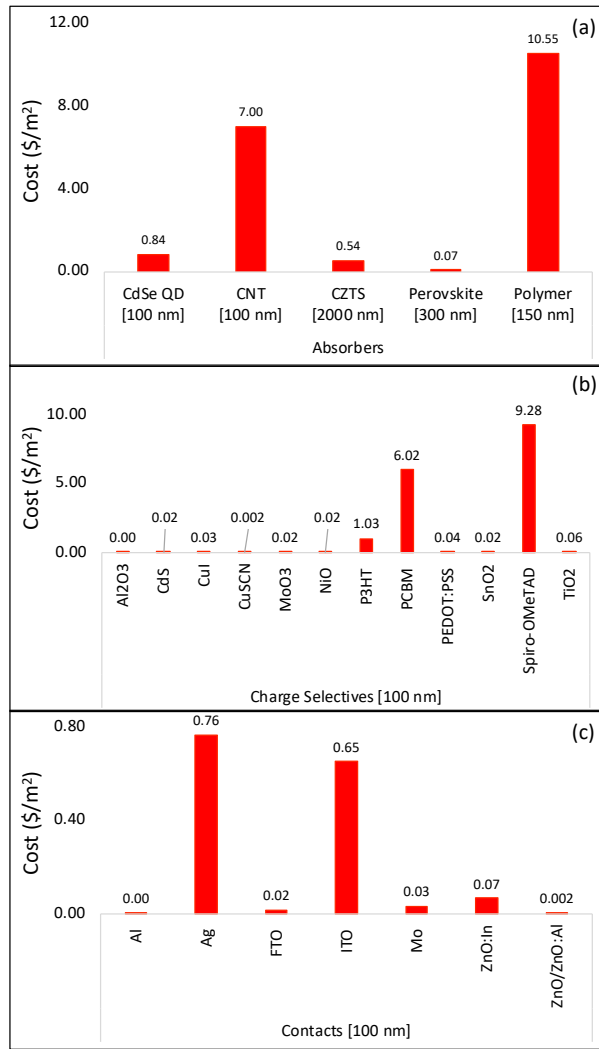


Figure 4-3 Material cost of the different layers used as absorber (a), charge selective (b) and contact (c) materials

Except Ag and ITO, the costs of all contact materials are less than 10 cent/m². Note that despite the high cost, Ag is commercially used in c-Si technology. Similarly, ITO material is also used in commercial market in smart phones and in the windows of planes. Therefore, it may be concluded that all the assessed contact materials may potentially play a role in the future emerging PV market.

4.3.3 Eco-Efficiency of the Material Selection

Eco-efficiency concept for emerging materials was built based on the cost of CO₂ emissions from different PV layers (Figure 4.4). The materials that have high cost but low (Cha et al., 2007)GWP are polymer and CNT absorbers, and Spiro-OMeTAD and PCBM charge selective while the materials with low cost but high GWP are CdS, ITO, ZnO:In, and ZnO:ZnO:Al. Except these materials, all the analysed PV materials are suitable for emerging PV market.

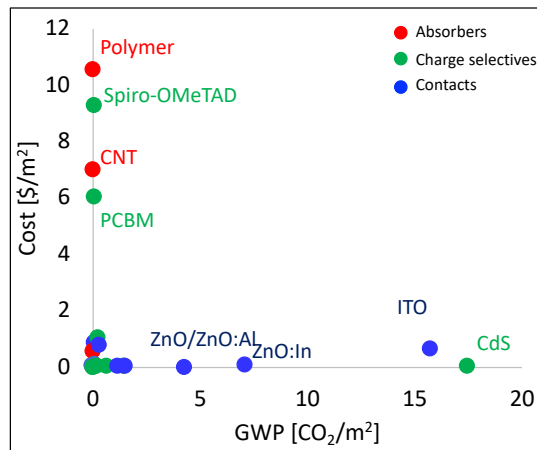


Figure 4-4 The cost of CO₂ emissions from different PV layers

4.4 Conclusions

In this study, I aimed to create inventories that offer insight into the environmental impacts, and cost of all the materials used in emerging PV technologies. The results show that CO₂ emissions from the absorber layers, are much less than the CO₂ emissions from

contact and charge selective layers. CdS and ITO are the highest impact charge selective and contact materials, respectively. The cost assessments showed that the organic materials such as polymer absorber, CNT, P3HT and Spiro-OMeTAD are the most expensive materials. All the remaining materials have a potential to be used in commercial PV market. Finally, the eco-efficiency analysis showed polymer, and CNT absorbers, Spiro-OMeTAD, PCBM and CdS charge selective and ITO, ZnO:In, and ZnO:ZnO:Al materials should be excluded from the emerging PV market.

Chapter 5

Conclusions

This dissertation aimed to increase the resolution of the emerging PVs' environmental footprint by conducting LCA. It consisted of three studies which incorporate economic and toxicological analysis of the materials used in emerging PVs.

In my first study, I evaluated the environmental impacts of vacuum, solution, and HTL-free perovskite solar cell devices using fabrication approaches that are amenable to large scale manufacturing. A comparison of environmental impacts was made with mono-Si as a reference point. I found that manufacturing of perovskite solar modules causes 10 to 30 % lower impacts than manufacturing mono-Si PV. However, if perovskite cells were to enter the market, their environmental impacts would be higher than those of all commercial PV technologies mainly because of their shorter lifetimes. Monte Carlo analysis varying lifetime and efficiencies of perovskite cells showed that HTL-free structure could perform equal or better than mono-Si cells with about 55 % cumulative probability.

To my surprise, the energy requirements of perovskite solar cells were not lower than those of commercial technologies. This result is likely due to incomplete specification of the commercial scale fabrication of perovskite solar cells. The EPBT and GWP varied from 1.0 to 1.5 years and 100-150 g CO₂ equivalence (per kWh). These values are within previously reported data for other perovskite solar cells. Solution-based methods with spray used in perovskite deposition were observed to decrease the overall electricity consumption.

Among the three structures modeled, the HTL-free structure had the lowest environmental impacts in all impact categories, except marine eutrophication. Marine eutrophication impact of the solution and HTL-free structure were dominated by organics (around 95 %). Material impacts attributed to the vacuum-based method were lower than other two methods, except for ecotoxicity. The ecotoxicity value of HTL free structure was around 30 % of the vacuum and solution-based methods because it is missing the HTL made from copper thiocyanate. The impact of lead used in the absorber layer was negligible, which is consistent with the literature.

In my second work, I studied the end use toxic impact of the emerging PV cells. For this purpose, a life cycle toxicity analysis on the metals used in the emerging PV technologies was conducted. A dissolution model to estimate LF of metals when PV devices are exposed to moisture was developed. The model incorporates PV properties and outdoor conditions. Using the LF information, we compared the toxic impacts from downstream

and upstream emissions of emerging PVs. The results show that the use phase (downstream) emissions of Pb and Cu in perovskite PVs can be more toxic than those of extraction phase (upstream) and, as such, omitting the toxicity from use phase may result in significant errors in the life cycle analysis of emerging PV. The suggested precautionary limits for LL can be considered to keep the metal related downstream toxicity lower than upstream. From analysing four different PV structures, I found that CdS (compared to ZnO and SnO₂) and PbS (compared to MAPbI₂) are less toxic alternatives for ESL and light absorber, respectively. In addition, it was shown that the metal emissions from PVs are expected to be several times less than the emissions from coal.

In my third study, I aim to create inventories that offer insight into the environmental impacts, and cost of all the materials used in emerging PV technologies. The result show that CO₂ emissions due to absorber layers, are much less than the CO₂ emissions due to contact and charge selective layers. CdS and ITO are the most impactful material that can be used as a charge selective and contact material, respectively. The cost assessments show that the organic materials such as polymer absorber, CNT, P3HT and Spiro-OMeTAD are the most expensive materials. All the remaining materials have a potential to be used in commercial PV market. Finally, the eco-efficiency analysis showed polymer, and CNT absorbers, Spiro-OMeTAD, PCBM and CdS charge selective and ITO, ZnO:In, and ZnO:ZnO:Al materials should be excluded from emerging PV market.

Chapter 6

Limitations and Recommendations to Future Works

One limitation of this work is excluding the end of life phase analysis from the life cycle assessments. Solar panels can be either recycled or landfilled in their end of life. Unfortunately, there is no federal law in the US regarding the recycling of the solar modules. The common practice used is recycling the glass substrate and landfilling the solar materials. Particularly, landfilling of solar material is considered as a harmless alternative since commercial PV modules do not consist of insoluble toxic materials. However, emerging technologies contain a lot of toxic and soluble materials, therefore, the landfilling scenario is not a convenient option for them. When I prepared my LCA models, there was limited data regarding how the emerging technologies should be recycled. Therefore, I did not include the end of life phase in my analysis. I recommend that future LCA studies to cover the emerging PVs' recycling phase, since there is recent experimental data that shows how emerging PVs can be recycled (Binek et al., 2016).

Second limitation is perhaps GaBi software package that used in this work. I noticed some significant differences between the data from Usetox and GaBi, although GaBi gives the

results for Usetox assessment tool. The disparities between the two analysis might be due to the assumption that GaBi makes in the assessment. However, GaBi does not disclosure the assumptions or the approximations that it uses in running the software, therefore, it is hard to find what causes the disparities. I suggest to future researcher to do detailed analysis regarding the differences between the LCA software packages on toxicity assessment. I believe if the three available sources run at the same time (GaBi, SimaPro and Usetox), then all the disparities regarding the toxicity calculations of the sources are enlightened and perhaps, the reasons can be found.

References

Albrecht, S., Rech, B., 2017. Perovskite solar cells: On top of commercial photovoltaics. *Nat. Energy* 2, 16196. <https://doi.org/10.1038/nenergy.2016.196>

Alsema, E.A., 2006. Energy Requirements and CO₂ Mitigation Potential of PV Systems.

Anctil, A., 2011. Fabrication and life cycle assessment of organic photovoltaics.

Anctil, A., Fthenakis, V., 2006. Life Cycle Assessment of Organic Photovoltaics.

Babbitt, C.W., Lindner, A.S., 2005. A life cycle inventory of coal used for electricity production in Florida. *J. Clean. Prod.* 13, 903–912. <https://doi.org/10.1016/j.jclepro.2004.04.007>

Bailie, C.D., Christoforo, M.G., Mailoa, J.P., Bowring, A.R., Unger, E.L., Nguyen, W.H., Burschka, J., Pellet, N., Lee, J.Z., Grätzel, M., Noufi, R., Buonassisi, T., Salles, A., McGehee, M.D., 2014. Semi-transparent perovskite solar cells for tandems with silicon and CIGS. *Energy Environ. Sci.* 8, 956–963. <https://doi.org/10.1039/C4EE03322A>

Bauer, D., Diamond, D., Li, J., Sandalow, D., Telleen, P., Wanner, B., 2011. Critical Materials Strategy.

Benmessaoud, I.R., Horváth, E., Maco, B., Spina, M., Lashuel, H.A., Forró, L., 2016. Health hazards of methylammonium lead iodide based perovskites: cytotoxicity studies. *Toxicol. Res. (Camb)*. 5, 407–419. <https://doi.org/10.1039/c5tx00303b>

Berhe, T.A., Su, W.-N., Chen, C.-H., Pan, C.-J., Cheng, J.-H., Chen, H.-M., Tsai, M.-C., Chen, L.-Y., Dubale, A.A., Hwang, B.-J., 2016. Organometal halide perovskite solar cells: degradation and stability. *Energy Environ. Sci.* 9, 323–356. <https://doi.org/10.1039/C5EE02733K>

Bhandari, K.P., Collier, J.M., Ellingson, R.J., Apul, D.S., 2015. Energy payback time (EPBT) and energy return on energy invested (EROI) of solar photovoltaic systems: A systematic review and meta-analysis. *Renew. Sustain. Energy Rev.* 47, 133–141. <https://doi.org/10.1016/j.rser.2015.02.057>

Binek, A., Petrus, M.L., Huber, N., Bristow, H., Hu, Y., Bein, T., Docampo, P., 2016. Recycling Perovskite Solar Cells to Avoid Lead Waste. *ACS Appl. Mater. Interfaces* 8,

12881–12886. <https://doi.org/10.1021/acsami.6b03767>

Bishop, C., 2011. Vacuum deposition onto webs, films and foils.

Brun, N.R., Wehrli, B., Fent, K., 2016. Ecotoxicological assessment of solar cell leachates: Copper indium gallium selenide (CIGS) cells show higher activity than organic photovoltaic (OPV) cells. *Sci. Total Environ.* 543, 703–714. <https://doi.org/10.1016/j.scitotenv.2015.11.074>

Burschka, J., Pellet, N., Moon, S.J., Humphry-Baker, R., Gao, P., Nazeeruddin, M.K., Grätzel, M., 2015. Sequential deposition as a route to high-performance perovskite-sensitized solar cells. *Nature* 499, 316.

Chen, C., Li, C., Li, F., Wu, F., Tan, F., Zhai, Y., ZhC., W., Chen, C.L., F. Li, F.W., Tan, F., Zhai, Y., Zhang, W., 2014. Efficient perovskite solar cells based on low-temperature solution-processed (CH₃NH₃) PbI₃ perovskite/CuInS₂ planar heterojunctions. *Nanoscale Res. Lett.* 9, 1–8.

Cai, M., Wu, Y., Chen, H., Yang, X., Qiang, Y., Han, L., 2017. Cost-Performance Analysis of Perovskite Solar Modules. *Adv. Sci.* 4. <https://doi.org/10.1002/advs.201600269>

Celik, I., 2014. Source Apportionment of Trace Elements in Ankara. Middle East Technical University.

Celik, I., Mason, B.E., Phillips, A.B., Heben, M.J., Apul, D.S., 2017a. Environmental Impacts from Photovoltaic Solar Cells Made with Single Walled Carbon Nanotubes. *Environ. Sci. Technol.* 51, 4722–4732. <https://doi.org/10.1021/acs.est.6b06272>

Celik, I., Phillips, A.B., Song, Z., Yan, Y., Ellingson, R.J., Heben, M.J., Apul, D., 2017b. Energy Payback Time (EPBT) and Energy Return on Energy Invested (EROI) of Perovskite Tandem Photovoltaic Solar Cells. *IEEE J. Photovoltaics* 8, 2156–2161.

Celik, I., Phillips, A.B., Song, Z., Yan, Y., Ellingson, R.J., Heben, M.J., Apul, D., 2017c. Environmental analysis of perovskites and other relevant solar cell technologies in a tandem configuration. *Energy Environ. Sci.* <https://doi.org/10.1039/C7EE01650F>

Celik, I., Tamimi, L. M., Al-Khatib, I. A., & Apul, D. S. (2017). Management of rainwater harvesting and its impact on the health of people in the Middle East: case study from Yatta town, Palestine. *Environmental monitoring and assessment*, 189(6), 271.

Celik, I., Phillips, A.B., Song, Z., Yan, Y., Ellingson, R.J., Heben, M.J., Apul, D., 2017d. Environmental analysis of perovskites and other relevant solar cell technologies in a tandem configuration. *Energy Environ. Sci.* 10. <https://doi.org/10.1039/C7EE01650F>

Celik, I., Song, Z., Cimaroli, A.J.A.J., Yan, Y., Heben, M.J.M.J., Apul, D., 2016a. Life

Cycle Assessment (LCA) of perovskite PV cells projected from lab to fab. *Sol. Energy Mater. Sol. Cells* 156, 157–169. <https://doi.org/10.1016/j.solmat.2016.04.037>

Celik, I., Song, Z., Heben, M.J., Yan, Y., Apul, D.S., 2016b. Life cycle toxicity analysis of emerging PV cells, in: 2016 IEEE 43rd Photovoltaic Specialists Conference (PVSC). IEEE, pp. 3598–3601. <https://doi.org/10.1109/PVSC.2016.7750343>

Celik, I., Song, Z., Phillips, A.B., Heben, M.J., Apul, D., 2018. Life cycle analysis of metals in emerging photovoltaic (PV) technologies: A modeling approach to estimate use phase leaching. *J. Clean. Prod.* 186. <https://doi.org/10.1016/j.jclepro.2018.03.063>

Çelik, İ., & Demirer, G. N. (2015). Biogas production from pistachio (*Pistacia vera* L.) processing waste. *Biocatalysis and Agricultural Biotechnology*, 4(4), 767-772.

Cha, K., Lim, S., Hur, T., 2007. Eco-efficiency approach for global warming in the context of Kyoto Mechanism 7, 4–10. <https://doi.org/10.1016/j.ecolecon.2007.09.016>

Chang, N.L., Yi Ho-Baillie, A.W., Basore, P.A., Young, T.L., Evans, R., Egan, R.J., 2017. A manufacturing cost estimation method with uncertainty analysis and its application to perovskite on glass photovoltaic modules. *Prog. Photovoltaics Res. Appl.* 25, 390–405. <https://doi.org/10.1002/pip.2871>

Chatzisideris, M.D., Espinosa, N., Laurent, A., Krebs, F.C., 2016. Ecodesign perspectives of thin-film photovoltaic technologies: A review of life cycle assessment studies. *Sol. Energy Mater. Sol. Cells* 1–9. <https://doi.org/10.1016/j.solmat.2016.05.048>

Christians, J.A., Fung, R.C., Kamat, P. V., 2013. An inorganic hole conductor for organolead halide perovskite solar cells. Improved hole conductivity with copper iodide. *J. Am. Chem. Soc.* 136, 136(2), 758-764.

Collier, J., Celik, I., Apul, D., 2016. Development of a new online learning module on solar energy sustainability, in: 2016 IEEE 43rd Photovoltaic Specialists Conference (PVSC). IEEE, pp. 3296–3299. <https://doi.org/10.1109/PVSC.2016.7750275>

Collier, J., Wu, S., Apul, D., 2014a. Life cycle environmental impacts from CZTS (copper zinc tin sulfide) and Zn₃P₂ (zinc phosphide) thin film PV (photovoltaic) cells. *Energy* 74, 314–321. <https://doi.org/10.1016/j.energy.2014.06.076>

Conings, B., Baeten, L., Dobbelaere, C., D., D’Haen, J., Manca, J., Boyen, H.G., 2014. Perovskite-based hybrid solar cells exceeding 10% efficiency with high reproducibility using a thin film sandwich approach. *Adv. Mater.* 26, 2041–2046.

Darling, S.B., You, F., 2013. The case for organic photovoltaics. *RSC Adv.* 3, 17633–17648. <https://doi.org/10.1039/C3RA42989J>

Darling, S.B., You, F., Veselka, T., Velosa, A., 2011. Assumptions and the levelized cost

of energy for photovoltaics. *Energy Environ. Sci.* 4, 3133. <https://doi.org/10.1039/c0ee00698j>

Dhere, N.G., 2005. Reliability of PV modules and balance-of-system components, in: Conference Record of the 32nd IEEE Photovoltaic Specialists Conference. IEEE, pp. 1570–1576. <https://doi.org/10.1109/PVSC.2005.1488445>

Docampo, P., Ball, J.M., Darwich, M., Eperon, G.E., Snaith, H.J., 2013. Efficient organometal trihalide perovskite planar-heterojunction solar cells on flexible polymer substrates. *Nat. Commun.* 4, 2761.

Ellingson, R.J., Beard, M.C., Johnson, J.C., Yu, P., Micic, O.I., Nozik, A.J., Shabaev, A., Efros, A.L., 2005. Highly Efficient Multiple Exciton Generation in Colloidal PbSe and PbS Quantum Dots.

Engelenburg, B. Van, Alsema, E., 1993. Environmental aspects and risks of amorphous silicon solar cells.

Espinosa, N., García-Valverde, R., Urbina, A., Krebs, F.C., 2011. A life cycle analysis of polymer solar cell modules prepared using roll-to-roll methods under ambient conditions. *Sol. Energy Mater. Sol. Cells* 95, 1293–1302. <https://doi.org/10.1016/j.solmat.2010.08.020>

Espinosa, N., Hösel, M., Angmo, D., Krebs, F.C., 2012. Solar cells with one-day energy payback for the factories of the future. *Energy Environ. Sci.* 5, 5117–5132. <https://doi.org/10.1039/C1EE02728J>

Espinosa, N., Serrano-luján, L., Urbina, A., Krebs, F.C., 2015. Solution and vapour deposited lead perovskite solar cells: Ecotoxicity from a life cycle assessment perspective. *Sol. Energy Mater. Sol. Cells* 137, 303–310. <https://doi.org/10.1016/j.solmat.2015.02.013>

Espinosa, N., Zimmermann, Y.-S., dos Reis Benatto, G.A., Lenz, M., Krebs, F.C., 2016. Outdoor fate and environmental impact of polymer solar cells through leaching and emission to rainwater and soil. *Energy Environ. Sci.* 9, 1674–1680. <https://doi.org/10.1039/C6EE00578K>

Fraunhofer Institute for Solar Energy Systems ISE, 2016. Photovoltaic Report.

Fthenakis, V., 2009. Sustainability of photovoltaics: The case for thin-film solar cells. *Renew. Sustain. Energy Rev.* 13, 2746–2750. <https://doi.org/10.1016/j.rser.2009.05.001>

Fthenakis, V., 2004. Life cycle impact analysis of cadmium in CdTe PV production, *Renewable and Sustainable Energy Reviews*. <https://doi.org/10.1016/j.rser.2003.12.001>

Fthenakis, V., Kim, H.C., 2011. Photovoltaics: Life-cycle analyses. *Sol. Energy* 85, 1609–

1628. <https://doi.org/10.1016/j.solener.2009.10.002>

Fthenakis, V., Kim, H.C., Frischknecht, R., 2011. Life cycle inventories and life cycle assessment of photovoltaic systems. IEA.

Fthenakis, V., Wang, W., Kim, H.C., 2009. Life cycle inventory analysis of the production of metals used in photovoltaics. *Renewable and Sustainable Energy Reviews*, 13(3), 493–517. [htt. Renew. Sustain. Energy Rev. 13, 493–517.](http://www.sciencedirect.com/science/article/pii/S136403210900012) <https://doi.org/10.1016/j.rser.2007.11.012>

Fthenakis, V.M., 2000. End-of-life management and recycling of PV modules. *Energy Policy* 28, 1051–1058. [https://doi.org/10.1016/S0301-4215\(00\)00091-4](https://doi.org/10.1016/S0301-4215(00)00091-4)

Fthenakis, V.M., Fuhrmann, M., Heiser, J., Lanzirotti, a., Fitts, J., Wang, W., 2005. Emissions and encapsulation of cadmium in CdTe PV modules during fires. *Prog. Photovoltaics Res. Appl.* 13, 713–723. <https://doi.org/10.1002/pip.624>

Fthenakis, V.M., Kim, H.C., Alsema, E., 2008. Emissions from Photovoltaic Life Cycles. *Energy* 42, 2168–2174. <https://doi.org/10.1021/es071763q>

García-Valverde, R., Cherni, J. a., Urbina, A., 2010. Life cycle analysis of organic photovoltaic technologies. *Prog. Photovoltaics Res. Appl.* 18, 535–538. <https://doi.org/10.1002/pip.967>

Geisler, G., Hofstetter, T.B., Hungerbühler, K., 2004. Production of fine and speciality chemicals: procedure for the estimation of LCIs. *Int. J. Life Cycle Assess.* 9, 101–113. <https://doi.org/10.1007/BF02978569>

Goe, M., Gaustad, G., 2014. Strengthening the case for recycling photovoltaics: An energy payback analysis. *Appl. Energy* 120, 41–48. <https://doi.org/10.1016/j.apenergy.2014.01.036>

Goedkoop, M., Heijungs, R., Huijbregts, M., De Schryver, A., Struijs, J., Van Zelm, R., 2008. A life cycle impact assessment method which comprises harmonised category indicators at the midpoint and the endpoint level 1. *ReciPe* 2008.

Gong, J., Darling, S., You, F., 2015. Perovskite Photovoltaics: Life-Cycle Assessment of Energy and Environmental Impacts. *Energy Environ. Sci.* 8, 1953–1968. <https://doi.org/10.1039/C5EE00615E>

Graedel, T.E., Allenby, B.R., 2010. *Industrial ecology and sustainable engineering*. Prentice Hall.

Graetzel, M., Janssen, R., Mitzi, D., Sargent, E., 2012. Materials interface engineering for solution-processed photovoltaics. *Nature*.

Graetzel, M., Janssen, R.A.J., Mitzi, D.B., Sargent, E.H., 2012. Materials interface engineering for solution-processed photovoltaics. *Nature* 488, 304–312. <https://doi.org/10.1038/nature11476>

Green, M.A., Ho-Baillie, A., Snaith, H.J., 2014. Green, M. A., Ho-Baillie, A., & Snaith, H. J. The emergence of perovskite solar cells. *Nat. Photonics* 8.

Guo, Y., Liu, C., Tanaka, H., Nakamura, E., 2015. Air-stable and solution-processable perovskite photodetectors for solar-blind UV and visible light. *J. Phys. Chem. Lett.* 6, 535–539.

Gustafsson, J.P., 2006. Visual minteq. Capturado em 26.

Hagedorn, G., and Hellriegel, E., 1992. Umweltrelevante Masseneinträgen bei der Herstellung verschiedener Solarzellentypen. Munchen.

Hagedorn, G., S. Lichtenberg and H. Kuhn, K., 1989. Energieverbrauch für die Herstellung von Solarzellen und photovoltaischen Kraftwerken. Munchen.

Hailegnaw, B., Kirmayer, S., Edri, E., Hodes, G., Cahen, D., 2015. Rain on Methyl-Ammonium-Lead-Iodide Based Perovskites: Possible Environmental Effects of Perovskite Solar Cells. *J. Phys. Chem. Lett.* 150407164831001. <https://doi.org/10.1021/acs.jpcclett.5b00504>

Hauck, M., Ligthart, T., Schaap, M., Boukris, E., Brouwer, D., 2017. Environmental benefits of reduced electricity use exceed impacts from lead use for perovskite based tandem solar cell. *Renew. Energy.* <https://doi.org/10.1016/j.renene.2017.04.044>

Hauschild, M.Z., Huijbregts, M., Jolliet, O., Macleod, M., Margni, M., Van De Meent, D., Rosenbaum, R.K., McKone, T.E., 2008. Building a model based on scientific consensus for life cycle impact assessment of chemicals: The search for harmony and parsimony. *Environ. Sci. Technol.* 42, 7032–7037. <https://doi.org/10.1021/es703145t>

Henderson, A.D., Hauschild, M.Z., van de Meent, D., Huijbregts, M. a J., Larsen, H.F., Margni, M., McKone, T.E., Payet, J., Rosenbaum, R.K., Jolliet, O., 2011. Usetox fate and ecotoxicity factors for comparative assessment of toxic emissions in life cycle analysis: sensitivity to key chemical properties. *Int. J. Life Cycle Assess.* 16, 701–709. <https://doi.org/10.1007/s11367-011-0294-6>

Heo, J.H., Im, S.H., Noh, J.H., Mandal, T.N., Lim, C.S., Chang, J.A., Grätzel, M., 2013. Efficient inorganic–organic hybrid heterojunction solar cells containing perovskite compound and polymeric hole conductors. *Nat. Photonics* 7, 486.

Hong, J., Chen, W., Qi, C., Ye, L., Xu, C., 2016. Life cycle assessment of multicrystalline silicon photovoltaic cell production in China. *Sol. Energy* 133, 283–293. <https://doi.org/10.1016/j.solener.2016.04.013>

- Huijbregts, M.A.J., Thissen, U., Jager, T., van de Meent, D., Ragas, A.M.J., 2000. Priority assessment of toxic substances in life cycle assessment. Part II: assessing parameter uncertainty and human variability in the calculation of toxicity potentials. *Chemosphere* 41, 575–88. [https://doi.org/10.1016/S0045-6535\(00\)00031-X](https://doi.org/10.1016/S0045-6535(00)00031-X)
- Hwang, K., Jung, Y.S., Heo, Y.J., Scholes, F.H., Watkins, S.E., Subbiah, J., ..., Vak, D., 2015. Toward large scale roll-to-roll production of fully printed perovskite solar cells. *Adv. Mater.* 27(7), 1241-1247. 27, 1241–1247.
- IEA, 2013. Medium-Term Renewable Energy Market Report 2013 Market trends and projections to 2018.
- International Energy Agency, 2014. Technology roadmap: solar photovoltaic energy.
- IRENA - International Renewable Energy Agency, 2016. Roadmap for a renewable energy future.
- ISO, 2006. ISO,14044:environmentalmanagement – life cycleassessment – require- ments andguidelines, International Organizationfor Standardization,2006. (accessed 10.26.16).
- Jeon, N.J., Noh, J.H., Yang, W.S., Kim, Y.C., Ryu, S., Seo, J., Seok, S.I., 2015. Compositional engineering of perovskite materials for high-performance solar cells. *Nature*, 517(7535), 476. 517, 476.
- Jolliet, O., Margni, M., Charles, R., Humbert, S., Payet, J., Rebitzer, G., Rosenbaum, R., 2003. IMPACT 2002+: A new life cycle impact assessment methodology. *Int. J. Life Cycle Assess.* 8, 324–330. <https://doi.org/10.1007/BF02978505>
- Jørgensen, M., Carlé, J.E., Søndergaard, R.R., Lauritzen, M., Dagnæs-Hansen, N. a., Byskov, S.L., Andersen, T.R., Larsen-Olsen, T.T., Böttiger, A.P.L., Andreasen, B., Fu, L., Zuo, L., Liu, Y., Bundgaard, E., Zhan, X., Chen, H., Krebs, F.C., 2013. The state of organic solar cells - A meta analysis. *Sol. Energy Mater. Sol. Cells* 119, 84–93. <https://doi.org/10.1016/j.solmat.2013.05.034>
- Jørgensen, M., Norrman, K., Krebs, F.C., Jørgensen, M., 2008a. Stability/degradation of polymer solar cells. *Sol. Energy Mater. Sol. Cells* 92, 686–714. <https://doi.org/10.1016/j.solmat.2008.01.005>
- Jørgensen, M., Norrman, K., Krebs, F.C., Jørgensen, M., Norrman, K., Krebs, F.C., 2008b. Stability/degradation of polymer solar cells. *Sol. Energy Mater. Sol. Cells* 92, 686–714. <https://doi.org/10.1016/j.solmat.2008.01.005>
- Journey Staff, 2012. Reduce. <http://www.coca-colacompany.com/stories/reduce>.
- Jr, P., Carlito, S., Savenije, T., Mohamed, A., Kaibo, Y., Arkady, Y., Tobjörn, P., Harlang, T., 2014. Organometal halide perovskite solar cell materials rationalized: ultrafast charge generation, high and microsecond-long balanced mobilities, and slow recombination. *J. Am. Chem. Soc.* 136, 5189–5192.

Jung, H.S., Park, N.G., 2015. Perovskite solar cells: from materials to devices. *Small* 11, 10–25.

Katagiri, H., Jimbo, K., Maw, W.S., Oishi, K., Yamazaki, M., Araki, H., Takeuchi, A., 2009. Development of CZTS-based thin film solar cells. *Thin Solid Films* 517, 2455–2460. <https://doi.org/10.1016/j.tsf.2008.11.002>

Ke, W., Fang, G., Liu, Q., Xiong, L., Qin, P., Tao, H., Yang, G., 2015. Low-temperature solution-processed tin oxide as an alternative electron transporting layer for efficient perovskite solar cells. *J. Am. Chem. Soc.* 137, 6730–6733.

Kim, G.-H., Arquer, F.P.G. de, Yoon, Y.J., Lan, X., Liu, M., Voznyy, O., Yang, Z., Fan, F., Ip, A.H., Kanjanaboos, P., Hoogland, S., Kim, J.Y., Sargent, E.H., 2015. High-Efficiency Colloidal Quantum Dot Photovoltaics via Robust Self-Assembled Monolayers.

Kim, H.C., Cha, K., Fthenakis, V., Sinha, P., Hur, T., 2014. Life cycle assessment of cadmium telluride photovoltaic (CdTe PV) systems. *Sol. Energy* 103, 78–88. <https://doi.org/10.1016/j.solener.2014.02.008>

Kushnir, D., Sandén, B.A., 2008. Energy Requirements of Carbon Nanoparticle Production. *J. Ind. Ecol.* 12, 360–375. <https://doi.org/10.1111/j.1530-9290.2008.00057.x>

Latunussa, C.E.L., Ardente, F., Blengini, G.A., Mancini, L., 2016. Life Cycle Assessment of an innovative recycling process for crystalline silicon photovoltaic panels. *Sol. Energy Mater. Sol. Cells* 1–11. <https://doi.org/10.1016/j.solmat.2016.03.020>

Lee, M.M., Teuscher, J., Miyasaka, T., Murakami, T.N., Snaith, H.J., 2012. Efficient hybrid solar cells based on meso-superstructured organometal halide perovskites. *Science* (80-.). 1228604.

Li, X., Tschumi, M., Han, H., Babkair, S.S., Alzubaydi, R.A., Ansari, A.A., 2015. Outdoor performance and stability under elevated temperatures and long-term light soaking of triple-layer mesoporous perovskite photovoltaics. *Energy Technol.* 3, 551–555.

Liu, M., Johnston, M.B., Snaith, H.J., 2013. Efficient planar heterojunction perovskite solar cells by vapour deposition. *Nature* 501, 395.

Lizin, S., Van Passel, S., De Schepper, E., Maes, W., Lutsen, L., Manca, J., Vanderzande, D., 2013. Life cycle analyses of organic photovoltaics: a review. *Energy Environ. Sci.* 6, 3136. <https://doi.org/10.1039/c3ee42653j>

MacLeod, M., Woodfine, D.G., Mackay, D., McKone, T., Bennett, D., Maddalena, R., 2001. BETR North America: A regionally segmented multimedia contaminant fate model for North America. *Environ. Sci. Pollut. Res.* 8, 156. <https://doi.org/10.1007/BF02987379>

Maddalena, R.L., McKone, T.E., Layton, D.W., Hsieh, D.P.H., 1995. Comparison of multi-media transport and transformation models: Regional Fugacity model vs. CalTOX.

Chemosphere 30, 869–889. [https://doi.org/10.1016/0045-6535\(94\)00447-3](https://doi.org/10.1016/0045-6535(94)00447-3)

Meijer, A., Huijbregts, M.A.J., Schermer, J.J., Reijnders, L., 2003. Life-cycle assessment of photovoltaic modules: Comparison of mc-Si, InGaP and InGaP/mc-Si solar modules. *Prog. Photovoltaics Res. Appl.* 11, 275–287. <https://doi.org/10.1002/pip.489>

Michael, V., 2012. Fabrication of OLED on FTO and ITO Coated Substrates. De Montfort University.

Noh, J., Jeon, N., Choi, Y., Nazeeruddin, M., 2013. Nanostructured TiO₂/CH₃NH₃PbI₃ heterojunction solar cells employing spiro-OMeTAD/Co-complex as hole-transporting material. *J. Mater.*

Noyes, A.A., Whitney, W.R., 1897. The rate of solution of solid substances in their own solutions. *J. Am. Chem. Soc.* 19, 930–934. <https://doi.org/10.1021/ja02086a003>

NREL, 2017. Best-Research-Cell Efficiencies [WWW Document]. URL <https://www.nrel.gov/pv/assets/images/efficiency-chart.png> (accessed 1.4.17).

Owens, T., Ungers, L., Briggs, T., 1980. Estimates of occupational safety and health impacts resulting from large-scale production of major photovoltaic technologies.

Park, N.G., 2015. Perovskite solar cells: an emerging photovoltaic technology. *Mater. Today* 18, 65–72.

Phylipsen, G.J., Alsema, E.A., 1995. Environmental life-cycle assessment of multicrystalline silicon solar cell modules. *Analysis* 65.

Pizzol, M., Christensen, P., Schmidt, J., Thomsen, M., 2011a. Eco-toxicological impact of “metals” on the aquatic and terrestrial ecosystem: A comparison between eight different methodologies for Life Cycle Impact Assessment (LCIA). *J. Clean. Prod.* 19, 687–698. <https://doi.org/10.1016/j.jclepro.2010.12.008>

Pizzol, M., Christensen, P., Schmidt, J., Thomsen, M., 2011. Impacts of “metals” on human health: a comparison between nine different methodologies for Life Cycle Impact Assessment (LCIA). *J. Clean. Prod.* 19, 646–656. <https://doi.org/10.1016/j.jclepro.2010.05.007>

Po, R., Carbonera, C., Bernardi, A., Tinti, F., Camaioni, N., 2012. Polymer- and carbon-based electrodes for polymer solar cells: Toward low-cost, continuous fabrication over large area. *Sol. Energy Mater. Sol. Cells* 100, 97–114. <https://doi.org/10.1016/j.solmat.2011.12.022>

Qin, P., Tanaka, S., Ito, S., Tetreault, N., Manabe, K., Nishino, H., Grätzel, M., 2014. Inorganic hole conductor-based lead halide perovskite solar cells with 12.4% conversion efficiency. *Nat. Commun.* 5, 3834.

- Rand, B.P., Genoe, J., Heremans, P., Poortmans, J., 2007. Solar Cells Utilizing Small Molecular Weight Organic Semiconductors. *Prog. Photovolt Res. Appl.* 15, 659–676. <https://doi.org/10.1002/pip>
- Raugei, M., Bargigli, S., Ulgiati, S., 2007. Life cycle assessment and energy pay-back time of advanced photovoltaic modules: CdTe and CIS compared to poly-Si. *Energy* 32, 1310–1318. <https://doi.org/10.1016/j.energy.2006.10.003>
- Raugei, M., Fthenakis, V., 2010. Cadmium flows and emissions from CdTe PV: future expectations. *Energy Policy* 38, 5223–5228. <https://doi.org/10.1016/j.enpol.2010.05.007>
- Rix, A., Steyl, J., Rudman, M.J., Terblanche, U., van Niekerk, J., 2015. First Solar 's CdTe module technology – performance , life cycle , health and safety impact assessment.
- Roes, A.L., Alsema, E.A., Blok, K., Patel, M.K., 2009. Ex-ante environmental and economic evaluation of polymer photovoltaics. *Prog. Photovoltaics Res. Appl.* 17, 372–393. <https://doi.org/10.1002/pip.891>
- Romeo, A., Terheggen, M., Abou-Ras, D., Bätzner, D.L., Haug, F.J., Kälin, M., ..., Tiwari, A.N., 2004. Development of thin-film Cu (In, Ga) Se₂ and CdTe solar cells. *Prog. Photovoltaics Res. Appl.* 12(2-3), 93-111. 12., 93–111.
- Ryberg, M., Vieira, M.D.M., Zgola, M., Bare, J., Rosenbaum, R.K., 2014. Updated US and Canadian normalization factors for TRACI 2.1. *Clean Technol. Environ. Policy* 16, 329–339. <https://doi.org/10.1007/s10098-013-0629-z>
- Şengül, H., Theis, T.L., 2011. An environmental impact assessment of quantum dot photovoltaics (QDPV) from raw material acquisition through use. *J. Clean. Prod.* 19, 21–31. <https://doi.org/10.1016/j.jclepro.2010.08.010>
- Serrano-Lujan, L., Espinosa, N., Larsen-Olsen, T.T., Abad, J., Urbina, A., Krebs, F.C., 2015. Tin- and lead-based perovskite solar cells under scrutiny: An environmental perspective. *Adv. Energy Mater.* 5, 1–5. <https://doi.org/10.1002/aenm.201501119>
- Shahan, Z., 2015. Global Solar Power Capacity About To Hit 200 GW [WWW Document]. <http://cleantechnica.com/2015/07/11/global-solar-power-capacity-about-to-hit-200->. URL <http://cleantechnica.com/2015/07/11/global-solar-power-capacity-about-to-hit-200-gw/> (accessed 7.24.16).
- Shockley, W., Queisser, H.J., 1961. Detailed Balance Limit of Efficiency of *p-n* Junction Solar Cells. *J. Appl. Phys.* 32, 510–519. <https://doi.org/10.1063/1.1736034>
- Sinha, P., 2016. Potential environmental hazards of photovoltaic panel disposal: Discussion of Tammaro et al. (2015). *J. Hazard. Mater.* <https://doi.org/10.1016/j.jhazmat.2016.04.021>

Sinha, P., 2015. Cadmium telluride leaching behavior: Discussion of Zeng et al. (2015). *J. Environ. Manage.* 163, 184–185. <https://doi.org/10.1016/j.jenvman.2015.08.015>

Sinha, P., 2013. Life cycle materials and water management for CdTe photovoltaics. *Sol. Energy Mater. Sol. Cells* 119, 271–275. <https://doi.org/10.1016/j.solmat.2013.08.022>

Sinha, P., Balas, R., Krueger, L., Wade, A., 2012. Fate and transport evaluation of potential leaching risks from cadmium telluride photovoltaics. *Environ. Toxicol. Chem.* 31, 1670–1675. <https://doi.org/10.1002/etc.1865>

Sinha, P., Kriegner, C.J., Schew, W. a., Kaczmar, S.W., Traister, M., Wilson, D.J., 2008. Regulatory policy governing cadmium-telluride photovoltaics: A case study contrasting life cycle management with the precautionary principle. *Energy Policy* 36, 381–387. <https://doi.org/10.1016/j.enpol.2007.09.017>

Sinha, P., Wade, A., 2015. Assessment of leaching tests for evaluating potential environmental impacts of PV module field breakage, in: *IEEE Journal of Photovoltaics*.

Snaith, H.J., Abate, A., Ball, J.M., Eperon, G.E., Leijtens, T., Noel, N. K., ..., Zhang, W., 2015. Anomalous hysteresis in perovskite solar cells. *The journal of physical chemistry letters*, 5(9), 1511-1515. *J. Phys. Chem. Lett.* 5, 1511–1515.

Song, Z., McElvany, C.L., Phillips, A.B., Celik, I., Krantz, P.W., Wathage, S.C., Liyanage, G.K., Apul, D., Heben, M.J., 2017. A technoeconomic analysis of perovskite solar module manufacturing with low-cost materials and techniques. *Energy Environ. Sci.* 10. <https://doi.org/10.1039/c7ee00757d>

Song, Z., Wathage, S.C., Phillips, A.B., Heben, M.J., 2016. Pathways toward high-performance perovskite solar cells: review of recent advances in organo-metal halide perovskites for photovoltaic applications. *J. Photonics Energy* 6, 022001. <https://doi.org/10.1117/1.JPE.6.022001>

Song, Z., Wathage, S.C., Phillips, A.B., Tompkins, B.L., Ellingson, R.J., Heben, M.J., 2015. Impact of Processing Temperature and Composition on the Formation of Methylammonium Lead Iodide Perovskites. *Chem. Mater.* 27, 4612–4619. <https://doi.org/10.1021/acs.chemmater.5b01017>

Stoumpos, C.C., Malliakas, C.D., Kanatzidis, M.G., 2013. Semiconducting tin and lead iodide perovskites with organic cations: phase transitions, high mobilities, and near-infrared photoluminescent properties. *Inorg. Chem.* 52, 9019–9038.

Stranks, S.D., Eperon, G.E., Grancini, G., Menelaou, C., Alcocer, M.J.P., Leijtens, T., Herz, L.M., Petrozza, A., Snaith, H.J., 2013. Electron-Hole Diffusion Lengths Exceeding 342, 341–345.

Sum, T.C., Mathews, N., 2014. Advancements in perovskite solar cells: photophysics

behind the photovoltaics. *Environ. Sci.* 7, 2518–2534.

Taylor, M., Daniel, K., Ilas, A., So, E., 2015a. Renewable Power Generation Cost in 2014.

Tsang, M.P., Sonnemann, G.W., Bassani, D.M., 2016. Life-cycle assessment of cradle-to-grave opportunities and environmental impacts of organic photovoltaic solar panels compared to conventional technologies. *Sol. Energy Mater. Sol. Cells* 156, 37–48. <https://doi.org/10.1016/j.solmat.2016.04.024>

Van Zelm, R., Huijbregts, M.A.J., Van De Meent, D., 2009. USES-LCA 2.0-a global nested multi-media fate, exposure, and effects model. *Int. J. Life Cycle Assess.* 14, 282–284. <https://doi.org/10.1007/s11367-009-0066-8>

Vaseghi, G., Celik, I., Burian, S., & Apul, D. (2017). Economic, Environmental, And Social Criteria Evaluation of Rainwater Harvesting System Options for An Office And Lab Building On the University of Utah Campus. *Frontiers in Civil Engineering*, 2, 115-147.

Wang, D., Wright, M., Elumalai, N.K., Uddin, A., 2016. Stability of perovskite solar cells. *Sol. Energy Mater. Sol. Cells* 147, 255–275. <https://doi.org/10.1016/j.solmat.2015.12.025>

Wang, W., Winkler, M.T., Gunawan, O., Gokmen, T., Todorov, T.K., Zhu, Y., Mitzi, D.B., 2014. Device Characteristics of CZTSSe Thin-Film Solar Cells with 12.6% Efficiency. *Adv. Energy Mater.* 4, 1301465. <https://doi.org/10.1002/aenm.201301465>

Wec, 2013. World Energy Scenarios: Composing energy futures to 2050. Rep. From <Http://Www.Worldenergy.Org/> 1–288.

Wernet, G., Bauer, C., Steubing, B., Reinhard, J., Moreno-Ruiz, E., Weidema, B., 2016. The ecoinvent database version 3 (part I): overview and methodology. *Int. J. Life Cycle Assess.* 21, 1218–1230. <https://doi.org/10.1007/s11367-016-1087-8>

Wong, J.H., Royapoor, M., Chan, C.W., 2016. Review of life cycle analyses and embodied energy requirements of single-crystalline and multi-crystalline silicon photovoltaic systems. *Renew. Sustain. Energy Rev.* 58, 608–618. <https://doi.org/10.1016/j.rser.2015.12.241>

Xu, J., Buin, A., Ip, A.H., Li, W., Voznyy, O., Comin, R., Kanjanaboos, P., 2015. Xu, J., Buin, A., Ip, A. H., Li, W., Voznyy, O., Comin, R., ... & Kanjanaboos, P. (2015). Perovskite–fullerene hybrid materials suppress hysteresis in planar diodes. *Nature communications*, 6, 7081. *Nat. Commun.* 6, 7081.

Ye, S., Sun, W., Li, Y., Yan, W., Peng, H., Bian, Z., Huang, C., 2015. CuSCN-based inverted planar perovskite solar cell with an average PCE of 15.6%. *Nano Lett.* 15, 3723–3728.

Yin, W.-J., Yang, H., Kang, J., Yang, S., Wei, H., 2015. Halide Perovskite Materials for solar cells: a theoretical review. *J. Mater. Chem.* 8926–8942.

You, J., Hong, Z., Yang, Y., Chen, Q., Cai, M., Song, T., 2014. Low-temperature solution-processed perovskite solar cells with high efficiency and flexibility.

Yue, D., You, F., Darling, S.B., 2014. Domestic and overseas manufacturing scenarios of silicon-based photovoltaics: Life cycle energy and environmental comparative analysis. *Sol. Energy* 105, 669–678. <https://doi.org/10.1016/j.solener.2014.04.008>

Zhang, J., Gao, X., Deng, Y., Li, B., Yuan, C., 2015. Life cycle assessment of titania perovskite solar cell technology for sustainable design and manufacturing. *ChemSusChem*.

Zhao, Y., Nardes, A.M., Zhu, K., 2014. Effective hole extraction using MoO_x-Al contact in perovskite CH₃NH₃PbI₃ solar cells. *Appl. Phys. Lett.* 104(21), 213906. 104, 213906.

Zhou, H., Chen, Q., Li, G., Luo, S., Song, T.B., Duan, H.S., Yang, Y., 2014. Interface engineering of highly efficient perovskite solar cells. *Science* (80-.). 345, 542–546.

Zimmermann, Y.-S., Niewersch, C., Lenz, M., Zohra Ku, H., F-X Corvini, P., Scha, A., Wintgens, T., Kül, Z.Z., Corvini, P.F.-X., Schäffer, A., Wintgens, T., 2014. Recycling of Indium From CIGS Photovoltaic Cells: Potential of Combining Acid-Resistant Nanofiltration with Liquid–Liquid Extraction. *Environ. Sci. Technol.* 48, 13412–13418. <https://doi.org/10.1021/es502695k>

Zimmermann, Y.-S., Schäffer, A., Corvini, P.F.-X., Lenz, M., 2013. Thin-film photovoltaic cells: long-term metal(loid) leaching at their end-of-life. *Environ. Sci. Technol.* 47, 13151–9. <https://doi.org/10.1021/es402969c>

Zimmermann, Y.-S., Schäffer, A., Hugi, C., Fent, K., Corvini, P.F.-X., Lenz, M., 2012. Organic photovoltaics: Potential fate and effects in the environment. *Environ. Int.* 49, 128–140. <https://doi.org/10.1016/j.envint.2012.08.015>

Zweibel, K., 2005. The Terawatt Challenge for Thin-Film PV.

Appendix A

Appendix A provides supplementary information for Chapter 2.

A1. Stoichiometric Reactions Assumed for Synthesis of Compounds

SnCl₂:2H₂O, CH₃NH₃I and CuSCN were needed for the life cycle inventory but not available in the Ecoinvent database. To estimate the impacts from these compounds we analyzed how they would be synthesized and modeled the chemicals needed to synthesize them. The synthesis reactions and the device layers for which they are needed are shown in Table A. 1.

Table A-1 Synthesis of the compounds

| | |
|--------------------------|--|
| Electron Transport Layer | |
| 1. | $\text{Sn}_{(s)} + 2 \text{HCl}_{(aq)} \rightarrow \text{SnCl}_{2(aq)} + \text{H}_2$ |
| 2. | $\text{SnCl}_{2(aq)} + 2\text{H}_2\text{O} \rightarrow \text{SnCl}_2 \cdot 2\text{H}_2\text{O}$ |
| Absorber Layer | |
| 3. | $\text{Pb} + 2 \text{HNO}_3 \rightarrow \text{Pb}(\text{NO}_3)_2 + \text{H}_2$ |
| 4. | $3 \text{I}_2 + 6 \text{KOH} \rightarrow 5 \text{KI} + \text{KIO}_3 + 3\text{H}_2\text{O}$ |
| 5. | $\text{Pb}(\text{NO}_3)_{2(aq)} + 2 \text{KI}_{(aq)} \rightarrow \text{PbI}_{2(s)} + 2 \text{KNO}_{3(aq)}$ |
| 6. | $\text{N}_2 + \text{H}_4 + 2 \text{I}_2 \rightarrow 4 \text{HI} + \text{N}_2$ |
| 7. | $\text{CH}_3\text{NH}_2 + \text{HI} \rightarrow \text{CH}_3\text{NH}_3\text{I}$ |
| Hole Transport Layer | |

| | |
|-----|--|
| 8. | $2\text{Cu}_{(s)} + \text{H}_2\text{O}_{(g)} + \text{CO}_{2(g)} + \text{O}_2 \rightarrow \text{Cu}(\text{OH})_2 + \text{CuCO}_3$ |
| 9. | $\text{NH}_4\text{SCN} + \text{KOH} \rightarrow \text{KSCN} + \text{NH}_3(g) + \text{H}_2\text{O}$ |
| 10. | $2\text{KSCN} + \text{Cu}(\text{OH})_2 + \text{HCl} \rightarrow 2\text{CuSCN} + 2\text{KCl} + 2\text{H}_2\text{O}$ |

A.2 Life Cycle Inventory of the Solution and Vacuum Based and HTL Free Models

Routes for deposition of each layer for each model are given in Table A. 2. The inputs and outputs for each one of the route numbers is given in Table A. 3. Specific assumptions, cited studies, and EcoInvent names are also included in Table A. 3.

Table A. 1 Routes for solution and vacuum based methods and HTL free structure models

| Route for Solution Based | Route for Vacuum Based | Route for HTL free |
|--------------------------|------------------------|--------------------|
| 1,2,3a,4,5a | 1,2,3b,4,5a | 1,2,3a,5b |

Table A. 2 Inventory for solution, vacuum based and HTL free Perovskite PV cell devices. Where a reference is not given assumptions and data came directly from the University of Toledo PVIC lab. Deposition efficiency is abbreviated as D.E. in the assumptions column

| | Parameters | Explanation | Inputs | Assumptions | Reference |
|---|---------------------|---|--------------------------------------|------------------------|------------------------|
| 1 | Front contact layer | | | | |
| | Material Input | | Solar glass, acetone and isopropanol | | |
| | Cleaning of layer | | Mass (kg/ kg glass) | | |
| | Glass | RER: solar glass, low-iron, at regional storage | 5 kg | Assumed as FTO covered | (Collier et al., 2014; |

| | | | | |
|-------------------------------|---|---|----------------------------------|---------------------------------------|
| | | | Pilkington glass | García et al., 2010) |
| Acetone | RER: acetone, liquid, at plant | 8.90E-03 | | |
| Isopropanol | RER: isopropanol, at plant | 2.07E-03 | | |
| Energy Input | | Electricity (MJ/m ²) | | |
| Electricity (Ultrasonication) | US: electricity, production mix US | 7.00E+01 | For cleaning | |
| Wastes | | | | |
| Acetone | Emission to air | 8.90E-03 | | |
| Isopropanol | Emission to air | 2.07E-03 | | |
| Waste heat | Emission to air | 7.00E+01 | | |
| 2 | Electron Transport Layer | | | |
| | Material Input | SnCl ₂ :H ₂ O | | |
| | Formation of Layer (SnO ₂) | Mass (kg/m ²) | | |
| | Sn | RER: tin, at regional storage | 5.70E-01 | |
| | HCl | RER: hydrochloric acid, from the reaction of hydrogen with chlorine, at plant | 3.50E-01 | |
| | SnCl ₂ | Modeled according to reaction 1 in Table A. 1 | 9.11E-01 | Synthesized with 100 % rxn efficiency |
| | SnCl ₂ :H ₂ O | Modeled according to reaction 2 in Table A. 1 | 1.08E+00 | Synthesized with 100 % rxn efficiency |
| | H ₂ O | CH: water, deionised, at plant | 1.73E-01 | |
| | Precursor: SnCl ₂ :2H ₂ O | | 2.71E-03 | |
| | Energy Input | US: electricity, production mix US | Electricity (MJ/m ²) | (Ke et al., 2015) |
| | Chemical Rxn 1 and 2 in Table A. 1 | | 5.99E-07 | |
| | Pretreatment (1 h stirring, @ 70°C.) | | 1.94E+01 | |
| | Deposition (Spray deposition) | | 7.70E+01 | |

| | | | | | |
|-----|-----------------------------------|---|--|---------------------------------------|--|
| | Post-treatment (1 h, @ 180C) | | 4.54E+01 | | |
| | Carrier gas | | | | |
| | Nitrogen | RER: nitrogen, liquid, at plant | | | |
| | Waste | | | | |
| | Waste heat | Emitted to air | 1.46E+02 | D.E =80% | |
| | Tin | Emitted to industrial soil | 5.42E-04 | D.E = 80% | |
| | HCl | Emitted to wastewater | 7.00E-02 | D.E =80% | |
| | Nitrogen gas | Emitted to air | 1.65E-02 | D.E =80% | |
| 3.a | Absorber Layer | | | | |
| | Material Input | | PbI ₂ , CH ₃ NH ₂ I and N,N DMF | | |
| | Formation of Layer (Perovskite) | | Mass (kg/m ²) | | |
| | Pb | RER: lead, at regional storage | 1.66E-03 | | |
| | HNO ₃ | RER: nitric acid, 50% in H ₂ O, at plant | 1.01E-03 | | |
| | Pb(NO ₃) ₂ | Produced | 2.65E-03 | | |
| | N ₂ H ₄ | RER: hydrazine, at plant | 3.40E-05 | | |
| | I ₂ | | 8.53E-03 | | |
| | KOH | RER: potassium hydroxide, at regional storage | 1.08E-03 | | |
| | KI | | 2.66E-03 | Synthesized with 100 % rxn efficiency | |
| | PbI ₂ | | 3.69E-03 | Synthesized with 100 % rxn efficiency | |
| | HI | | 3.07E-03 | Synthesized with 100 % rxn efficiency | |
| | CH ₃ NH ₂ | RER: methylamine, at plant | 7.45E-04 | | |
| | CH ₃ NH ₃ I | | 3.82E-03 | Synthesized with 100 % rxn efficiency | |

| | | | | |
|---|---|--|---|----------------------|
| Precursor N,N DMF | RER: N,N-dimethylformamide, at plant | 3.73E-01 | | |
| Energy Input | US: electricity, production mix US | Electricity (MJ/m ²) | | |
| Chemical Rxn | | 2.38E-08 | | |
| Pretreatment (2 h stirring, @ room temp.) | | 1.30E+02 | *Instead of 8 hours, stirring was assumed as 2 h *Electricity consumption of commercial stirrer is assumed to be 30% of thermal lab stirrer | (Garcia et al.,2010) |
| Deposition (Spray deposition) | | 2.70E+01 | | |
| Post-treatment (30 min, @ 70°C) | | 2.27E+01 | | |
| Carrier gas | | | | |
| Nitrogen | RER: nitrogen, liquid, at plant | 5.45E-01 | | |
| Waste | | | | |
| Methyl ammonium | Emission to wastewater | 7.64E-04 | D.E = 80% | |
| Lead | Emission to wastewater | 3.32E-04 | D.E = 80% | |
| Methyl formamide | Emission to wastewater | 7.46E-02 | D.E = 80% | |
| Waste heat | Emission to air | 1.79E+02 | | |
| Nitrogen gas | Emission to air | 5.60E-01 | | |
| 3.b Absorber Layer | | | | |
| Material input | | PbI ₂ and CH ₃ NH ₂ I | | |
| Formation of layer(Perovskite) | | Mass (kg/m ²) | | |
| Pb | RER: lead, at regional storage | 2.07E-03 | | |
| HNO ₃ | RER: nitric acid, 50% in H ₂ O, at plant | 1.26E-03 | | |
| Pb(NO ₃) ₂ | Produced | 3.31E-03 | | |

| | | | | |
|-----------------------------------|---|----------------------------------|---------------------------------------|----------------------|
| H ₂ | RER: hydrogen, liquid, at plant | 8.00E-05 | | |
| I ₂ | | 1.07E-02 | | |
| KOH | RER: potassium hydroxide, at regional storage | 1.35E-03 | | |
| KI | | 3.32E-03 | Synthesized with 100 % rxn efficiency | |
| PbI ₂ | | 4.61E-03 | Synthesized with 100 % rxn efficiency | |
| HI | | 3.84E-03 | Synthesized with 100 % rxn efficiency | |
| CH ₃ NH ₂ | RER: methylamine, at plant | 9.32E-04 | | |
| CH ₃ NH ₃ I | | 4.77E-03 | Synthesized with 100 % rxn efficiency | |
| Energy Input | US: electricity, production mix US | Electricity (MJ/m ²) | | (Garcia et al.,2010) |
| Chemical Rxn | | 2.98E-08 | | |
| Deposition (Co-evaporation) | | 6.91E+01 | 30 min duration | |
| Deposition (Vacuum) | | 2.65E+02 | 2 hour duration | |
| Carrier gas | | | | |
| Nitrogen | RER: nitrogen, liquid, at plant | 6.81E-01 | | |
| Waste | | | | |
| Methyl ammonium | Emission to air | 3.02E-04 | D.E =60% | |
| Lead | Emission to water | 6.64E-04 | D.E = 60% | |
| Waste heat | Emission to air | 3.34E+02 | | |
| Nitrogen | Emission to air | 6.81E-01 | | |
| 4 | Hole Transfer Layer | | | |
| | Material Input | CuSCN and Chlorobenzene | | |
| | Formation of layer (CuSCN) | Mass (kg/m ²) | | (Qin et al., 2014) |

| | | | | |
|---|---|----------------------------------|---|---|
| Cu | RER: copper, at regional storage | 1.25E-03 | | |
| CO ₂ | RER: carbon dioxide liquid, at plant | 4.34E-04 | | |
| O ₂ | | 1.58E-04 | | |
| Cu(OH) ₂ | | 9.63E-04 | Synthesized with 100 % rxn efficiency | |
| NH ₄ SCN | GLO: ammonium thiocyanate, at plant | 1.50E-03 | | |
| KOH | RER: potassium hydroxide, at regional storage | 1.11E-03 | | |
| KSCN | | 1.92E-03 | Synthesized with 100 % rxn efficiency | |
| Cu(OH) ₂ | | 9.63E-04 | Synthesized with 100 % rxn efficiency | |
| HCl | RER: hydrochloric acid, from the reaction of hydrogen with chlorine, at plant | 7.19E-04 | | |
| CuSCN | | 2.40E-03 | Synthesized with 100 % rxn efficiency | |
| H ₂ O | CH: water, deionised, at plant | 8.88E-04 | | |
| Precursor: Chlorobenzene | RER: monochlorobenzene, at plant | 4.00E-04 | Assumed instead of Dipopyl sulfide | |
| Energy Input | | Electricity (MJ/m ²) | | (García et al., 2010; Kushnir and Sandén, 2011) |
| Chemical Rxn | | 5.56E-08 | | |
| Pretreatment (1 h stirring, @ room temp.) | | 6.48E+01 | | |
| Deposition (Printing) | | 3.17E+01 | Assumed as the same as spray deposition | |
| Post-treatment (15 min, @ 70°C) | | 1.13E+01 | | |
| Waste | | | | |
| Copper | Emission to industrial waste | 4.80 E-04 | DE = 80 % | |

| | | | | | |
|----|------------------------------|------------------------------------|----------------------------------|-----------|----------------------------|
| | HCl | Emission to water | 1.44 E-04 | DE = 80 % | |
| | Waste heat | Emission to air | 1.12 E+02 | | |
| 5a | Back Contact | | | | |
| | Material Input | | Al | | |
| | Formation of layer (Al) | | Mass (kg/m ²) | | |
| | Al | RER: aluminum, primary, at plant | 3.53E-03 | | |
| | Energy Input | US: electricity, production mix US | Electricity (MJ/m ²) | | (García et al., 2010) |
| | Electricity (Evaporation) | | 3.46E+01 | | |
| | Electricity (Vacuum) | | 1.32E+02 | | |
| | Waste | | | | |
| | Aluminum | Emission to air | 1.77E-03 | DE = 50 % | |
| | Waste heat | Emission to air | 1.36E+02 | | |
| 5b | Back Contact | | | | |
| | Material Input | | Carbon and Isopropyl | | |
| | Formation of layer (C-paste) | | Mass (kg/m ²) | | (Mei et al., 2014) |
| | Graphite | GLO: carbon black, at plant | 2.00E-02 | | |
| | Isopropanol | RER: isopropanol, at plant | 2.00E-03 | | |
| | Energy Input | US: electricity, production mix US | Electricity (MJ/m ²) | | (Kushnir and Sandén, 2011) |
| | Spray deposition | | 1.13E+02 | | |
| | Waste | | | | |
| | Graphite | Emission to industrial soil | 4.00E-03 | DE = 80 % | |
| | Isopropanol | Emission to air | 4.00E-04 | DE = 80 % | |
| | Waste heat | Emission to air | 1.13E+02 | | |

A.3 Comparison of Primary Energy Demand (PED) of Selected Metals

Primary energy demands (MJ) of selected metals (for 1 kg of metals) are given in Figure A. 2. This figure is used to show why PED value of this study may be lower than previous studies (Gong et al., 2015). Silver, gold and aluminium are the metals that can be used for

back contact (Table A. 5). Indium is an alternative for top contact (ITO). Gong indicated PED of FTO as 122 MJ/m² while that of ITO as 323 MJ/m² (Figure 3, Gong et al., 2015). However, Figure A. 2 shows that the embedded energies of indium and silver are about 10 times and that of gold is about 1000 greater than aluminum. The high PED values that Gong et al.(2015) found likely resulted from indium usage in ITO, in addition to silver and gold usage in back contact. In TiO₂ module, Gong et al found the energy consumption for silver and gold layers as 60 %, and in ZnO module the of ITO glass were found 95 %.

Table A. 3 Material comparison with a literature study

| | Gong et al. (2015) (TiO ₂ module) | Gong et al.(2015) (ZnO module) | This study |
|--------------|---|-----------------------------------|------------|
| Top Contact | FTO | ITO | FTO |
| Back Contact | Gold | Silver | Aluminum |

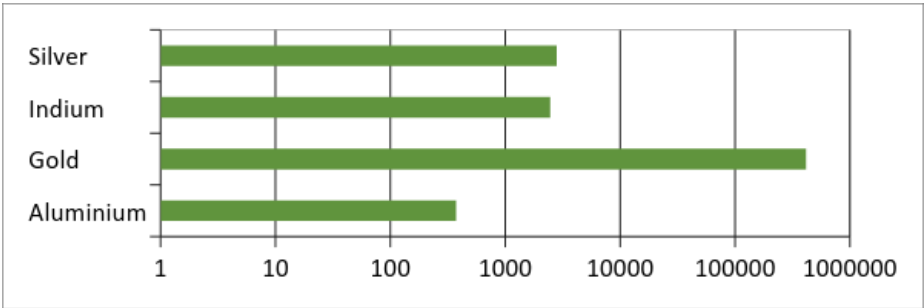


Figure A. 1 Comparison of primary energy consumption of selected metals (MJ/kg of metal) Properties of Modeled Deposition Methods and Structures

A.3. 1 Solution Based deposition

In Table A. 6, nine different environmental impacts of each layer are given. The table was used to compare solution-based deposition methods with vacuum and HTL free methods in Section 2.3.8 and in preparation Figure 2- 5.

Table A. 4 Impacts of solution-based perovskite PV production (per m²)

| | Acid. (kg SO ₂ - Eq.) | Ecotox. (CTU _e) | Eutro p. (kg N- Eq.) | GWP (kg CO ₂ - Eq.) | Human -tox., c. (CTU _h) | Human -tox.,n- c. (CTU _h) | PED (MJ) | Marin e eutrop (kg N- Eq.) | Fresh- water use (kg) |
|--------------|---|--------------------------------|-------------------------------|---|--|--|-------------|--|--------------------------------|
| Substrate | 1.5E-01 | 6.8E+01 | 6.4E-02 | 2.0E+01 | 9.3E-07 | 3.4E-06 | 3.0E+02 | 2.1E-03 | 4.4E+01 |
| ETL | 4.6E-01 | 5.6E+02 | 3.4E-01 | 3.9E+01 | 3.1E-06 | 9.2E-06 | 6.6E+02 | 5.6E-03 | 1.3E+02 |
| Perovskite | 4.4E-01 | 1.5E+02 | 3.1E-01 | 3.9E+01 | 2.2E-06 | 7.4E-06 | 6.3E+02 | 8.0E-02 | 1.0E+02 |
| HTL | 1.6E-01 | 6.3E+02 | 1.4E-01 | 2.3E+01 | 1.4E-06 | 5.4E-06 | 3.9E+02 | 3.0E-03 | 6.3E+01 |
| Back Contact | 2.4E-01 | 1.4E+02 | 1.3E-01 | 3.5E+01 | 1.9E-06 | 6.6E-06 | 5.6E+02 | 4.0E-03 | 9.2E+01 |
| Total | 1.4E+00 | 1.5E+03 | 9.8E-01 | 1.6E+02 | 9.6E-06 | 3.2E-05 | 2.6E+03 | 9.4E-02 | 4.4E+02 |

A.3.2. Vacuum-based deposition

In Table A. 5, 6 and 9 different environmental impacts of each layer are given. The table was used to compare vacuum-based deposition methods with solution and HTL free methods in Section 2.3.8 and in preparation Figure 2-9.

Table A. 5 Impacts of vacuum based perovskite PV production (per m²)

| | Acid. (kg SO ₂ - Eq.) | Ecotox. (CTU _e) | Eutrop (kg N- Eq.) | GWP (kg CO ₂ - Eq.) | Human -tox., c. (CTU _h) | Human -tox., n-c. (CTU _h) | PED (MJ) | Marine eutrop. (kg N- Eq.) | Fresh- water use (kg) |
|-----------|---|--------------------------------|--------------------------|---|--|--|-------------|-------------------------------------|-----------------------------|
| Substrate | 1.51E-01 | 6.86E+01 | 6.41E-02 | 2.01E+01 | 9.33E-07 | 3.38E-06 | 3.04E+02 | 2.09E-03 | 4.44E+01 |

| | | | | | | | | | |
|--------------|--------------|--------------|----------|--------------|----------|----------|--------------|----------|--------------|
| ETL | 4.56E-01 | 5.58E+0 2 | 3.36E-01 | 3.99E+0 1 | 3.14E-06 | 9.19E-06 | 6.64E+0 2 | 5.62E-03 | 1.35E+0 2 |
| Perovskite | 4.81E-01 | 2.76E+0 2 | 2.67E-01 | 6.98E+0 1 | 3.87E-06 | 1.32E-05 | 1.12E+0 3 | 9.41E-03 | 1.85E+0 2 |
| HTL | 1.59E-01 | 6.27E+0 2 | 1.39E-01 | 2.35E+0 1 | 1.42E-06 | 5.40E-06 | 3.89E+0 2 | 2.97E-03 | 6.28E+0 1 |
| Back contact | 2.38E-01 | 1.38E+0 2 | 1.33E-01 | 3.48E+0 1 | 1.94E-06 | 6.60E-06 | 5.61E+0 2 | 4.01E-03 | 9.22E+0 1 |
| Total | 1.48E+0 0 | 1.67E+0 3 | 9.39E-01 | 1.88E+0 2 | 1.13E-05 | 3.78E-05 | 3.04E+0 3 | 2.41E-02 | 5.19E+0 2 |

A.3.3 HTL free structure

In Table A. 8, 9 different environmental impacts of each layer are given. The table was used to compare HTL free structure methods with vacuum and solution-based methods in Section 3.8.

Table A. 6 Impacts of HTL free perovskite PV production (per m²)

| | Acid. (kg SO ₂ - Eq.) | Ecotox. (CTU _e) | Eutrop (kg N- Eq.) | GWP (kg CO ₂ - Eq.) | Human -tox., c. (CTU _h) | Human -tox., n-c. (CTU _h) | PED (MJ) | Marine eutrop. (kg N- Eq.) | Fresh- water use (kg) |
|------------|---|--------------------------------|--------------------------|---|--|--|-------------|-------------------------------------|-----------------------------|
| Substrate | 1.5E-01 | 6.8E+0 1 | 6.4E-02 | 2.0E+0 1 | 9.3E-07 | 3.3E-06 | 3.0E+0 2 | 2.0E-03 | 4.4E+01 |
| ETL | 4.5E-01 | 1.8E+0 2 | 3.3E-01 | 4.0E+0 1 | 3.4E-06 | 9.1E-06 | 6.6E+0 2 | 5.6E-03 | 1.3E+02 |
| Perovskite | 4.4E-01 | 1.5E+0 2 | 3.0E-01 | 3.9E+0 1 | 2.1E-06 | 7.3E-06 | 6.3E+0 2 | 7.9E-02 | 1.0E+02 |
| C-paste | 1.6E-01 | 9.9E+0 1 | 1.1E-01 | 2.6E+0 1 | 1.3E-06 | 4.7E-06 | 4.7E+0 2 | 2.7E-03 | 6.8E+01 |
| Total | 1.2E+0 0 | 5.0E+0 2 | 8.2E-01 | 1.2E+0 2 | 7.6E-06 | 2.4E-05 | 2.0E+0 3 | 9.0E-02 | 3.5E+02 |

A.4 Comparison of Electricity Consumption Mix of Different Regions and Countries

Comparison of electricity mix of selected regions and countries are summarized in Figure A. 8. This figure was prepared to show the different impacts of unit electricity mix

production in selected regions. This figure was specifically used to explain CO₂ equiv. of perovskite PV cells which were modeled in for different electricity mix. Espinosa et al.(2015) used Denmark low grid, Gong et al. (2015) used US mix in their calculations, and we also used US electricity mix in our study. Central Europe, China and Germany were given for comparison. China and Germany are the world’s largest solar panel manufacturers (Wheeland, 2014). China electricity mix is dominated by acidification and GWP, while German electricity mix is dominated by ecotoxicity, eutrophication, human-toxicity, marine eutrophication and fresh water use. Impacts from central Europe were found between Denmark’s and Germany’s mix as it was expected.

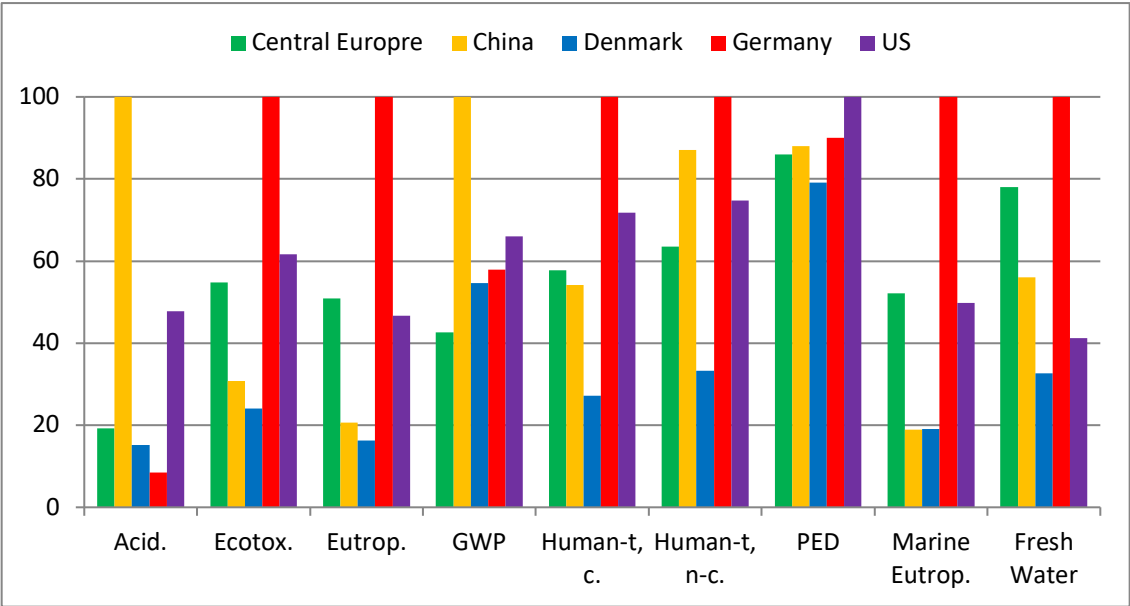


Figure A. 2 Normalized impact comparison of unit production-mixture of the selected countries and regions

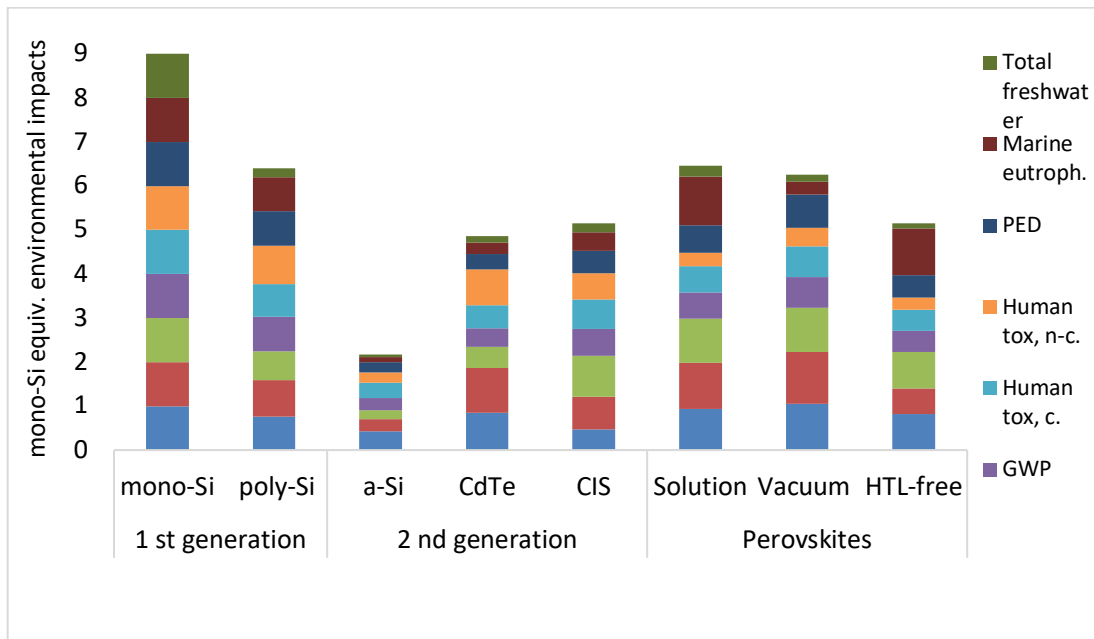


Figure A. 3 Comparison of Perovskite devices with commercial PV technologies when normalized to mono-Si for selected impact categories. Note that process energy for all technologies are set to RER, Electricity production mix.

Figure A. 3 prepared to show the impact of shifting from US Electricity mix to RER electricity mix. Comparison with Figure 2- 3 show GWP and acidification are greatly affected this change. The total mono-Si equiv. of HTL-free structure becomes as low as CdTe and CIS while these of Solution and Vacuum are close to poly-Si.

A.5 EPBT Calculation

EPBT calculation was done using approach of Bhandari et al., 2015; Raugei et al., 2012.

$$EPBT = \frac{PED \times \varepsilon}{I \times \eta \times PR \times CF} \quad (\text{Equation A. 1})$$

where,

$EPBT$ = energy payback time (years),

PED = primary energy demand (MJ_{primary}/m^2),

ε = electrical to primary energy conversion factor (%), 35 %,

PR = Performance Ratio (%)

η = Efficiency (%)

I = insolation constant ($kWh/m^2\text{-yr}$);

CF = Conversion factor, 3.6 MJ/kWh

A.6 Environmental Impacts of Materials Used

Table A. 8 was used to prepare Figure 2- 9.

Table A. 7 Toxicity of materials used in Modeled PV Technologies per kWh electricity.

| | | Acid. (kg SO ₂ - Eq) | Ecotox. (CTUe) | Eutrop. (kg N- Eq.) | GWP (kg CO ₂ - Eq.) | Human- tox., c. (CTUh) | Human- tox., n- c. (CTUh) | PED (MJ) | Marine eutrop. (kg N- Eq.) | Fresh- water use (kg) |
|-----------------------|----------------|--|-------------------|---------------------------|---|------------------------------|------------------------------------|-------------|-------------------------------------|-----------------------------|
| Solution Based Method | Aluminum | 1.4E-07 | 2.1E-04 | 1.1E-07 | 3.2E-05 | 9.0E-12 | 9.9E-12 | 5.0E-04 | 2.8E-09 | 9.9E-05 |
| | Carbon P. | 0.0E+00 | 0.0E+00 | 0.0E+00 | 0.0E+00 | 0.0E+00 | 0.0E+00 | 0.0E+00 | 0.0E+00 | 0.0E+00 |
| | Copper | 2.2E-09 | 3.5E-05 | 6.9E-09 | 3.3E-08 | 5.8E-14 | 1.7E-12 | 5.8E-07 | 6.5E-11 | 8.8E-07 |
| | Lead | 5.0E-08 | 8.5E-05 | 2.1E-08 | 2.3E-06 | 4.1E-13 | 1.2E-11 | 3.3E-05 | 5.3E-10 | 1.6E-05 |
| | Tin | 3.3E-04 | 8.3E-02 | 7.2E-05 | 1.3E-02 | 1.9E-09 | 4.2E-09 | 2.3E-01 | 2.7E-06 | 7.0E-02 |
| | Solar glass | 6.7E-05 | 1.4E-02 | 1.1E-05 | 7.2E-03 | 1.6E-10 | 8.0E-10 | 9.0E-02 | 5.3E-07 | 7.5E-03 |
| | Inorg. Add. | 5.2E-06 | 7.9E-03 | 7.2E-06 | 9.3E-04 | 8.6E-11 | 5.9E-10 | 1.9E-02 | 6.0E-07 | 7.1E-03 |
| | Org. Add. | 2.4E-04 | 2.9E-02 | 1.3E-04 | 2.1E-03 | 1.3E-10 | 7.3E-10 | 6.1E-02 | 9.8E-05 | 7.6E-03 |
| | Waste Str. | 2.7E-06 | 1.2E+00 | 4.2E-04 | 0.0E+00 | 1.4E-10 | 1.0E-09 | 0.0E+00 | 1.1E-06 | 0.0E+00 |
| | Total | 6.5E-04 | 1.3E+00 | 6.4E-04 | 2.3E-02 | 2.4E-09 | 7.3E-09 | 4.0E-01 | 1.0E-04 | 9.2E-02 |

| | | | | | | | | | | |
|---------------------|-------------|---------|---------|---------|---------|---------|---------|---------|---------|---------|
| Vacuum Based Method | Aluminum | 1.2E-07 | 1.7E-04 | 9.1E-08 | 2.6E-05 | 7.2E-12 | 7.9E-12 | 4.0E-04 | 2.3E-09 | 7.9E-05 |
| | Carbon P. | 0.0E+00 |
| | Copper | 1.8E-09 | 2.8E-05 | 5.5E-09 | 2.7E-08 | 4.6E-14 | 1.4E-12 | 4.7E-07 | 5.2E-11 | 7.1E-07 |
| | Lead | 5.2E-08 | 8.8E-05 | 2.1E-08 | 2.4E-06 | 4.3E-13 | 1.2E-11 | 3.4E-05 | 5.5E-10 | 1.6E-05 |
| | Tin | 2.6E-04 | 6.6E-02 | 5.8E-05 | 1.0E-02 | 1.5E-09 | 3.3E-09 | 1.8E-01 | 2.2E-06 | 5.6E-02 |
| | Solar glass | 5.4E-05 | 1.1E-02 | 8.6E-06 | 5.7E-03 | 1.3E-10 | 6.4E-10 | 7.2E-02 | 4.3E-07 | 6.0E-03 |
| | Inorg. Add. | 3.0E-06 | 3.0E-06 | 3.0E-06 | 3.0E-06 | 4.8E-11 | 4.0E-10 | 3.0E-06 | 3.0E-06 | 3.0E-06 |
| | Org. Add. | 4.0E-06 | 1.9E-02 | 1.9E-05 | 9.8E-04 | 6.5E-11 | 3.7E-10 | 2.8E-02 | 1.1E-07 | 3.2E-03 |
| | Waste Str. | 5.3E-06 | 9.3E-01 | 2.1E-04 | 0.0E+00 | 1.1E-10 | 8.1E-10 | 0.0E+00 | 2.2E-06 | 2.2E-06 |
| | Total | 3.3E-04 | 1.0E+00 | 3.0E-04 | 1.7E-02 | 1.9E-09 | 5.6E-09 | 2.8E-01 | 8.0E-06 | 6.5E-02 |
| HTL-free Structure | Aluminum | 0.0E+00 |
| | Carbon P. | 2.0E-07 | 1.0E-04 | 3.2E-08 | 7.5E-05 | 8.8E-13 | 6.1E-12 | 2.6E-03 | 4.9E-10 | 1.7E-05 |
| | Copper | 0.0E+00 |
| | Lead | 6.0E-08 | 1.0E-04 | 2.5E-08 | 2.8E-06 | 4.9E-13 | 1.4E-11 | 3.9E-05 | 6.3E-10 | 1.9E-05 |
| | Tin | 3.9E-04 | 9.9E-02 | 8.6E-05 | 1.6E-02 | 2.3E-09 | 5.0E-09 | 2.8E-01 | 3.3E-06 | 8.3E-02 |
| | Solar glass | 8.0E-05 | 1.7E-02 | 1.3E-05 | 8.7E-03 | 1.9E-10 | 9.5E-10 | 1.1E-01 | 6.4E-07 | 9.0E-03 |
| | Inorg. Add. | 5.1E-06 | 5.1E-06 | 5.1E-06 | 5.1E-06 | 1.0E-10 | 7.0E-10 | 5.1E-06 | 5.1E-06 | 5.1E-06 |
| | Org. Add. | 3.1E-04 | 1.6E-02 | 1.6E-04 | 5.7E-03 | 1.9E-10 | 7.9E-10 | 1.8E-01 | 1.2E-04 | 1.4E-02 |
| | Waste Str. | 3.3E-06 | 5.8E-01 | 4.5E-04 | 0.0E+00 | 0.0E+00 | 0.0E+00 | 0.0E+00 | 1.4E-06 | 0.0E+00 |
| | Total | 7.9E-04 | 7.2E-01 | 7.2E-04 | 3.0E-02 | 2.8E-09 | 7.5E-09 | 5.6E-01 | 1.3E-04 | 1.1E-01 |

Appendix B

Appendix B provides supplementary information for Chapter 3.

B. 1 Typical PV Structure

The typical PV Structure and a possible damage on a solar glass is shown in Figure A. 1.

This figure helps to visualize the leaching process explained in Section 2.2.

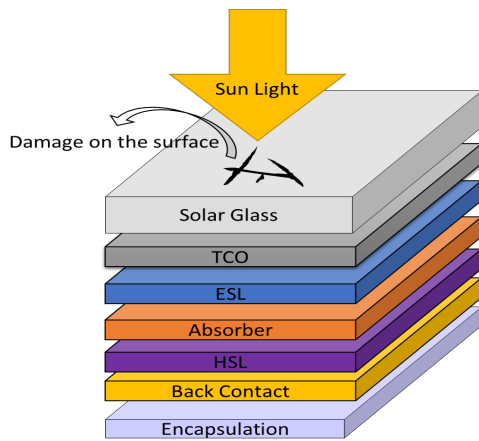


Figure B. 1: Typical PV structure and possible representations of a damage on glass layer

B. 2 Derivation of LF

To estimate the loss factors (LF) of different metal contents in the worst scenario, we consider the dissolution of these metals in rain water using the Noyes-Whitney equation

Equation (B.1):

$$\frac{dm}{dt} = A \times \left(\frac{D}{d}\right) \times (C_s - C_b) \quad \text{Eq B. 1}$$

where dm/dt is dissolution rate which is the change in mass of solute per time, m is the mass of the dissolved material, t is time, A is the surface area exposed to the solvent, D is diffusion coefficient of metal ion, d is thickness of the boundary layer, C_s is the saturated mass concentration at the surface, and C_b is mass concentration in the bulk solvent. Assuming $C_b = 0$ for the concentration in the bulk solvent, LF can be found by integrating Equation (1):

$$\int dm = A \times \frac{D}{d} \int C_s dt \quad \text{Eq A. 2}$$

Since

$$C_s = MW \times S_s \quad \text{Equation B. 3}$$

where MW is molecular weight of the metals, and S_s is the saturated molar concentration of the metal compounds. When we take the integral and divide the both sides to M_u ,

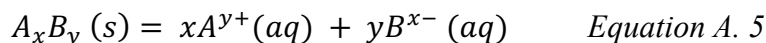
$$m_t - m_0 = A \times \frac{D}{d} \times MW \times S_s \times t$$

where $m_0 = 0$, $m_t = M_d$ (downstream emission from PV content), and divide the both sides to M_u

$$LF = \frac{M_d}{M_u} = \frac{A \times D \times MW \times S_s}{d \times M_u} t \quad \text{Equation B. 4}$$

where M_u is initial metal mass (upstream) in the PV panels.

For a metal compound A_xB_y , dissolution can be described by



where a saturated solution of A_mB_n in steady-state equilibrium is governed by the solubility product constant, defined as $K_{sp} = [A^{y+}]^x[B^{x-}]^y$. When the dissolution reaches the equilibrium concentration, $[A^{y+}] = S_s$, where S_s is saturated molar concentration of the metal ions,

$$K_{sp} = (S_s)^m [(y/x)S_s]^y = (y/x)^y (S_s)^{x+y} \quad \text{Equation B. 6}$$

or

$$S_s = \left(\frac{x}{y}\right)^{\frac{y}{x+y}} x (K_{sp})^{1/(x+y)}, \quad \text{Equation B. 7}$$

Combing Eqs. 2 and 5, LF can be determined by the solubility of the metal content as:

$$LF = \frac{A \times D \times MW \times t}{d \times M_u} \left(\frac{x}{y}\right)^{\frac{y}{x+y}} (K_{sp})^{1/(x+y)} \quad \text{Equation B. 8}$$

B. 3 Estimation of LF

All the parameters used in estimation of LF for realistic case are tabulated in Table B.1. The LF calculation in the manuscript was based on realistic case assumptions. A possible best-case scenario and worst-case scenario are also included in Table B2. As it is seen, all PbI_2 content is lost even in the best-case scenario. The error bars given in Figure 3-2 and Figure 3-4 represent the best and worst-case scenarios shown in Table A.2. Table A.3 is also provided to show the LF factors that were used to prepare Figure 3- 4. The only difference between the assumption in Table B.1 and B.3 is the different M_u values, which corresponds the initial mass available in the layers.

Table B. 1 Physical parameters of metal compounds and the estimated metal LF values.

| | K_{sp} | D (cm/s) | MW | $(x/y)^{(y/x+y)}$ | $K_{sp}^{(1/m+n)}$ | M_u | A (m ²) | LF |
|------------------|----------|----------|----------|-------------------|--------------------|----------|---------------------|----------|
| CdS | 1.00E-27 | 7.19E-06 | 1.12E+02 | 1.00E+00 | 3.16E-14 | 5.00E-01 | 3.0E-04 | 1.06E-08 |
| CuSCN | 1.77E-13 | 1.00E-05 | 6.36E+01 | 1.00E+00 | 4.21E-07 | 5.00E-01 | 3.0E-04 | 1.11E-01 |
| PbI ₂ | 9.80E-09 | 9.45E-06 | 2.07E+02 | 6.30E-01 | 9.90E-05 | 5.00E-01 | 3.0E-04 | 1.00E+02 |
| PbS | 3.00E-28 | 9.45E-06 | 2.07E+02 | 1.00E+00 | 1.73E-14 | 5.00E-01 | 3.0E-04 | 1.41E-08 |
| NiO | 5.48E-16 | 7.05E-06 | 5.87E+01 | 1.00E+00 | 2.34E-08 | 5.00E-01 | 3.0E-04 | 4.02E-03 |
| SnO ₂ | 1.09E-38 | 6.20E-06 | 1.19E+02 | 6.30E-01 | 2.22E-13 | 5.00E-01 | 3.0E-04 | 5.72E-08 |
| ZnO | 2.19E-17 | 7.03E-06 | 6.54E+01 | 1.00E+00 | 4.68E-09 | 5.00E-01 | 3.0E-04 | 8.92E-04 |
| SnS | 1.00E-26 | 6.20E-06 | 1.19E+02 | 1.00E+00 | 1.00E-13 | 5.00E-01 | 3.0E-04 | 3.06E-08 |

Table B.2 The variation of LF among the different scenarios.

| | Best-case | Realistic | Worst-case |
|--------------------------------|-------------------------------|----------------------------|-----------------------------|
| Breakage density of module (A) | 0.01% | 0.03% | 0.1% |
| Boundary layer (d) | 4 mm | 1 mm | 1 mm |
| Time (t) | 1 week - rains 3 hrs in a day | 1 yr- rains once in 4 days | 1 yr- rains every other day |
| | LF | LF | LF |
| CdS | << 0.01 % | << 0.01 % | << 0.01 % |
| CuSCN | 0.01% | 11.14% | 85 % |
| PbI ₂ | 100 % | 100 % | 100 % |
| PbS | << 0.01 % | << 0.01 % | << 0.01 % |
| NiO | << 0.01 % | 0.40% | 3.06 % |
| SnO ₂ | << 0.01 % | << 0.01 % | << 0.01 % |
| ZnO | << 0.01 % | << 0.01 % | 0.68 % |
| SnS | << 0.01 % | << 0.01 % | << 0.01 % |

Table B.3 Physical parameters of metal compounds and the estimated metal LF values used in Figure 3-4. Except M_u , the other input parameters (K_{sp} , D , MW etc.) used in calculation of LF are the same with Table B.1

| | M_u | LF |
|------------------|----------|-----------|
| CdS | 4.00E-02 | 0.00016% |
| CuSCN | 3.50E-02 | 100% |
| PbI ₂ | 6.40E-01 | 100% |
| PbS | 1.78E+00 | 0.000005% |
| NiO | 4.20E-01 | 5.68% |
| SnO ₂ | 3.30E-01 | 0.00008% |
| ZnO | 3.10E-01 | 1.71% |
| ZnO | 2.00E-01 | 2.65% |
| SnS | 2.83E+00 | 0.00001% |

B.4 Do results change if Usetox is used instead of ReCiPe?

Figure 3- 4 suggested that CdS (compared ZnO and SnO₂), PbS (compared to PbI₂ and CZTS) and NiO (compared to CuSCN) are less toxic alternatives for ESL, light absorber and HSL layers. We further analyzed these results with Usetox. As it is seen, metal toxicity ranking decision in the selected metals generally would not affect the results. Only exception was observed in Ni vs. Cu comparison. ReCiPe result suggest Ni is less toxic alternative than Cu while Usetox suggests Cu is less toxic. The contradiction between the two toxicity models regarding Ni and Cu was also noted by Pizzol.(Pizzol et al., 2011)

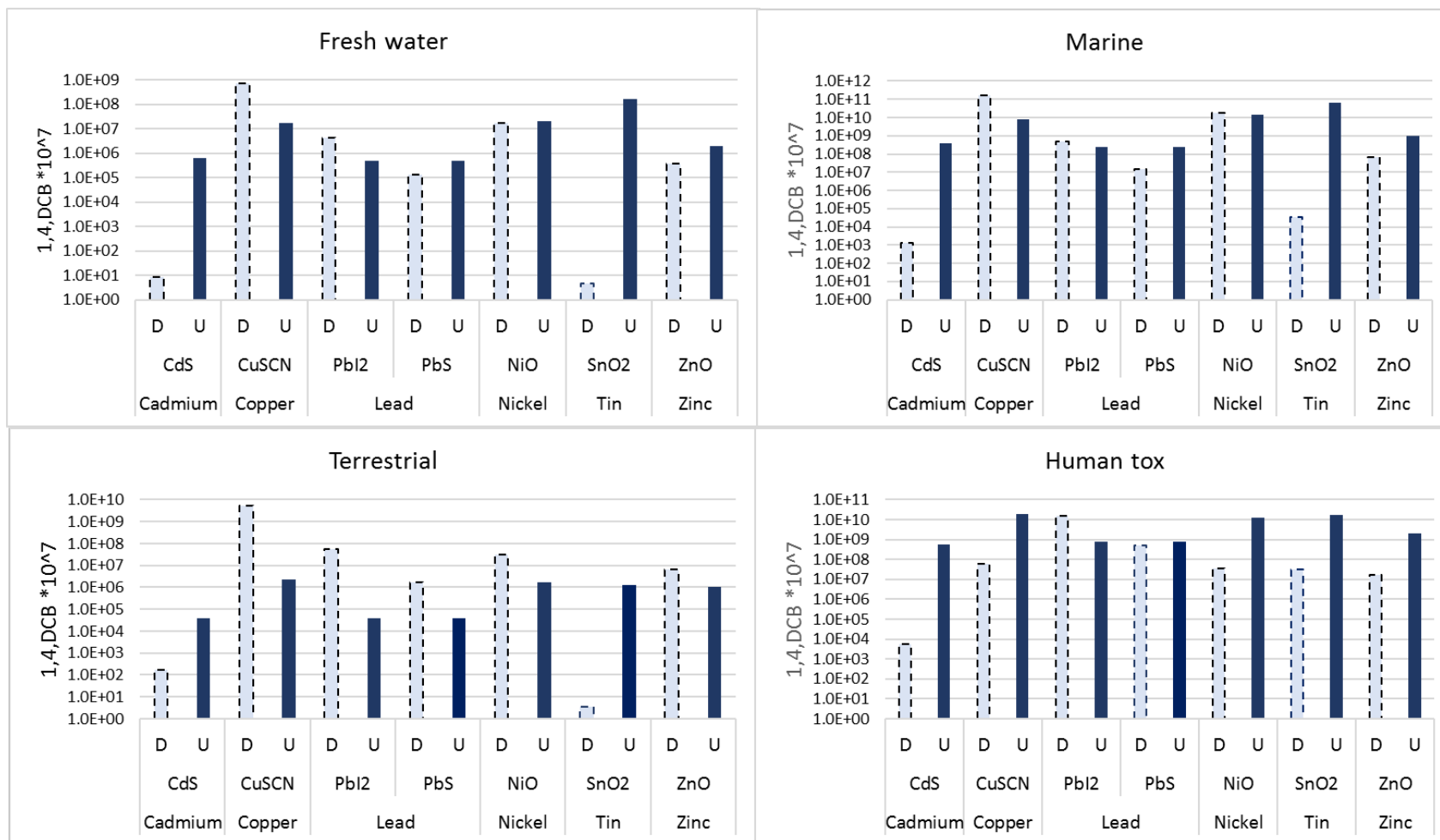


Figure B. 2 Downstream (D) and upstream (U) toxicity from metals used in emerging PV. These data are for midpoint impact categories.

These data were normalized using ReCiPe's hierarchist end point model to prepare Figure 3-2 and Figure

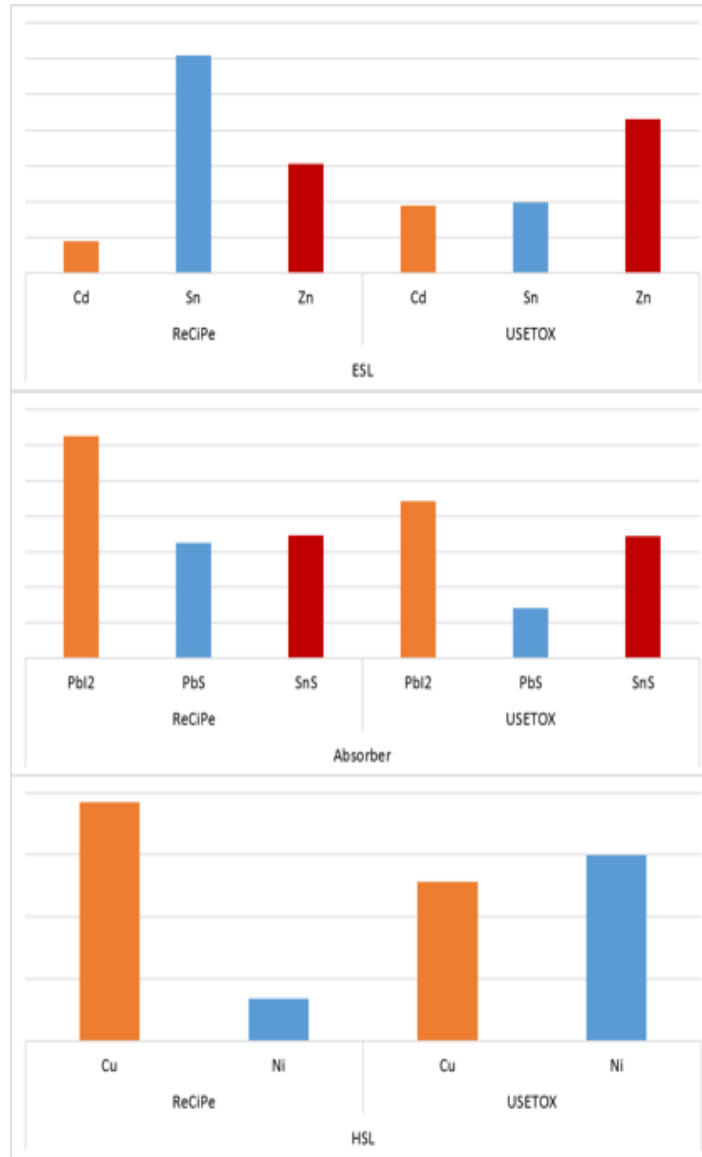


Figure B. 3 Toxicity impacts of the metals used in different studies for ESL, absorber and HSL. The graph was prepared in log scale to show a clear comparison between the different toxicity tools. Since different toxicity tools have different units, y-axis was left blank.

B. 5 Metal Releases from Coal-Fired Power Plants

The data used in Table 3 was taken from Babbitt and Lander's study (Babbitt and Lindner, 2005). The data represents the coal-fired power plants in Florida. However, the coal for Florida power plants is supplied by various sources from Rocky Mountains to Appalachian Basin. As such, the data is representative of coal-fired power plants in the US average. The pulverized coal-fired power technology was used in the study.

Babbitt and Lander [3] presented the metal emissions per 1,000 kg of coal combustion. They showed that 1,000 kg of coal can generate ~ 9.68 GJ (2.689 MWh). We normalized the data to g/MWh (Table A.4).

The data regarding Cd release from coal-fired power plants were directly extracted from the literature (Rix et al., 2015) since Babbitt and Lander did not provide Cd data.

Table B.4 Downstream and upstream metal emissions of coal-fired power plants

| g/MWh | Coal mining (Upstream) | Coal combustion (Use phase) |
|-------|------------------------|-----------------------------|
| Cu | 3.94 | 4.87 |
| Ni | 0.47 | 0.58 |
| Pb | 0.37 | 0.45 |
| Zn | 1.10 | 1.37 |

B. 6 Metal Releases from Mining the Metals Used in Emerging PV Technologies

Upstream metal emissions associated with emerging PV technologies were taken from EcoInvent 3.3(Wernet et al., 2016) (Table B. 5). These data are provided for gram of metal emitted per gram of metal mined. We multiply this data with gram of metal mined per m² of module (m₀) to obtain gram of metal emitted per m² of module. To be able to compare to coal electricity, we need mass of metal emitted per MWh of electricity generated not per m² of module. To convert the area of module to electricity generated, we made assumptions on insolation (1,700 MWh/yr/m²), lifetime (25 yr), efficiency (0.2), and performance ratio (0.75). Based on these assumptions the energy generated per unit area of module is:

$$\text{Energy generation from 1 m}^2 \text{ hypothetical emerging PV module} = 1.700 \frac{\text{MWh}}{\text{yr} \times \text{m}^2} \times 25 \text{ yr} \times 0.75 \times 0.20 = 6.375 \text{ MWh/m}^2$$

Energy generated per unit area is then multiplied with gram of metal emitted per unit area of module to obtain gram of metal emitted per MWh electricity generated (Table B. 6).

Table B.5 Grams of metals emitted per gram of metal mined. These metal mining emissions are used as the upstream emissions of emerging PV technologies.

| Mass of emissions (g) | Emissions from mining/extraction phase of different metals | | | | | |
|-----------------------|--|----------|----------|----------|----------|----------|
| | 1g Cd | 1 g Cu | 1 g Pb | 1 g Ni | 1 g Sn | 1 g Zn |
| Cd | 1.94E-07 | 2.23E-07 | 1.40E-05 | 1.85E-07 | 6.80E-07 | 4.97E-06 |
| Cu | 3.57E-05 | 1.18E-06 | 1.00E-03 | 3.98E-04 | 6.29E-04 | 6.70E-04 |
| Pb | 3.80E-06 | 6.01E-05 | 8.94E-04 | 3.95E-05 | 4.92E-05 | 2.27E-04 |
| Ni | 1.20E-06 | 1.28E-06 | 4.93E-06 | 3.45E-06 | 1.26E-05 | 3.80E-06 |
| Sn | 9.91E-08 | 1.90E-07 | 4.50E-07 | 1.33E-07 | 4.76E-07 | 3.15E-07 |
| Zn | 3.00E-06 | 9.60E-06 | 1.69E-04 | 7.91E-06 | 3.33E-05 | 2.08E-03 |

Table B. 6 Upstream metal emissions from emerging PVs. m(o)

| Components of the hypothetical emerging PV | M_u (g/m ²) | Upstream Emissions (g/m ²) | Upstream Emissions (g/MWh) |
|--|---------------------------|--|----------------------------|
| Cd | 4.00E-02 | 1.25E-05 | 1.96E-06 |
| Cu | 3.50E-02 | 2.80E-03 | 4.39E-04 |
| Pb | 6.40E-01 | 8.00E-04 | 1.26E-04 |
| Ni | 4.20E-01 | 4.17E-05 | 6.54E-06 |
| Sn | 2.83E+00 | 1.80E-06 | 2.82E-07 |
| Zn | 3.10E-01 | 8.49E-04 | 1.33E-04 |

Appendix C

I prepared Appendix C to share my personal experiences regarding the use of GaBi LCA Software package.

C.1 How to start using GaBi?

I suggest to new GaBi users to work on paper clip example a few times before starting own LCA models. I remember a few times that I made mistakes in saving the LCA model. First, the users should create the a “project” than within that project, a “plan” should be saved. Please note that GaBi allows users to save plans without defining project. In these cases, users cannot find their plans in their future attempts even though they saved the plans before exit GaBi. Watching the paper clip example a few times, may help to eliminate these mistakes.

C.2 How to extract the data from GaBi?

I find moving the data from GaBi to excel very useful. After running the model, in the coming page, click on the “Balance” tab. Then, click on the arrow in the first line. Next, select the impact assessment tool. In the coming page, you’ll see all the impacts that the selected impact assessment tool contains. When you click on the “total” column, you’ll see the breakdown of all the inventory used in the model. This data can be moved to excel by using Ctrl+A.

C.3 How do I create PV LCA models?

Initially, I prepared large LCA modules that have all the layers. Then, I switch to preparing single layer models for each layer. Well, two approaches have its own advantages and disadvantageous but I decided preparing single layer in each LCA plan is more convenient since one layer could be use in different PVs, therefore, working the data in excel is much easier to work in GaBi. I prepare separate excel pages for each layer in excel and prepare the final result in the excel.

C.4 How to work on an available PV LCA inventory in EcoInvent?

There are number of LCA models in EcoInvent. If a user wants to breakdown the complete inventory, this is the way to make it in GaBi: 1) search for “photovoltaic”, select the unit process (u-so, not “agg”) for desired technology (e.g., silicon, CdTe, or CIS). 2) Right click on the process and select “DB settings” 3) On the left side of the coming window, a long list of sub-processes required for making a complete PV process. For example, how much electricity is required, how heavy is the silicon material etc can be found in this window. If users want to complete data, e.g., CO₂ emissions from mono-crystalline silicon PV, then, choose the “agg” process in the first step.